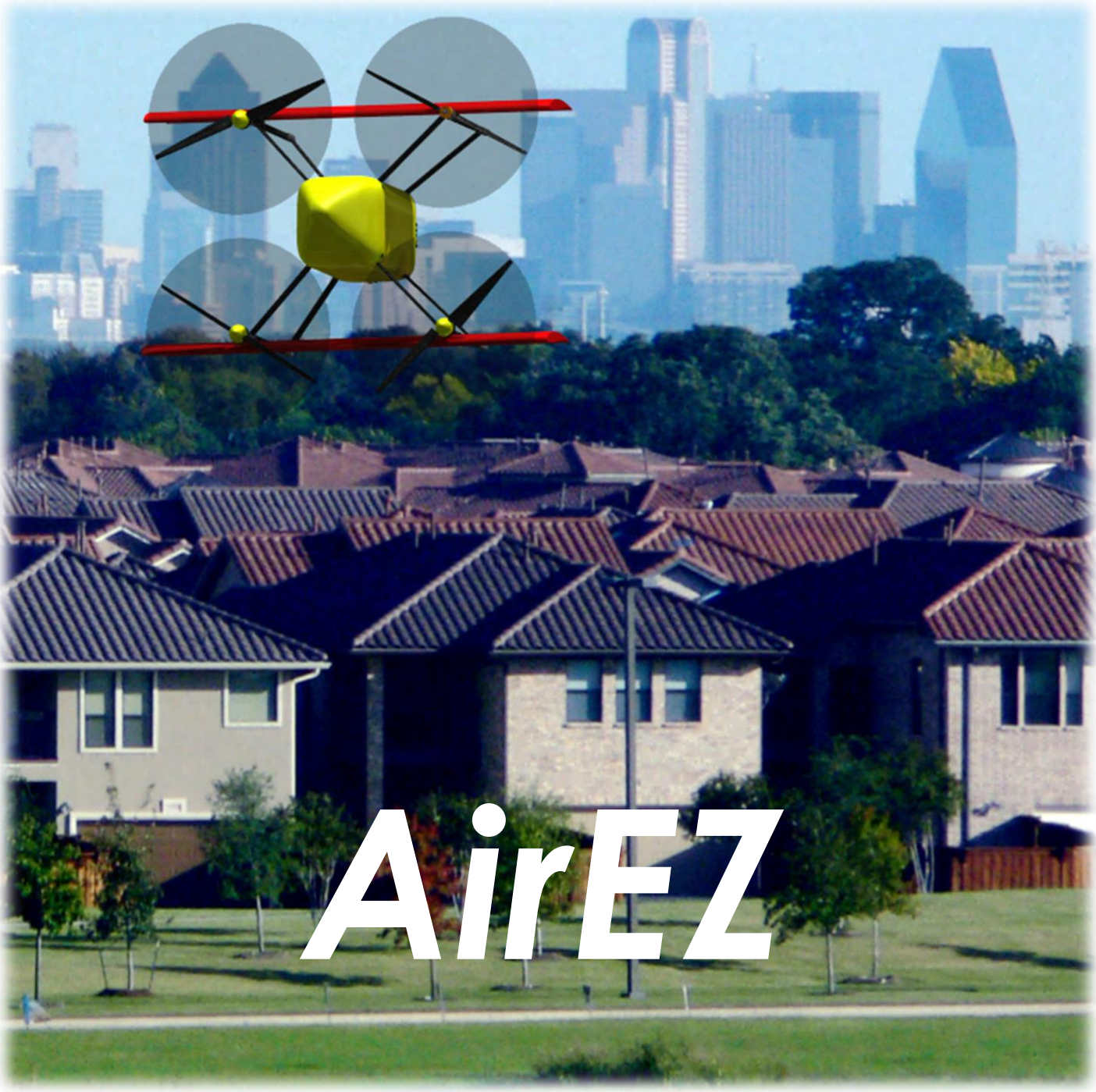

UNIVERSITY OF MARYLAND

Alfred Gessow Rotorcraft Center
Department of Aerospace Engineering
University of Maryland
College Park, MD 20740 U.S.A.

Stacy Sidle
Graduate Student (Team Leader)
stacy.sidle@gmail.com

Christopher Bogdanowicz
Graduate Student
cbogdano@terpmail.umd.edu

Brandon Gudenius
Graduate Student
bgudenius1@gmail.com

Daigo Shishika
Graduate Student
shishika@umd.edu

Xing Wang
Graduate Student
wxing@umich.edu

Justin Winslow
Graduate Student
jstnwnslw@gmail.com

Dr. Vengalatore Nagaraj
Faculty Advisor
vnagaraj@umd.edu

Dr. Inderjit Chopra
Faculty Advisor
chopra@umd.edu

Alfred Gessow Rotorcraft Center
Department of Aerospace Engineering
University of Maryland
College Park, MD 20740 U.S.A.

The members of the University of Maryland Graduate Student Team grant their permission for the following proposal for the 32nd Annual AHS Student Design Competition and the accompanying Executive Summary to be posted to the AHS website in accordance with the Request for Proposal.

ACKNOWLEDGEMENTS

The *AirEZ* design team wishes to acknowledge the following people for their invaluable discussion, guidance, and support throughout the course of this project.

University of Maryland Faculty

Dr. Vengalattore T. Nagaraj – Senior Research Scientist, Dept. of Aerospace Engineering, University of Maryland, College Park

Dr. Inderjit Chopra – Alfred Gessow Professor and University Distinguished Professor, Director of Alfred Gessow Rotorcraft Center (AGRC), Dept. of Aerospace Engineering, University of Maryland, College Park

Dr. Derek A. Paley – Associate Professor, Director of Collective Dynamics and Control Laboratory, Dept. of Aerospace Engineering, University of Maryland, College Park.

Dr. J. Sean Humbert – Associate Professor, Director of Autonomous Vehicle Laboratory, Dept. of Aerospace Engineering, University of Maryland, College Park

Industry Professionals

Dr. Graham Drozeski – Aurora Flight Sciences

Charley Kilmain – Director, Rotor and Drive System Design, Bell Helicopter Textron, Inc.

Dr. Dev G. Raheja – President, Raheja Consulting, Inc.

Dr. Nick Roy – Robust Robotics Group, Computer Science and Artificial Intelligence Laboratory, Massachussetts Institute of Technology

Dr. Ken Uleck – Senior Manager, Air Vehicle Engineering, Textron Systems

Special thanks goes:

Dr. Graham Bowen-Davies
Dr. Bharath Govindarajan
Dr. Vikram Hrishikeshavan
Dr. Ananth Sridharan
Dr. Derrick Yeo
Joseph Schmaus
William Staruk
Elizabeth (Weiner) Ward
Brandyn Phillips

Contents

List of Figures

List of Tables

Nomenclature

Symbol	Units	Description
AR	–	Aspect ratio
BL	–	Blade loading coefficient
DL	lb/ft^2	Disk loading
c	ft	Rotor chord
C_d	–	Drag coefficient
C_{d_0}	–	Zero-lift drag coefficient
C_f	–	Skin friction coefficient
C_l	–	Lift coefficient
C_T	–	Thrust coefficient
$C_{l_{\text{stall}}}$	–	Maximum lift coefficient
f	–	Fineness ratio
FF	–	Form factor
$GTOW$	lbs	Gross takeoff weight
M	–	Mach number
N_b	–	Number of blades
R	ft	Rotor radius
ρ	slugs/ft^3	Air density
Q	–	Interference factor
R	–	Reynolds number
S	ft^2	Wing planform area
S_{ref}	ft^2	Reference area
S_{wet}	ft^2	Wetted area
σ	–	Solidity
V_{stall}	ft/s	Stall speed
V_{tip}	ft/s	Tip speed
W	lbs	Weight

1 Introduction

With the introduction of expedited delivery processes such as Amazon Prime, an increasing number of customers will come to rely on rapid delivery of their purchases, with a growing expectation of delivery within days or even hours. Unmanned aerial vehicles, or UAVs as they are more commonly known, offer an opportunity to expand the range of delivery services currently offered and allow for faster-than-ever delivery of smaller packages.

High-profile companies such as Amazon and Google are developing their own UAV technology for rapid package delivery. The American Helicopter Society (AHS) has addressed this growing field of interest by issuing its 32nd Annual Student Design Competition Request for Proposal (RFP), which desires an aerial vehicle that will work as part of an entire system of systems for quick delivery of packages from a central warehouse directly to the customer. In response to the RFP, the University of Maryland Graduate Design Team proudly presents the *AirEZ* delivery system.

AirEZ is a quadrotor biplane tailsitter vehicle capable fast and efficient delivery of packages. Working as part of the complete system of systems concept, the *AirEZ* vehicle safely and reliably delivers multiple packages to customers in a 50 mi x 50 mi region within a two-hour window, and does so efficiently day after day. The advanced onboard avionics suite and communication systems allow *AirEZ* to coordinate between the hundreds of vehicles in the local airspace while successfully navigating through the urban canyons.

The capabilities of the *AirEZ* delivery system are unprecedented and represent a paradigm shift in the delivery services market. This report will outline the methodology utilized in arriving at the final *AirEZ* system design, explain the features of the system that make it a superior concept for accomplishing this demanding delivery mission, as well as address the challenges that need to be addressed before such a system can be realistically implemented. Part 1 discusses the overall system operation. Part 2 gives details of the vehicle.

Part I - System Level Design

2 *AirEZ* Concept of Operations

The *AirEZ* system has been designed to optimally fulfill the requirements of the RFP. This chapter will outline the concept of operations for the entire system for a basic delivery mission.

2.1 Warehouse Operations

The central warehouse serves as the base of operations for the entire delivery system. The functions undertaken in the central warehouse are as follows:

- **Package handling:** All packages to be delivered are stored in the warehouse at the start of the delivery day. For the purposes of the *AirEZ* system design, the warehouse is assumed to be an existing system with a high level of automation in terms of the picking and transport of packages from their locations in storage to the loading area. When orders are received, packages are located and picked from storage and transported to the loading area using an automated conveyor system or robotic arms. In simulations, a warehouse picking time of 10 minutes is assumed.
- **Vehicle storage and maintenance:** Simulations showed that to reliably complete the specified RFP mission, a fleet of at least 400 *AirEZ* vehicles is required. To ensure there are always enough vehicles to complete the delivery mission, 480 vehicles are kept at the warehouse. A maintenance schedule in which 10% of the fleet are being inspected and repaired is kept to ensure all vehicles are safe to fly.
- **Battery charging:** The *AirEZ* vehicle utilizes battery power. Spare batteries are charged continually throughout the day so that when a vehicle returns to the warehouse from delivering a package, the spent battery is exchanged with a fully charged battery and the vehicle is reloaded for another round of deliveries. In this way, the downtime between delivery missions is minimized.
- **Vehicle monitoring:** The *AirEZ* vehicle operates completely autonomously from the time it leaves the warehouse until it returns. However, to protect against any unforeseen problems, monitoring stations display information relayed through the central management computer about individual vehicle missions, specifically vehicle location and speed, as well as mission status updates (e.g., en route to customer, delivering a package, etc.). Twenty vehicle monitors keep track of 20 vehicles each.
- **Order processing:** The central management computer also processes all the orders received at the warehouse. When an order is received, information about its weight, size, and destination are also known. This information is used to determine efficient routing and assignment of multiple packages to each vehicle. In addition, the customer provides a cell phone number to receive text updates on the status of their delivery.
- **Vehicle loading:** Vehicle assignment and routing occur while the package is being picked and transported to the loading area. At that point, the packages are sorted automatically and diverted to the loading zone for the assigned vehicle.

2.2 Vehicle Operations: Basic Mission

Once the packages have been loaded, the vehicle departs the warehouse and begins the delivery mission. The vehicle's onboard computer is preloaded with aerial maps of the entire region, including height information for buildings to avoid. In addition, route information as well as the package dimensions are stored, and the vehicle begins navigating to its first delivery location.

When the vehicle is ready to depart, it lifts off the ground vertically and climbs to a safe elevation for transition to forward flight. The most efficient transition maneuver is determined based on the vehicle's height above ground level. In forward flight, the vehicle uses its forward facing camera to actively sense and avoid any unknown obstacles that might not have been represented on its map. The vehicle continues to fly in this way to the first customer's location, where it transitions back to helicopter flight mode, again using an efficient transition maneuver.

In the hover condition, the vehicle's on-board cameras sync with its IMU data and create a depth map that enables determination of a safe landing zone. Simultaneously, sonar, infrared, and LiDAR sensors work together to create a comprehensive sense and avoid capability, enabling the vehicle to land safely while avoiding obstacles such as animals and power lines.

After landing, the vehicle's delivery mechanism is activated. The payload bay door opens and servos operate two augers on either side of the package(s) to force them through the door. Preloaded package size information allows the delivery mechanism to only operate long enough for the first package to fall from the vehicle. At this point the, the servos run in reverse to re-center the remaining packages. The vehicle then takes off again in hover and continues to the next customer.

This delivery process is repeated until all assigned packages have been delivered. After the final package is delivered, the vehicle returns to the warehouse. At the warehouse, battery compartment is opened and the used battery is removed and replaced with a fully charged battery, so the vehicle can quickly begin another delivery mission. The battery changing time is less than 5 minutes due to the simple design of the battery compartment and hinged nose cone.

2.3 Overweight/Oversize Packages

The *AirEZ* vehicle has been sized to carry a payload of up to 5 lbs, approximately 85% of all the package requests. *AirEZ* is capable of fulfilling 100% of package requests in the 2,500-mile delivery zone that are 5 lb or less. For packages beyond this weight, a smaller battery is used and *AirEZ* will still be able to deliver many of these packages. Figure 2.1 shows the radius of action for the *AirEZ* vehicle based on the payload. All packages up to 5 lbs are deliverable on time in the delivery area. For packages between 5 and 8 lbs, the delivery range is shortened to 58.7 mi, allowing coverage of all but a small portion of the delivery zone. For 8-12 lb packages, the delivery range is 28.8 miles, covering 26% of the delivery area. The *AirEZ* vehicle does not have the ability to deliver packages greater than 12 lb, but this is only 5% of all the package requests. Arrangements may be made for oversize packages to be delivered by truck. For packages that do not fit in the payload compartment, slung load delivery is feasible though not practical economically, so they, too can be delivered by truck.

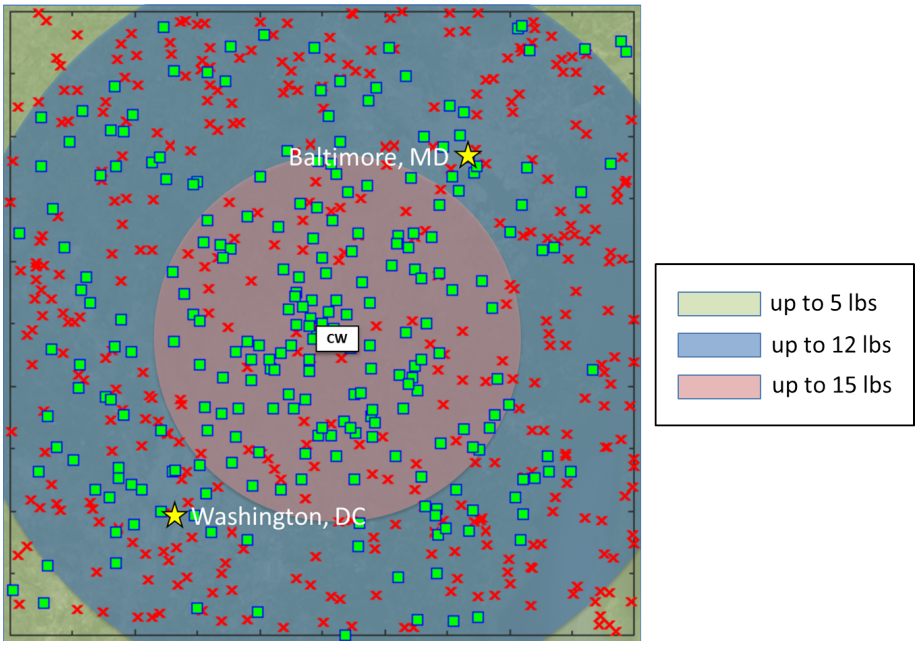

FIGURE 2.1: Radius of action of *AirEZ* vehicle

2.4 Additional Capabilities

Although *AirEZ* has been designed to meet the needs of a logistics company to deliver packages to customers, the alternative uses for the *AirEZ* vehicle, given its size and capabilities are numerous. For instance, as a reconnaissance vehicle, *AirEZ* could be dispatched to offshore windmills for inspection using the many cameras on board. Similarly, *AirEZ* could be used as a method of surveillance for border patrol or the identify illegal logging or mining.

AirEZ could also be particularly useful in military situations, where the unmanned, autonomous capabilities of the system could be used to get necessary supplies, like water, ammunition, or first aid, to soldiers in the battlefield. Additionally, *AirEZ* could provide surveillance for perimeter defense, serving as an early warning system.

This range of capabilities demonstrates that *AirEZ* is a versatile platform.

2.5 Barriers to Entry

It should be noted that although the *AirEZ* system has the capability to serve as an autonomous aerial delivery platform, the current FAA rules are not compatible with any autonomous aerial system. As it stands currently, UAVs must be flown by a human pilot who maintains a line of sight with the vehicle at all times. Obviously, there is no system that could deliver within a 50 mi x 50 mi area under these restraints. Furthermore, air traffic control systems are not equipped to handle the volume of communications that would accompany the volume of vehicles associated with the *AirEZ* system. Additionally, the concerns of state and local governments over the safety and happiness of residents could lead to excessive regulations prohibiting flyover in residential areas. Residents may also have concerns about small UAVs flying over their property. Although the *AirEZ* system is safe, it can take time to overcome ingrained prejudices.

AirEZ System Concept of Operations

Central Warehouse

Central Computer

Vehicle Monitoring

Vehicle Maintenance

UAV Fleet

Battery Charging

1. **Package requests 1-3 received**
2. **Packages assigned to a delivery vehicle and route to request locations determined**
3. **Packages picked from storage and transported to loading**
4. **Packages loaded onto vehicle**

GPS Satellite

Package Request 3

8. Vehicle returns to central warehouse for new battery and new delivery

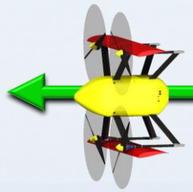

LATAS
Low Altitude Tracking and Avoidance

Air Traffic Control

Commercial Aircraft

7. Package 3 delivered

Radio Mesh Networking

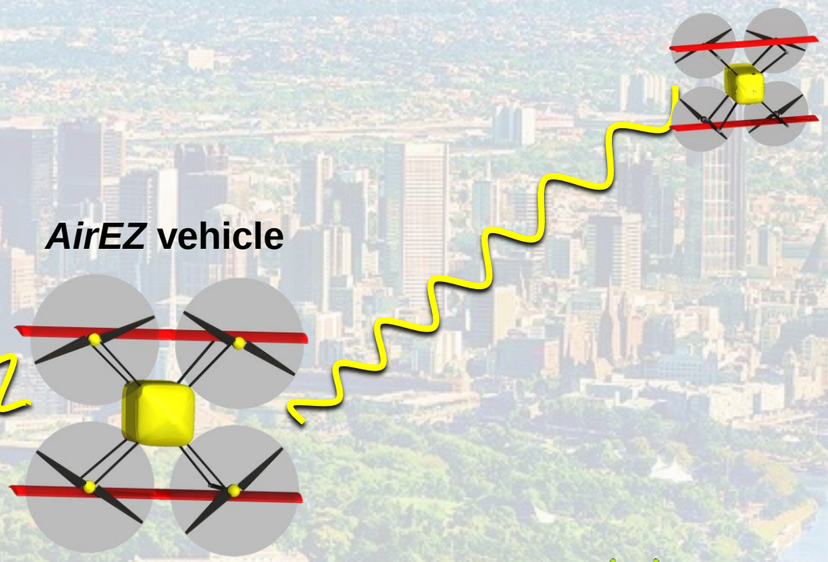

***AirEZ* vehicle**

5. Package 1 delivered

Package Request 1

Cellular Network

6. Package 2 delivered

Package Request 2

Routing Strategy

With multiple package delivery **61%** **reduction in required number of vehicles compared to single package delivery**

Cost Function

Vehicle routing is optimized specifically for the *AirEZ* delivery system using Modified Traveling Salesman Problem, which minimizes the following cost function:

$$F = K_1F_{dist} + K_2F_{wait} + K_3F_{energy} + K_4F_{spread} + F_{weight} + F_{volume}$$

The optimization achieves:

- **Fast delivery (short customer waiting time)**
- **Short traveled distance**
- **Low energy consumption**

while complying to the limitation (range, package weight/size) imposed by the vehicle specification.

Simulation Algorithm

Randomly generate requests

- Time
- Location
- Weight
- Size

March simulation in time

time = 0 min

(1) Check for new requests

(2) Assign packages to vehicle and optimize route (**modified TSP** detailed in Appendix)

Package size within cargo-bay limitation (90%)

- W_{pkg} < 5 lb (77%): **multi-package** delivery with full range & full speed *
- 5 < W_{pkg} <11 lb (7%) : single-package delivery with full range & **low speed** **
- 11 < W_{pkg} <12 lb (1%) : single-package delivery with **low range** & **low speed** ***

Oversized packages (10%): delivered by truck

- 12 < W_{pkg} lb (5%) : delivered by truck

(3) Update vehicle states (Location, Loading, Charging, etc.)

(4) Update package states (Requested, Out for delivery, Delivered)

time = *time* + 1 min

return to (1)

* Number of carried packages depends on the size
** Cruise speed varies between 55 kts to 32 kts
*** Range varies between 80 mi to 55 mi

Post process

- Success rate
- Energy usage
- Traveled distance
- Time history

Package Assignment Algorithm

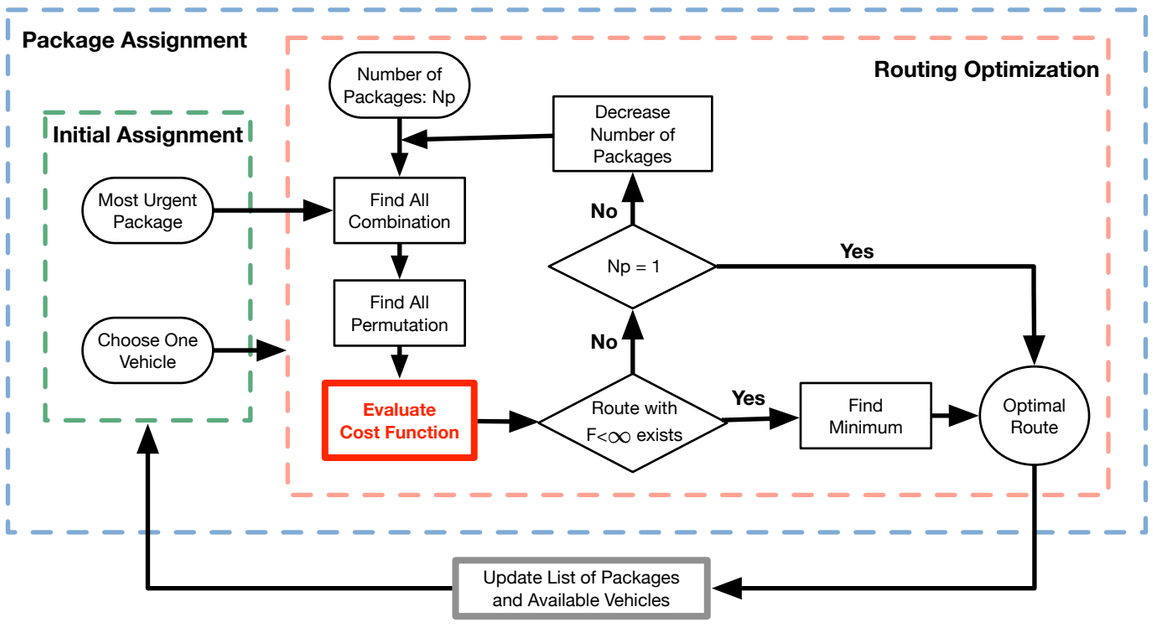

Multi-Vehicle Optimization & Directional Spreading

By regulating the directional spreading of the route, the total traveled distance from all routes are minimized with computationally simple algorithm.

With this method, suboptimal solution to multi-vehicle optimization (computationally expensive) are obtained by a single vehicle optimization.

The method is validated by numerical experiments.

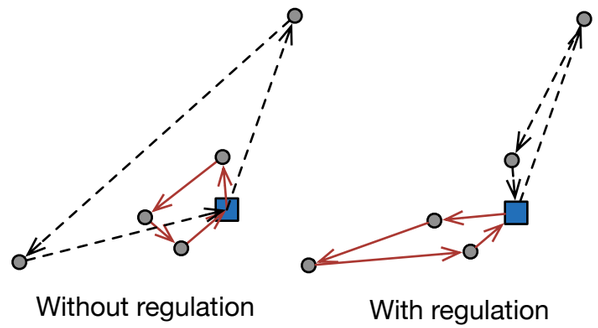

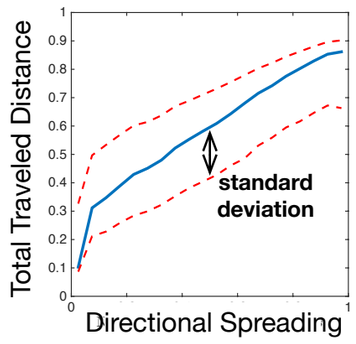

Wind Compensation

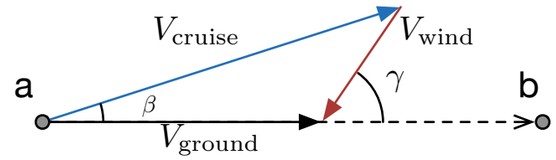

Weather information is incorporated in the optimization to ensure completion of the mission

3 Logistics Simulation

The RFP included a requirement for a simulation of the system of systems for an average day. The delivery scenario to be modeled is one in which 5,000 package requests are made uniformly randomly during an 8-hour period and distributed uniformly randomly throughout the 50 × 50-mile delivery region. The packages should then be delivered from the central warehouse to the customer within 2 hours.

An in-house simulation was developed to model the operation of the *AirEZ* system during a typical delivery day using a modified Traveling Salesman Problem which is detailed in the foldout-Routing Strategy. Results of these simulations were used throughout the design to explore the impact of certain design decisions as well as to determine values for the requested measures of effectiveness (MoEs). This chapter describes the development and implementation of the simulation program as well as the aspects of the system design that were modeled and the results of those studies.

3.1 Parameters and Assumptions

3.1.1 Package Size Assumptions

Although the distribution of package weights are specified in the RFP, the distribution of the package sizes are not specified. The package size has a significant effect on the number of packages that can be carried in a single trip. As shown in Section 3.3, the capability of carrying multiple packages is very important to improve the efficiency of the delivery, because the total traveled distance can be decreased with the help from efficient vehicle routing strategy (see flodout-Routing Strategy).

To accommodate different possibilities, simulations were performed with three different assumptions:

A1) Only one package fits in the vehicle.

A2) Package size is distributed within the specified (12 × 12 × 16 in) dimension.

A3) Ignore the size and only assume the maximum number ($N_{\text{pkg,max}}$) that can fit in the vehicle.

With the fuselage size (see Section 6), a strict interpretation of the RFP leads to the worst case assumption A1. A more realistic and reasonable assumption is that the package size is distributed within the dimension specified by the RFP, wherein folded-normal distribution was used together with the data obtained from USPS for the distribution. Finally, the most relaxed assumption A3 only considers the maximum number of packages that the vehicle can carry.

These different assumptions are kept as unknowns throughout the analysis to avoid any bias in the design. Towards the end of this chapter, simulation results are shown for all three cases.

3.1.2 Simulation Parameters

Important simulation parameters are summarized in Figure 3.1. Since the key engineering/design parameters were not specified in the RFP, extensive simulations were performed to determine the best package delivery system. The inputs to the simulation include vehicle specifications, number of vehicles, and time constants (e.g., time for package picking, loading, unloading, vehicle recharging, etc.). The freedom in the system design also includes features that can not be simply

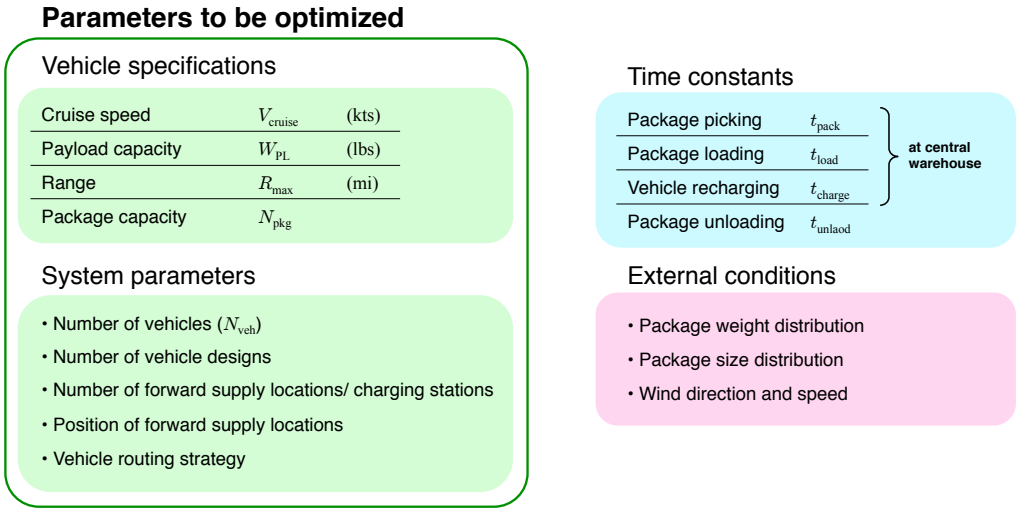

FIGURE 3.1: List of parameters

parametrized by numbers (e.g., use of forward supply locations). The effect of those parameters were explored to make design decisions. The design decisions considered in this chapter are:

1. Number of different vehicle designs
2. Use of forward supply locations
3. Use of charging stations
4. Vehicle specifications

The simulation shows how the packages are requested and transported during the day, and it can be used to compute the success rate (i.e., the fraction of packages delivered within 90 min or 2 hours after the request). Once a threshold for the desired success rate is specified, the simulation can be used to obtain the minimum number of vehicles required to achieve that success. The number of vehicles is then used to estimate $N_{\text{pkg/veh/day}}$(number of packages delivered per vehicle per day) and the vehicle acquisition cost. Other outputs of the simulation include distance traveled and consumed energy, which affect the operational cost and CO_2 emissions.

It is shown, in the following sections, that the most effective choice is to design only one type of vehicle that has sufficiently long range and large cargo space to perform multiple package delivery.

3.2 Package Transport Methods

Covering a 50 x 50 mile area while carrying possible payloads of up to 20 lb is a challenging task for small-size UAVs. In order to achieve this task while maximizing the MoEs, the architecture of the overall package transport method as well as the vehicle specifications were considered. The questions to be answered in this section are

- Does designing more than one vehicle improve the MoEs?
- Does having other operating locations improve the MoEs?

The vehicle specifications, including cruise speed, payload capacity, and the capability of carrying multiple packages, affect the performance of the system as shown in Section 3.3. Since the requirements on the vehicle specifications and delivery architecture are interrelated, vehicle specifications were kept as variables, and the use of two or more vehicle types and/or the use of forward supply locations were considered. Depending on the use of different vehicle types and forward supply locations, a vehicle routing strategy (see foldout-Routing Strategy) was developed for each case in order to get the best performance for each option.

At the same time, the vehicle specifications were narrowed down so it fits the best for the operation required by the candidate delivery architecture. The sizing of the vehicle was also considered in the process. In this way, the optimization of the vehicle specifications and the overall package transport architecture (system of systems) was an iterative process between many different subsystems, such as rotor design, power system, vehicle performance and sizing.

The following notations are used in this section: vehicle cruise speed (V_{cruise}), vehicle package capacity ($N_{\text{pkg,max}}$), vehicle payload capacity (W_{PL}), vehicle production cost per empty weight (X), and number of packages delivered per vehicle per day ($N_{\text{pkg/veh/day}}$).

3.2.1 Multiple Vehicle Designs

One of the most important decisions to be made is the number of different vehicle designs. An observation of the package weight distribution specified in the RFP is that most (around 85%) of the packages weigh less than 5 lbs. Using a large vehicle capable of carrying 20 lbs payload (covering 99% of all the packages) to deliver such light-weight packages may not be efficient since the operating payload fraction becomes smaller. Therefore, using vehicles with different payload capacities for different package weights could be more efficient than using just one type of vehicle. However, designing multiple vehicles requires much higher development costs. Studies of the costs and benefits relating to multiple vehicle designs are discussed in the following sections.

Vehicle Types

The list of possible approaches to utilize different vehicle designs are the following:

v1. Use a single large (20lb-payload) vehicle

v2. Use a small vehicle with payload capacity (W_{PL}) to carry light packages and a large vehicle to carry heavy packages.

v3. Use a small vehicle with payload capacity (W_{PL}) to carry light packages and use multiple of small vehicles cooperatively to carry heavy packages.

v4. Use fast and slow vehicles for delivery to far and close locations.

v5. Use long-range and short-range vehicles for delivery to far and close locations.

v6. Use a large vehicle to carry and deploy small vehicles.

v7. Use a ground vehicle to carry and deploy small vehicles.

It is shown in the following chapter that the development cost has a significant impact on the overall cost, and therefore, using more than two vehicle designs is not cost efficient. This point is shown by the comparison between the options v1 to v3 which is shown in the following chapter. The result (disadvantage of multiple vehicle design) applies for the options v4 to v7.

The trade study was performed for W_{PL}=10, 5, and 3 lbs. The vehicle cruise speed (V_{cruise}) and package capacity ($N_{\text{pkg,max}}$) were also varied to see how those parameters affect the performance in each case.

In the case where there are more than one vehicle designs with possibly overlapping tasks, the combination of the number of vehicles are determined based on the estimated acquisition cost. The combination is determined based on the estimates on the vehicle production cost and $N_{\text{pkg/veh/day}}$. It is assumed in this analysis that the production cost of a single vehicle is approximately proportional to its empty weight. The unknown unit cost is treated as a variable X \$/lb. The estimates on the empty weight of the vehicles were obtained by the preliminary sizing (see Chapter 3 for details).

Trade Study: Low Cost vs. High $N_{\text{pkg/veh/day}}$

The total acquisition cost (development cost + production cost) and the $N_{\text{pkg/veh/day}}$ was used to compare different cases. Figure 3.2 (left) shows the total acquisition cost as a function of X

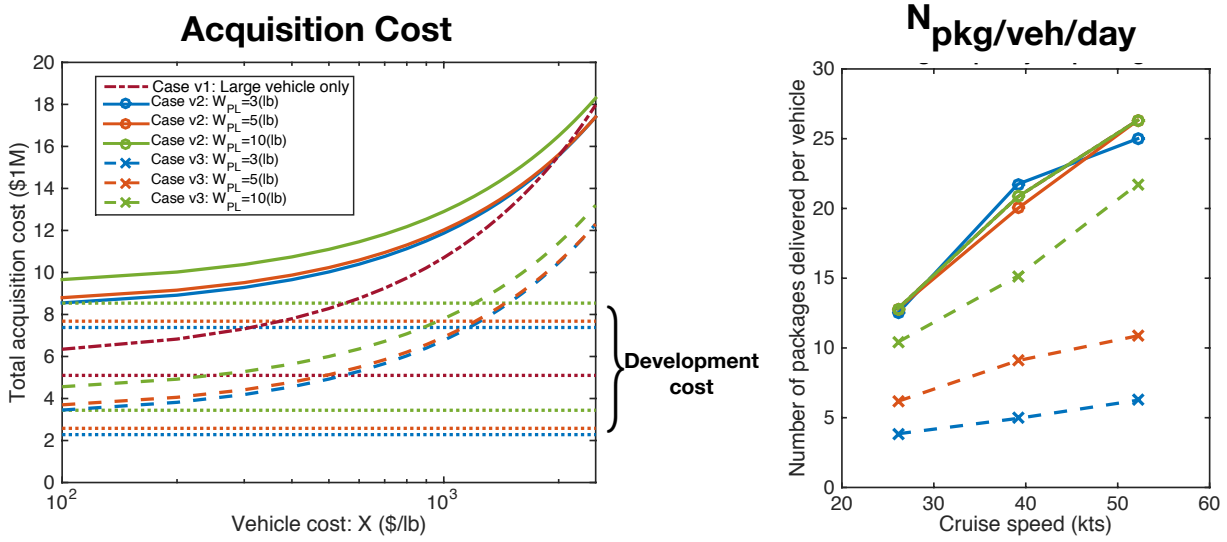

FIGURE 3.2: Comparison between multiple vehicle design options

\$/lb. It shows that for a reasonable vehicle production cost (up to around X=1,000 \$/lb), the development cost is the dominant factor in the acquisition cost, which makes Case v3 the most cost effective choice. Figure 3.2 (right) shows how $N_{\text{pkg/veh/day}}$ changes with different cases and vehicle specifications. In terms of the $N_{\text{pkg/veh/day}}$, Case v3 is detrimental because of a larger number of vehicles. From the cases and parameters considered, Case v3 with 10-lb payload vehicle has a good compromise between the acquisition cost and the $N_{\text{pkg/veh/day}}$.

Conclusion: The vehicle development cost becomes a dominant factor if there are multiple vehicle designs, especially when there are larger vehicles. This is why approaches v4 to v7 are not suitable for a cost effective operation. This disadvantage of large vehicle design lead the design of *AirEZ* vehicle towards smaller and lighter one. Another result is the conflict between low cost and high $N_{\text{pkg/veh/day}}$, i.e., low cost is achieved by a small vehicle design, but small vehicles cannot delivery many packages. Therefore, multiple aspects including $N_{\text{pkg/veh/day}}$, cost,

customer experience/safety, and size were comprehensively considered to decide on Case v3 with payload W_{PL}=5 lb.

3.2.2 Forward Supply Locations

The range is another important requirement for the delivery vehicles since they have to cover such a large geographical area. Longer range vehicles require more power and, as a result, end up being larger and heavier, both attributes that were not desired. One way to alleviate the range requirement is to have forward supply locations (FSLs) that would serve as waypoints for package requests beyond a certain radius from the central warehouse. In this section, the studies done on the use of FSLs as well as the rationale behind the decision to not using any FSLs are presented.

Type of Forward Supply Location

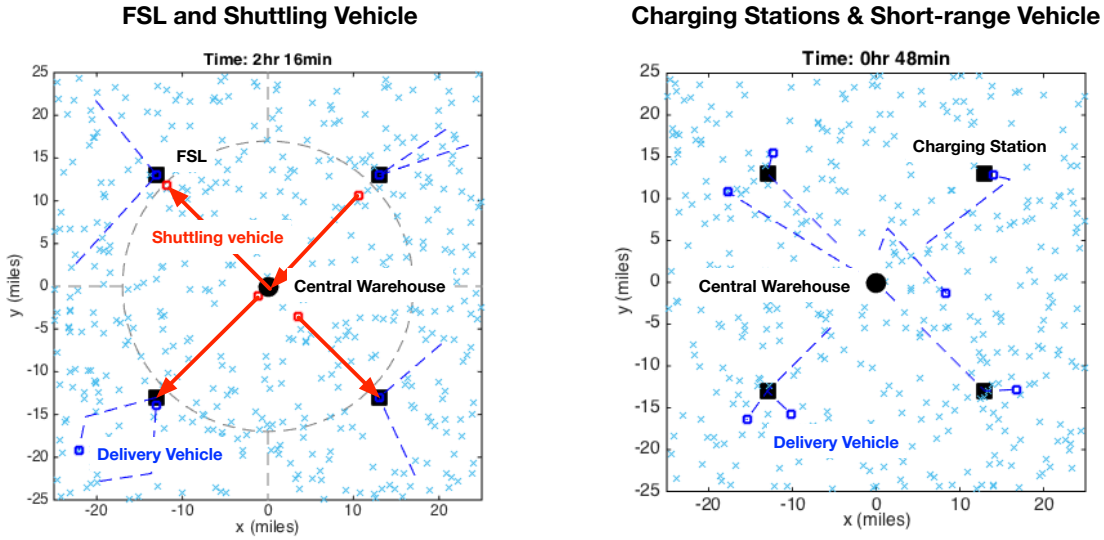

FIGURE 3.3: Snapshot of simulations with forward supply locations

The following options were considered:

f1. Use a long range vehicle that can cover the entire area; no FSL is used.

f2. Use shuttling vehicles to carry packages to the FSL and use delivery vehicles to deliver packages from FSL to customers.

f3. Use the FSLs as charging (or refueling) stations. The vehicles stop by at the charging stations depending on the assigned customer locations.

Different routing strategies were developed for each of the three cases to effectively use FSLs and different types of vehicles. For Case f2, the simulation showed that there is no significant effect on the performance other than the alleviation on the range requirement. However, this approach requires two vehicle designs, driving up the development cost. In addition, the packages have to be transferred from the shuttling vehicle to the delivery vehicle at the FSL, and this adds

time loss in the overall delivery process. For these reasons, Case f2 was abandoned. Case f3 is advantageous in terms of the smaller development cost. In addition, if the vehicle uses electric propulsion, the exhausted battery can be replaced with a fully charged one at the FSL, which should be a shorter process than smaller than transferring the package from the shuttling vehicle to the delivery vehicle as is required in Case f2. For these reasons, Case f3 was considered the only reasonable option for the use of FSLs. The overall decision of whether or not to use FSLs is considered in the next section.

For a valid comparison, the location of the charging station was optimized to obtained the best performance for the case with the charging station. (Details omitted for page constraints.)

Trade Study: Long Range vs. Charging Stations

Since the use of FSLs has an impact on the operational cost, the estimation on the acquisition costs and operational costs were used to compared Case f1 and f3. With the optimal positioning of the charging stations, simulation was used to estimate required number of vehicles, consumed energy, and the number of vehicles being recharged at the charging station at each instant in time.

To estimate the bounds on the cost to operate charging stations, land area and the number of operators for each station were bounded as 1,000-5,000 ft^2 and 1 to 5 operators, which was based on the instantaneous number of vehicles being recharged at the station: mean=6, maximum=17.

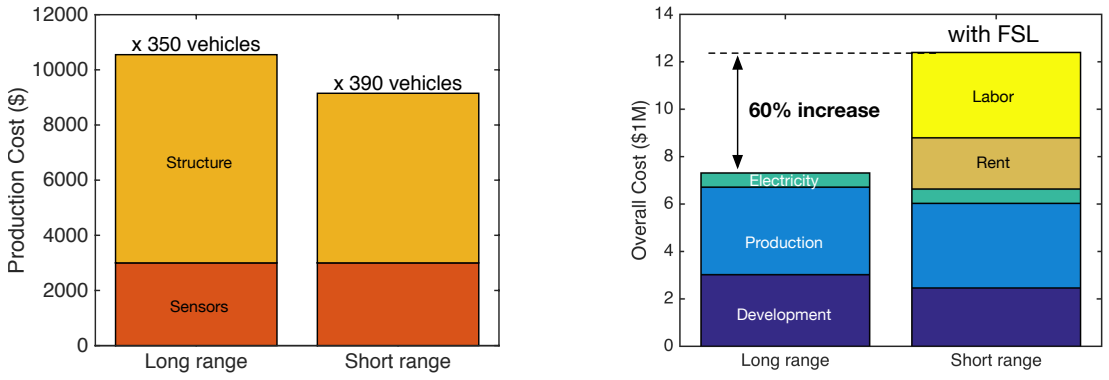

FIGURE 3.4: Cost comparison between long-range vehicle and short-range vehicle with charging station.

Figure 3.4 shows the estimated vehicle production cost, and the total cost for the two cases. The total cost for acquisition and operation was calculated for three years of operation (as specified in the RFP). The results showed that even with the mildest assumptions on the operational cost for the charging station (1,000 ft^2 area and 1 operator), the rental cost and labor cost were greater than the benefit from designing a vehicle with shorter range.

Conclusion: The benefits of using short-range vehicle (less acquisition cost and less electricity) were smaller than the disadvantage from operating charging stations. Another expected benefit of short-range vehicle was the size, however, the size reduction was less than 5%. For these reasons, the long-range vehicle with no FSLs was selected as the design choice.

3.3 Effect of Vehicle Specifications

Simulations were also conducted to find the vehicle specifications that are suited for the tasks. In this section, the effect of vehicle specifications to the performance of delivery is shown by the simulation results.

3.3.1 Effect of Multiple Package Delivery

One of the specifications that was considered using simulation was the possibility that each vehicle could carry more than one package. Figure 3.5 shows the effect of the limits on the package capacity (assumption A3 in Section 3.1.1). It can be seen that allowing vehicles to carry multiple packages has a significant impact on the number of vehicles required.

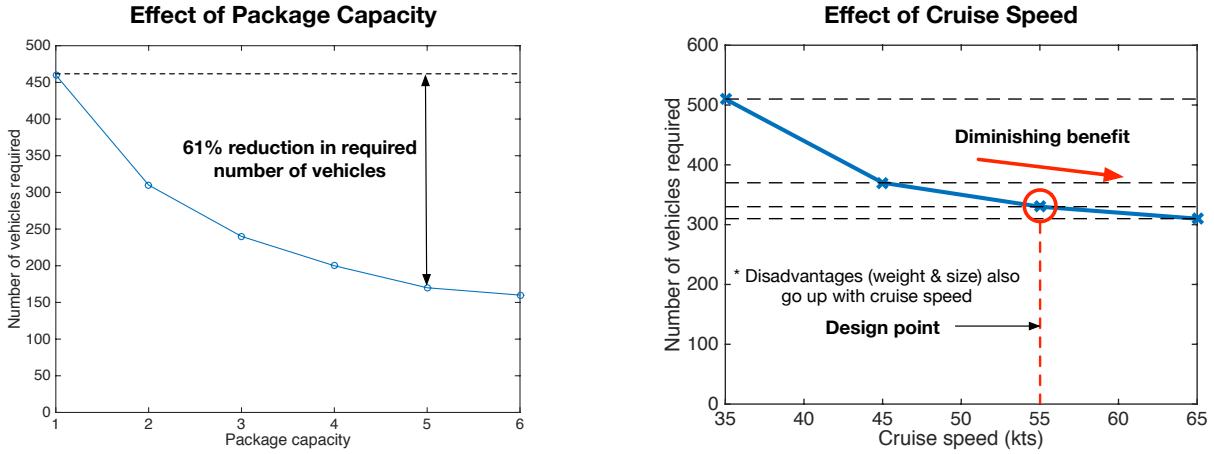

FIGURE 3.5: Effect of package capacity on number of vehicles necessary

The main reason for this effect is because combined with an efficient routing strategy, multiple package delivery decreases the total traveled distance. While it is desirable to maximize the number of delivered packages per trip, there are mainly three constraints on this capability: (1) Payload capacity, (2) Cargo space, and (3)Cruise speed. First two (payload capacity and cargo space) constrain how many packages can be loaded on the vehicle. The third (cruise speed) constrains how many customer locations vehicle can travel within the 2 hours limit. Typically, one of these three specifications acts as a "bottleneck" and determines how many package can be delivered in a single trip. Hence, the amount of benefit gained by improving one aspect is highly dependent on other two aspects. For example, if the multi-package capability is mainly constrained by the payload capacity, then increasing the cargo space does not significantly help the vehicle to carry more packages. Instead, only the adverse effect from larger fuselage drag will increase.

Therefore, it is important to have these three specifications to be balanced since every specification has an adverse effect on either vehicle size or weight. If they are not balanced well, the adverse effect can increase more than the benefit.

3.3.2 Effect of Cruise Speed

Increasing the cruise speed will not only decrease the time to travel the same distance, but also has the potential of decreasing the total traveled distance by allowing multiple package

delivery. However, as mentioned in the previous section, finding the right balance between payload capacity, cargo space, and vehicle speed is important. In this section, the effect of cruise speed is explored, and then the value that is suited for the payload capacity (5-lb) and the 12 x 12 x 16 (in) cargo space discussed in Chapter 12 is found.

It shows that the benefit from higher cruise speed starts diminishing after 55 kts. From this result and the limitation on the vehicle size and weight (see Section 6), the value 55 kts was chosen as the baseline. Also, how much the vehicle capabilities are fully utilized was studied by analyzing the histogram of the carried payload, carried number of package, and traveled distance. The study showed that the package size capacity is the "bottleneck" for the multiple package delievery.

Conclusion: The benefit from increasing the cruise speed starts to diminish after 55kts. Moreover, the constraining factor for the multiple package delivery is the package size. Therefore, increasing the vehicle speed does not improve the efficiency dramatically. Instead, the weight and size penalty from those changes will be greater. Hence, the baseline cruise speed 55 kts is kept as the choice instead of increasing it further.

3.4 Package Delivery Simulation

The preceding sections discussed the construction and assumptions of the simulation as well as how it was utilized in making design decisions. The vehicle routing strategy was also developed to enable an efficient operation of the *AirEZ* vehicle. In this section, a more detailed results of the simulation are shown with the selected package transport methods, designed vehicle specifications, and optimized vehicle routing strategy.

Also, the flexibility of the *AirEZ* system to different customer requirements are shown. By modifying the parameters used in the simulation and adjusting the number of vehicles, the same *AirEZ* vehicle can be used to achieve even faster package delivery.

3.4.1 Simulation Algorithm of *AirEZ* Delivery System

After the trade studies detailed in the preceding sections, the design parameters for *AirEZ* delivery system were chosen as follows:

System information		Vehicle parameters	
Vehicle design	1	Cruise speed	55 kts
Vehicles	480	Maximum range	80 mi
Forward supply location	0	Maximum payload	5 lbs
Charging station	0	Total package capacity	6

The vehicle routing strategy designed using modified Traveling Salesman Problem is detailed in foldout-Routing Strategy. The number of vehicles was selected based on the minimum number required to complete the mission (400), additional vehicles required to achieve the same success rate on a windy day (40, see foldout for details), and 10 % margin for repair and maintenance (40).

The time constants in Figure 3.1 are assumed to be $t_{\text{pick}} = 10$ min, $t_{\text{load}} = 5$ min, $t_{\text{charge}} = 5$ min, $t_{\text{unload}} = 5$ min. The simulation algorithm constructed specifically for the selected *AirEZ* delivery system is shown in the foldout-Routing Strategy. The delivery method of overweight

packages are detailed in Chapter 3.4.5. Although the *AirEZ* vehicle has the capability of slung-load to carry oversized packages, it is decided that those packages should be delivered by trucks, based on trade studies performed in Chapter 13.

3.4.2 Time History of Typical Delivery Day

The operation of *AirEZ* system is with the time history of a delivery day. The importance of using sufficient number of vehicles as well as the amount of flexibility in the system are highlighted.

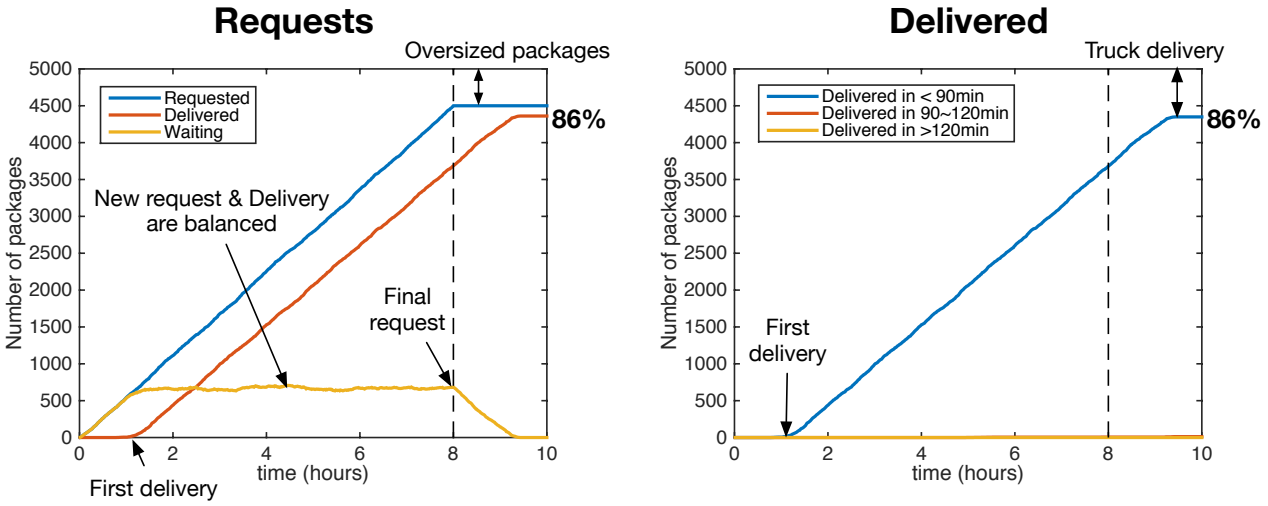

FIGURE 3.6: Time history of requests and deliveries.

Figure 3.6 shows how the number of requests, successful deliveries change over time for a typical delivery day. The first request is made at time = 0, and the last request is received at time = 8 hr (indicated as dashed line). With a sufficient number of vehicles, the number of waiting customers (yellow) converges to a constant value (500 customers) during the day, i.e., new requests and completed deliveries are balanced. The number of delivered packages does not go to 5000 at the end of the day because overweight packages (heavier than 12 lbs) and oversized packages are not delivered by the *AirEZ* vehicle. The rationale behind this is presented in Section 13. It is decided that the customer satisfaction will be maximized by limiting the size of the vehicle, instead of increasing the payload capacity to cover the overweight packages.

Number of Vehicles at Central Warehouse

In considering the required scale of the central warehouse, it is useful to know the estimated number of vehicles that are preparing for the next mission. Figure 3.7 shows how the numbers of vehicles at different stages change over time. The first request is made at time zero, and the loading (yellow) starts a few minutes later when the packages are picked up inside the central warehouse. During the day, the numbers fluctuate around constant value where most of the vehicles (around 85%) are out for delivery (red) and the rest are exchanging the batteries or loading new packages at the central warehouse. With the package-size assumption A2 (see Section 3.1.1), the number of vehicles exchanging battery at the central warehouse is around

20 in total. This number was used to estimate the number of people working at the central warehouse (see Chapter 4).

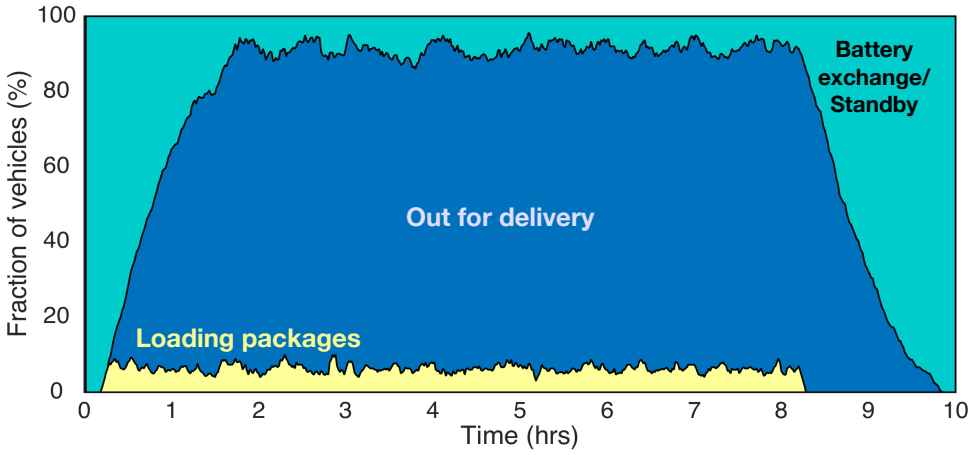

FIGURE 3.7: Fraction of vehicles at each stage.

Effective Choice of Vehicle Number

The number of vehicles was decided based on the success rate. Here, the importance of selecting the right amount of vehicle is discussed by considering the case where all the possible deliveries are completed in 90 minutes, and the case where some packages are delivered between 90 minutes and 2 hours. Different guarantees on the delivery time are achieved by changing the parameters in the routing strategy (see foldout-Routing Strategy). Simulation results of the two options are listed below:

Guaranteed delivery time	90 min	120 min
Success rate (delivery within 90 min)	86 %	46 %
Number of vehicle required	480	390
Cost per delivery	\$9.0	\$8.6

Since 90 % improvement in success rate is achieved by 5 % increase in the cost, the system that guarantees 90 minutes delivery is chosen.

3.4.3 Final Results and Extension

The MoEs specified by the RFP are summarized in this section. In addition, how the *AirEZ* vehicle can be used to achieve different customer requirements is discussed. By relaxing the delivery time window, the system can be acquired and operated with lower cost. On the other hand, delivery within 60 minutes can be achieved by increasing the number of vehicles.

The values specified by the RFP are shown in the following table: Changing the parameter (allowed customer waiting time) in the routing strategy and having different number of vehicles, the *AirEZ* system can achieve different guaranteed delivery time. Three cases including the 2 hour time limit specified by the RFP are shown in the following table.

Package size assumption	(A1)	(A2)	(A3)
Delivery in 90 min (%)	86	86	86
Delivery in 2 hours (%)	86	86	86
Number of vehicles required	540	480	300
Number of packages / vehicle	8	11	18
Delivery cost ($)	9.32	9.03	8.18
CO_2 emission per delivery mile (lb/mile)	0.096	0.067	0.054

Guaranteed delivery time	4 hours	2 hours	90 min	1 hour
Number of vehicles required	300	350	480	550
Delivery cost ($)	8.08	8.41	9.03	9.37

Conclusion: The high cruise speed of the *AirEZ* vehicle can be exploited (if required) to guarantee a delivery time of one hour, which is the half of the delivery time as required by the RFP.

3.4.4 Effect of Time constants and External conditions

In this section, the effect of parameters that were assumed in the simulations are varied to see the sensitivity of the *AirEZ* delivery system to those parameters. The pickup time of the packages at the central warehouse is one of the time constants that were assumed. Figure 3.8 shows how the pickup time affects the required number of vehicles. The effect is small when the package

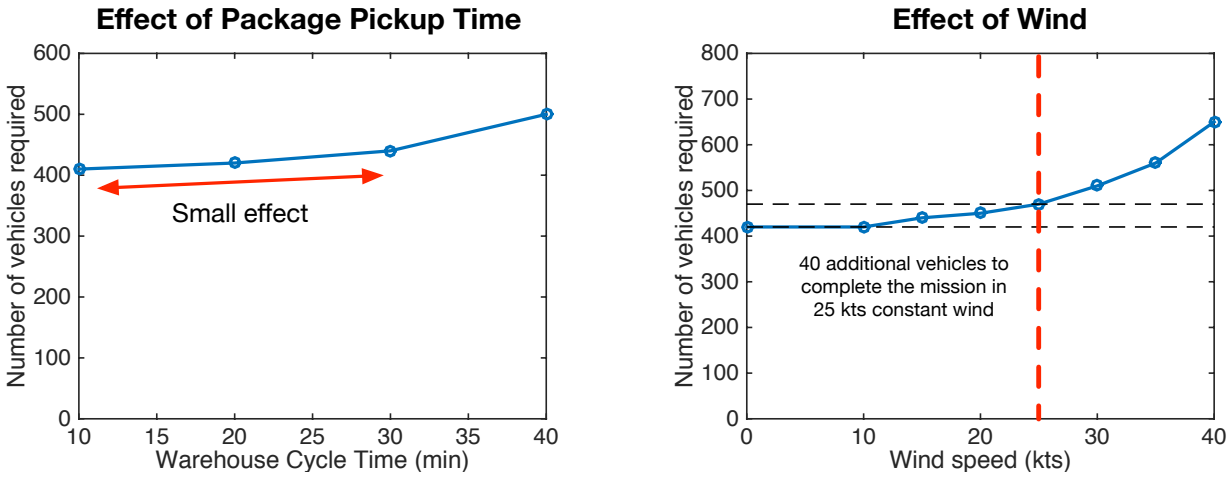

FIGURE 3.8: Effect of time package pickup time and external wind.

pickup time is less than 30 minutes.

The consideration on the effect of wind is shown in the foldout-Routing Strategy. The result shown in Figure 3.8 describes the effect of wind where the vehicles maintain 55 kts airspeed (ground speed depends on the direction of wind). Hence, the vehicles do not have to use excess power to compensate for the headwind (25 kts) if the system has additional 40 vehicles available.

Conclusion: By adjusting the number of vehicles, the *AirEZ* delivery system can complete its mission on windy condition, or in the case where package pickup time is longer.

3.4.5 Heavier Payloads

As detailed in the package weight breakdown specified by the RFP, approximately 15% of packages weigh more than the design payload of 5 lbs. In order to account for delivery of these packages, additional considerations were made in the vehicle routing strategy.

Figure 13.3(a) in Section 13 shows how the maximum range of the *AirEZ* vehicle is affected by the payload weight. Maximum range is found as a result of forcing the vehicle speed to be the designated speed for best range (V_{BR}). The vehicle power curve illustrated in Fig. 13.2 from Chapter13 shows V_{BR} to be 32.1 kts.

When carrying a 5 lb payload and operating at speed for V_{BR}, the vehicle is capable of flying 165 miles with 20 minutes of reserve battery life due to substantial power savings. As battery weight is sacrificed, range is reduced and maximum payload is increased. Figure 13.3(a) shows that the maximum vehicle payload is 12.85 lbs, which represents over 95% of all package weights. To make use of this maximum payload weight and subsequently increase the number of successful deliveries, this slower cruising speed is utilized.

When operating at V_{BR} the *AirEZ* vehicle is capable of delivering a 12 lb package within a radius of 29 miles from the central warehouse, while reserving 20 minutes of battery power. As this payload weight decreases, the *AirEZ* vehicle approaches its design maximum range value of 80 miles. This occurs at a payload weight of 11.0 lbs. Therefore, to deliver packages between 11.0 lbs and 12.0 lbs, a constraint is set on the package delivery that allows for only one package per trip and enforces a cruising speed of V_{BR}. Once packages are dropped, the vehicle is able to return to the warehouse at the design cruise speed, 55 kts. As the payload weight decreases towards the design weight of 5 lbs, the one package constraint remains fixed, however, allowable cruising speed is increased with decreasing package weight. At payloads of 5 lbs and below, the design cruise speed of 55 kts is utilized once again and multiple package trips are allowed. These design considerations allow for substantial increase in successful payload deliveries.

4 Cost Analysis

The life cycle costs of the *AirEZ* system are calculated based on an operating life of 300 days per year for 3 years as specified by the RFP. The *AirEZ* fleet consists of 480 vehicles with 400 active on a typical day. The life cycle cost of the *AirEZ* vehicle can be broken down into the following components; (i) development cost, (ii) acquisition cost, (iii) operating cost, and (iv) end of life cost. Operating cost can be further divided into direct and indirect costs. Direct operating costs account for unit-level maintenance, operations manpower, operating energy and repair parts, whereas indirect operating costs account for program management, information systems, general training and education.

The following costs and ground rules are specified in the RFP; 1. Development cost of $200,000/lb of vehicle empty weight, 2. Electricity cost of $0.18kW-hr, 3. Repair labor and vehicle operators/monitors cost of $100/hr, and 4. An operating life of 300 days per year for 3 years.

4.1 Development Cost

The RFP projects the development cost as $200,000/lb of vehicle empty weight, resulting in a development cost of $**4.13million**

Motors	\$396 x4 [a]
Rotor blades	\$111 x8 [b]
Rotor hubs	\$309 x4
Wings, fuselage, and landing Gear	\$2,058
Sense-and-Avoid Electronics and Communications	\$3,306
HUMS	\$3,306
2.04 kW-hr Batteries	\$449 x4 [c]
Acquisition cost per vehicle	**\$14,170**
Total acquisition cost for the fleet	**\$4.82million**

[a] Based on T-MOTORs U10 efficiency motor
[b] Based on T-MOTORS 30 in. diameter carbon fiber propeller
[c] Based on Li-Ion battery cost from Tesla's GigaFactory

TABLE 4.1: Vehicle acquisition cost.

Monitoring Station	\$2,000 x5
Higher bandwidth information systems	\$5,000
Loading Bay modifications for *AirEZ* vehicles	\$10,000 x14
Software costs	\$10,000
Total acquisition cost (Warehouse + fleet)	**\$6.77million**

TABLE 4.2: Warehouse acquisition costs.

4.2 Acquisition Cost

Acquisition costs for the motor and propeller were estimated based on similar components available off-the-shelf models, i.e., T-MOTOR's U10 Efficiency motor and T-MOTOR's 30" diameter carbon fiber propeller. The sense-and-avoid electronics suite is based entirely on off-the-shelf components currently available. The lithium-sulfur batteries are assumed to have the same production cost as lithium-ion batteries as produced by Tesla's Gigafactory (\$220/kW-hr) and each vehicle wears through about 4 batteries over 900 operating days. The rotor hubs are estimated to cost 50% of the combined blade and motor weight for a single rotor. The wings, fuselage, and landing gear are estimated assuming the combined cost is \$100 per lb of empty weight of the vehicle. The HUMS is assumed to be equal to the cost of the sense-and-avoid system.

The cost breakdown per vehicle and the acquisition costs for the warehouse are outlined in Tables 4.1 and 4.2.

4.3 Operating Cost

The RFP gives the cost of electricity as \$0.18/kW-hr and the cost of repair labor and operators/monitors as \$100/hr. Repair part cost is estimated at %15 of the total acquisition cost. Maintenance labor cost is estimated based on 80 man-hours of maintenance work per day (routine inspection and repair work). This relatively low amount of maintenance work is made possible by the dedication to a low maintenance design of every component and the HUMS system increasing the time between necessary inspections. There are 50 man-hours of work monitoring the HUMS information each day to respond to any emergencies. Based on the number of vehicles needing

Electricity	\$0.59 million
Repair Parts	\$1.01 million
Maintenance Labor	\$7.20 million
Battery Switching Labor	\$2.52 million
HUMS Monitoring Labor	\$4.5 million
Indirect operation costs	\$6.33 million [a]
Total operating costs	**\$22.17million**

[a] Assumed to be 40% of direct operating costs

TABLE 4.3: Total operating costs.

simultaneous battery swapping in the simulation, there are 140 man-hours of work dedicated to switching the batteries. Since switching the battery is an unskilled job, these employees would only need to be paid \$20/hr.

The cost breakdown of direct operating costs over 3 years is outlined in Table 4.3.

4.4 End of Life Cost

End of Life cost is dependent on recyclability of materials. The battery, motors, and aluminum joints can be recycled, while the composite parts cannot. We assumed a 28% net end of life cost for the vehicle resulting in a total end of life cost of **\$1.90million**

4.5 Total Life Cycle Cost

The total life cycle cost is the sum of the previously mentioned four costs, which is **\$34.96million**.

With the *AirEZ* system successfully delivering 86% of the requests, this amounts to 4,300 package deliveries per day and a cost per package delivered of \$9.03. This low value is possible by our dedication to a highly automated, low maintenance, and energy efficient design. This is very competitive with FedEx's same day delivery service cost of \$18.45 for a 12x12x16 in. 5 lb. package [1]. Assuming 400 vehicles fly for 10 hours every operating day, this leads to a cost per flight hour of \$9.71. With a fleet of 480 vehicles per warehouse, the acquisition cost per vehicle is \$14,104.

The development cost can be amortized over total vehicle fleet across all warehouses. Assuming a pilot program of one warehouse for each of the 10 most populous cities, a total fleet of 4800 vehicles would be needed. This amounts to the development costing \$860 per vehicle.

Cost Summary:

- Cost per vehicle (including development) - \$14,963
- Cost per flight hour - \$9.71
- Cost per package delivered - \$9.03
- Total Cost of *AirEZ* system for 3 years - **\$34.96 million**

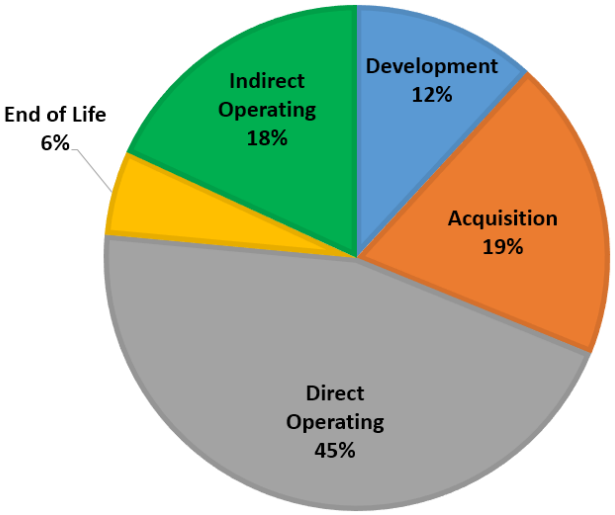

FIGURE 4.1: Three year Life Cycle Cost Breakdown

Part II - Aerial Vehicle Design

5 Vehicle Configuration Selection

5.1 Mission Requirements and Design Drivers

The RFP requires that a complete system of systems (SoS) be designed for aerial delivery of cargo to customers from a central node in a logistics company. Specifically, within an 8-hour window, 5000 requests will be made for delivery within two hours. These requests will be uniformly distributed throughout a delivery region measuring 50 mi x 50 mi.

Although the overall mission for the system is clearly specified in the RFP, the general requirements for the aerial vehicle are left to the designers' discretion. As a result, the design criteria appeared to be very open-ended, with options for multiple vehicle designs and inclusion of addition forward supply locations in the logistics infrastructure. The open-ended nature of the system design made the use of simulations essential for pinpointing specific vehicle and system requirements as well as determining the influence of the overall system configuration towards mission success. Details of these simulations and their impacts on the *AirEZ* system and vehicle design are discussed in detail in Chapter 3 and are referenced as needed in the following sections. The key results and observations from the simulations are: (i) Successfully completing each of the 5,000 delivery requests in the specified 2-hour time limit requires hundreds of vehicles. Figure 5.1 is a snapshot of a simulation showing the number of vehicles in flight at a given instant in time; (ii) The number of vehicles required to complete an entire of deliveries is highly dependent on vehicle speed; and (iii) For a given payload capacity, the ability to carry multiple packages per delivery reduces the number of vehicles needed.

In addition to these observations, the RFP also specifies five measures of effectiveness for the system of systems design:

- **MoE 1:** System acquisition and yearly operating costs

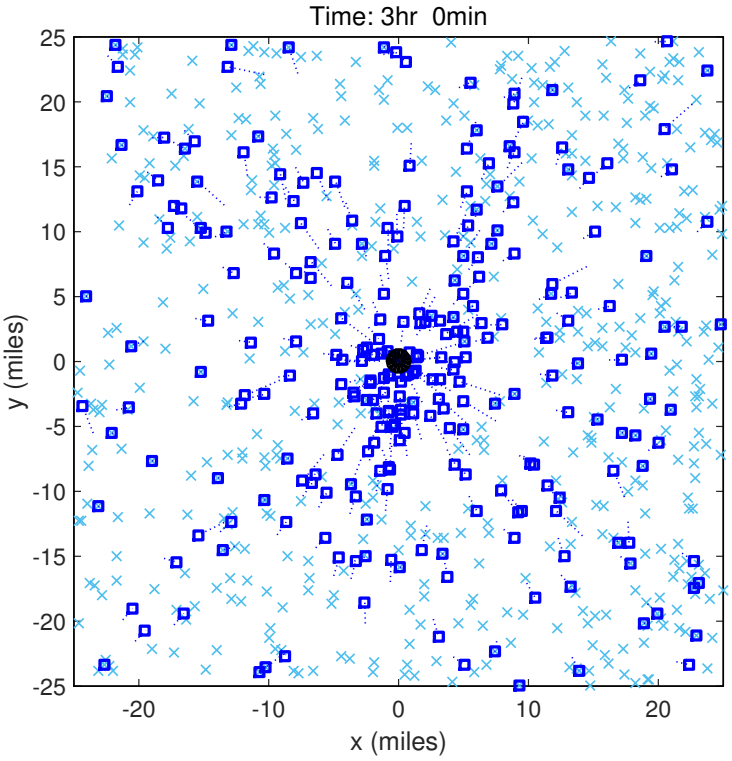

FIGURE 5.1: Snapshot of system mission. Customers that are awaiting delivery are indicated by the (x) while the blue squares represent vehicles that are out for delivery.

- **MoE 2:** Number of packages delivered per vehicle per day
- **MoE 3:** Number of events where the time between customer's request for a package and actual delivery exceeds 90 minutes
- **MoE 4:** Pounds of CO_2 emitted per delivery mile flown
- **MoE 5:** Percentage of delivery missions successfully completed

5.1.1 Selection Criteria

As a result of the initial simulation results, twelve criteria were identified for judging configurations during the preliminary selection process. These were:

1. **Ground Safety -** The vehicle will be spending much of its operating time in the presence or in the vicinity of warehouse personnel or delivery customers. It is of paramount importance that the vehicle be safe while operating close to the ground. While vehicles with multiple rotors might appear at a glance to be inherently less safe than a single rotor vehicle, distributing the lift over multiple rotors allows each rotor to be much smaller than a single main rotor (SMR), decreasing the rotor kinetic energy and consequently, the potential for injury.
2. **Operational Safety -** As stated previously, hundreds of vehicles will be flying on a given day, so it is desired that the vehicle operate autonomously to alleviate the need for hundreds of human pilots/controllers. Therefore, it is imperative that the vehicle be safe in flight (e.g., the vehicle should be able to land safely in the event of a power failure). Multiple

rotors, specifically four or more, provide multiple redundancies, increasing the likelihood that the vehicle can depend on these redundant systems and always operate and land in a safe manner.

3. **Payload Fraction -** As the primary purpose of this vehicle is to carry cargo, it is important that the vehicle have a high payload fraction, defined as the ratio of the payload weight to the gross take-off weight (GTOW). For a given payload, a higher payload fraction will result in a lower GTOW, which, in turn implies lesser power will be required during flight.
4. **Speed -** Since the RFP requires each package to be delivered within 2 hours, vehicle speed is obviously important. Compound configurations with lift and/or thrust augmentation through the use of wings and propellers generally have higher maximum speeds compared to traditional vehicle configurations such as SMR, coaxial, or tandem helicopters; which are plagued by limitations such as retreading blade stall and compressibility effects on the advancing side.
5. **Maintenance -** The RFP specifies a cost of $100 per hour for any vehicle repair labor needed. As a result, a vehicle that will be easy to maintain will be important in keeping the yearly operating costs as low as possible. This criteria favors a simple design with a minimal number of moving parts and easy access to the vehicle components.
6. **Ground Footprint -** The number of vehicles needed for a task of this magnitude as well as the urban environment specified in the RFP made it clear that the physical size of the vehicle on the ground was going to be very important. At every stage of the delivery process (warehouse, forward supply stations, delivery point) space will be limited. Therefore, it is necessary that the vehicle be as compact as possible.
7. **Hover Efficiency -** Although the vehicle will be spending the majority of its operating time in cruising flight, it still essential that it is able to hover efficiently.
8. **Forward Flight Efficiency -** Based on the initial simulation results discussed in Chapter 3, the delivery vehicle will need to be able to fly efficiently at speeds around 55 knots, which requires to a need for a high lift to drag ratio. This criterion favors configurations with some form of lift augmentation, like a wing, over conventional rotor configurations.
9. **Gust Tolerance -** The vehicle will be operating autonomously in urban canyons in which wind gusts are unavoidable. Therefore it is important that the vehicle is able to maintain stable flight in gusty environments.
10. **Maneuverability -** The inherent unpredictability of an urban delivery region demands that the chosen vehicle have the ability to quickly stop or change direction to avoid trees, buildings, other vehicles, and people or animals, as well as the ability to adapt to other unforeseen scenarios.
11. **Technological Risk -** Though a UAV delivery system does not yet exist, many companies are working to be the first to build such systems. Using completely unproven technologies is likely to delay implementation. Therefore the design of the vehicle must have a minimum TRL of 3.
12. **Acoustic Signature -** The vehicle will be operating primarily in residential areas, and so will need to be relatively quiet, particularly when hovering during delivery.
13. **Package Integration -** Since the vehicle is operating for the sole purpose of delivering packages, the ability to integrate the package into the vehicle is also a major consideration.

Such a design would protect the package from the elements and will result in a vehicle with predictable handling characteristics.

5.2 Analytical Hierarchy Process

Once the general selection criteria were established, the rankings of each design parameter were obtained by comparing their relative importance using an Analytical Hierarchical Process (AHP). The relative importance of each criterion as determined by the team is illustrated in Figure 5.2. As shown, the factors that most directly impact the vehicle's ability to deliver packages quickly, safely, and efficiently were weighted very highly. This is due to the fact that these three criteria help ensure a small, safe, and more user-friendly delivery vehicle. Other aspects such as low maintenance and low energy requirements help to lower cost which, while extremely important, was rated lower thansafety.

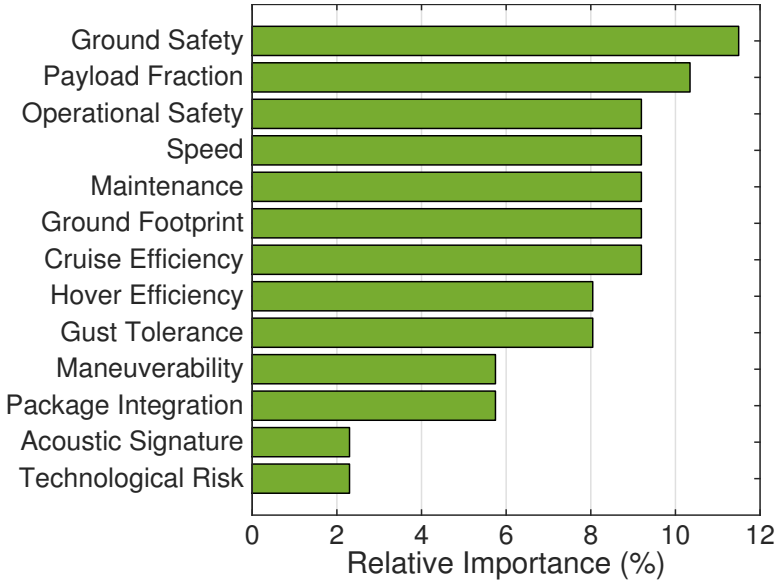

FIGURE 5.2: Relative ranking of vehicle selection criteria

5.3 Possible Configurations

A large number of configurations were considered in the initial design process of the *AirEZ* vehicle. These included conventional vehicles including fixed wing, single main rotor, coaxial rotor, and multi-rotor as well as novel designs such as tiltduct, tiltrotor, fan-in-wing, stoppable rotor, vectored thrust, compound helicopter, tailsitter, and ducted fan. Representative vehicles for these configurations are shown in Fig. 5.3. Although a hovering requirement was not explicitly mentioned in the RFP, precise delivery and navigation in a confined urban environment was deemed to be impractical without such a capability. Therefore, a pure fixed wing design was not considered. The VTOL configurations that were considered are discussed below:

5.3.1 Single Main Rotor Helicopters

The first configuration to be considered was a conventional single main rotor (SMR) with tail rotor. SMR helicopters are typically very efficient in hover, low empty weight fraction, and generally low maintenance. However, the high kinetic energy of the large single rotor poses

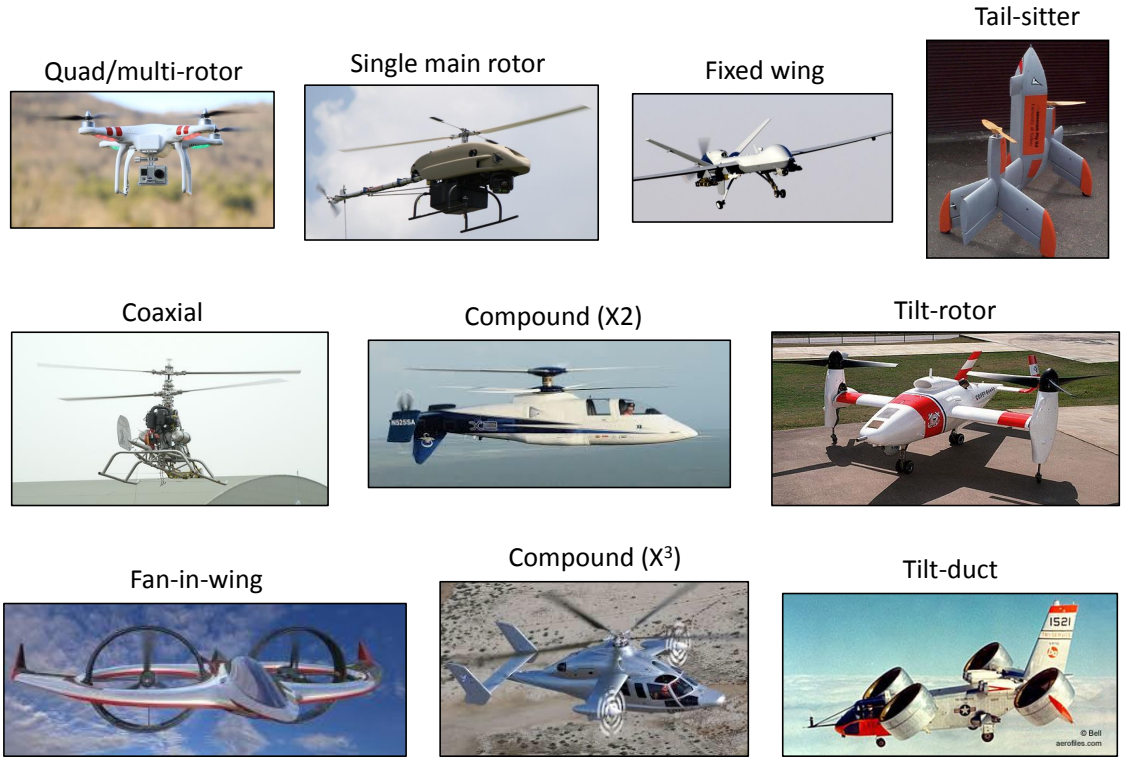

FIGURE 5.3: Representative images of vehicle configurations considered

greater risk of injury to personnel on the ground. In addition, the necessity of a tail rotor further increases the overall footprint of the vehicle. Furthermore, a SMR configuration has limited speed and range capabilities when compared to other configurations. For these reasons, the SMR was not deemed a suitable option for the *AirEZ* vehicle.

5.3.2 Twin Rotor Helicopters

Twin rotor configurations include tandem and coaxial helicopters, where two rotors are placed either one in front of the other or one on top of the other, respectively. The tandem configuration is typically used for heavy cargo missions, due to its low disk loading and high range of allowable center of gravity (c.g.) travel. However, tandem helicopters suffer from low forward flight efficiency as a result of the increased drag from two rotor hubs. Additionally, the multiple rotors would require increased maintenance because of complex hub designs. As a result, tandem and coaxial helicopter designs were not selected as the final design option for the *AirEZ* vehicle.

5.3.3 Compound Helicopters

Compound helicopters, such as the X2 and X^3 models shown in Fig. 5.3 are higher speed alternatives compared to conventional single and dual-rotor helicopter configurations. The presence of lift and/or thrust augmentation helps offload the rotor, which alleviates the constraints of conventional helicopter designs allowing for increased efficiency in forward flight. However, compound helicopters suffer form a reduced payload fraction, which is a consequence of the increased complexity required for the augmentation systems. Furthermore, these propulsion systems lead to increased weight and also a drastic increase in moving parts resulting in an increase in maintenance required. Therefore, an alternative to compound helicopters was sought in order to meet

mission requirements.

5.3.4 Convertible Helicopters

Convertible rotor vehicles, such as tilt-wing and tilt-rotor concepts were considered. These convertible designs offer the advantages of being able to take off and land vertically like a conventional helicopter, and then transition into forward flight like an airplane. In this regard, convertible configurations offer the high speed and long range desired for meeting the requirements of the RFP. However, the mechanical complexity required to tilt the rotors and/or wings in these designs result in much heavier vehicles and higher maintenance costs with overall increased system complexity. As a result, tilt-rotor or tilt-wing concepts were not considered favorably for meeting the mission goals.

5.3.5 Unconventional Designs

Less conventional designs, including fan-in-wing, flying duct, and tilt-duct configurations are more novel and unique approaches to the delivery mission. Unfortunately, these vehicles suffer from high mechanical complexity and bring an undesirable level of technological risk owing to their relatively low TRLs. These vehicles also lack efficiency in both hover and forward flight. As a result, these unconventional configurations were discounted from the vehicle selection process.

5.3.6 Multiple Rotor Helicopters

Multi-rotor configurations, e.g. quadrotors or octorotors, offer numerous advantages over the configurations usually considered for a full-scale vehicle. First, multiple rotors offer inherent redundancy leading to improved operational safety. The loss of one rotor and/or motor is not necessarily a debilitating handicap for these vehicles. Additionally, small-scale multi-rotor vehicles typically utilize electric motors and variable RPM for vehicle control, thus eliminating the need for a heavy, complicated transmission.

Although a pure multi-rotor configuration suffers from poor forward flight efficiency and low high-speed capability, its superiority to other configurations in terms of maintenance, safety, and maneuverability. Furthermore, the ability to augment the vehicle with additional lifting surfaces thus overcoming the low vehicle L/D made a multi-rotor design the best choice for the *AirEZ* vehicle.

5.4 Pugh Decision Matrix

An initial Pugh Decision Matrix was constructed using the selection criteria and comparing the possible configurations listed in the previous section. A standard single main rotor (SMR) was used as the baseline configuration. For each of the selection criteria, every configuration compared to the SMR and was rated on a scale of -3 to 3 to indicate the extent to which the configuration is better or worse than the SMR. These ratings were then scaled by the selection criteria scores and totaled to give a single score for each configuration. A spider plot with the results of this initial Pugh Matrix is shown in Figure 5.1. This figure shows each vehicle configuration's relative scoring magnitude for each design criterion.

The results of the initial Pugh Matrix, indicated that the vehicle must have multiple rotors. However, the need to explore the merits of different multi-rotor configurations was evident, and so a second Pugh Matrix was constructed. For this Pugh Matrix, the field of multi-rotors was

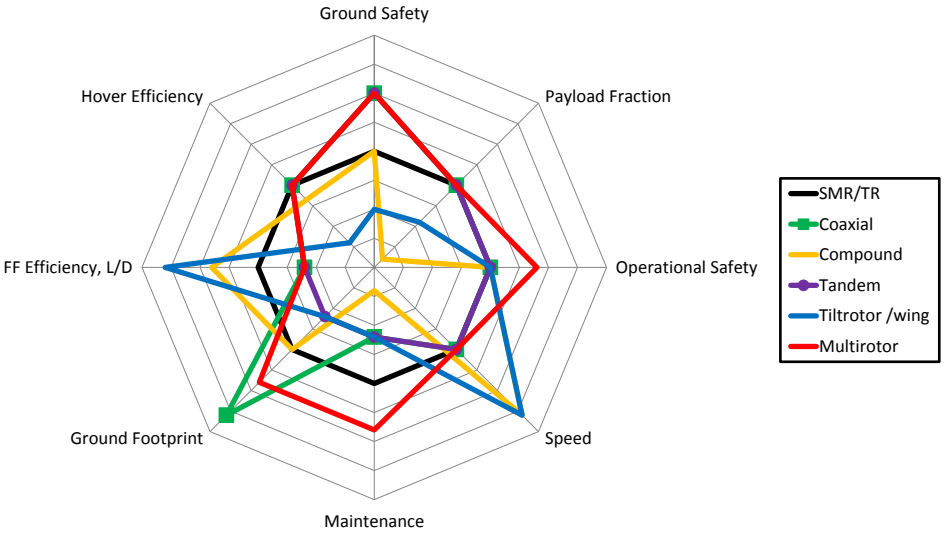

TABLE 5.1: Spider plot showing results of initial Pugh Decision Matrix

expanded to include an octorotor, quadrotor biplane, quad tilt-wing and tilting fan-in-wing. The quadrotor was selected as the baseline and the configurations were scored as before. This final Pugh Decision Matrix is shown in tabular form in Fig. 5.4. As a result of this process, the quadrotor and quadrotor biplane configurations came out as the best candidates for the *AirEZ* vehicle. At this point, some more quantitative comparisons were carried out to decide between these two narrowed-down configurations. Figure 5.5 shows a comparison of the power needed for both vehicles with a 5 lb payload. Forward flight speed was varied and representative values for fuselage drag, wing L/D were assumed. The augmented quadrotor-biplane vehicle is capable of reaching far greater maximum speeds (87 kts) as compared to a conventional quadrotor (55 kts) because of its ability to offload the rotor to the wings. From this analysis it was clear that the quad-rotor biplane would best fulfill the requirements of the RFP. This concept was designed, built, and tested successfully at $1/5^{\text{th}}$ model scale at the University of Maryland and has demonstrated hover, transition to forward flight, and transition back to hover (Figure 5.6).

5.5 The *AirEZ* Vehicle

The *AirEZ* vehicle is a novel quadrotor, tailsitter, biplane configuration. The vehicle features four rotors which are arranged and operated in the standard counter-rotating quadrotor convention. This integrated concept allows for maneuverability in hover and edge-wise flight typical of multi-rotor vehicles. Additionally, the rotors on the *AirEZ* vehicle are attached to two low aspect ratio wings which carry the vehicle in forward flight thus enabling the rotor to function as effective propellers. This ability to separate out the thrust and lift devices leads to a substantial increase in power savings and efficient forward flight compared to a conventional multi-rotor configuration. An extensive performance characterization of the *AirEZ* vehicle is detailed in Chapter 13.

All the forces and moments necessary for vehicle maneuvering and control are supplied by the rotors and consequently the vehicle requires no additional active control surfaces, ensuring a simple and lightweight design. With regard to transition maneuvers, the vehicle transitions between

	Weight	Quadrotor	Octorotor	Quad biplane	Quad biplane w/ telescoping wing	Multirotor biplane	Tilting Fan-in-wing	Quad tilt-wing	Flying duct
Ground Safety	10	0	0	0	0	0	1	1	2
Payload Fraction	9	0	0	-1	-2	-1	-2	-2	-1
Operational Safety	8	0	1	1	0	1	1	1	-1
Speed	8	0	0	1	2	1	1	1	1
Maintenance	8	0	-1	1	0	0	-1	-2	0
Ground Footprint	8	0	-1	0	0	0	-1	-1	1
L/D	8	0	0	2	3	2	1	2	1
Hover Efficiency	7	0	0	-1	-1	-1	-1	-1	0
Gust Tolerance	7	0	0	-1	-1	-1	-1	-2	-2
Maneuverability	5	0	1	-1	-1	0	-1	-1	-2
Package Integration	5	0	1	-1	-1	-1	1	1	-2
Acoustic Signature	2	0	1	0	0	1	1	2	1
Technological Risk	2	0	0	-1	-2	-1	-2	-2	-1
		0	**4**	**5**	**-6**	**4**	**-16**	**-21**	**-7**

FIGURE 5.4: Pugh Decision Matrix

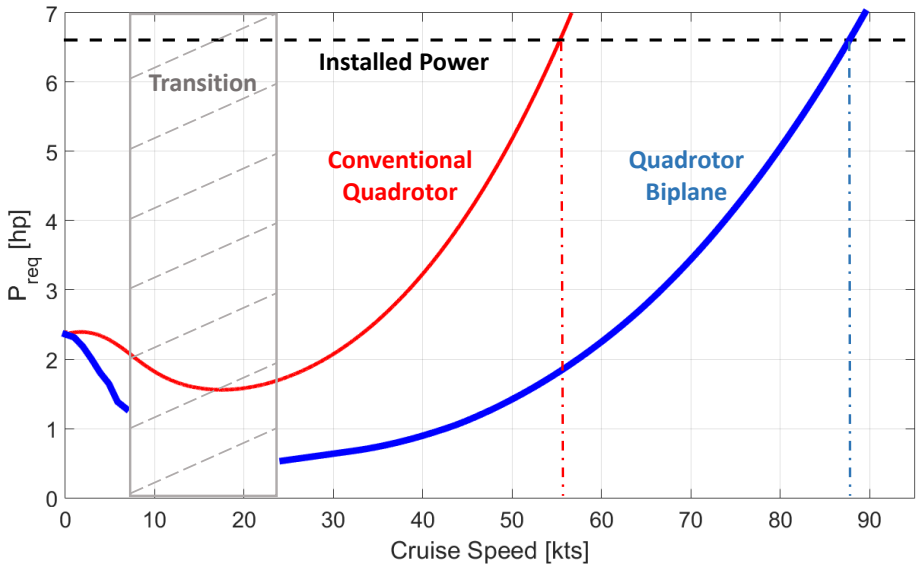

FIGURE 5.5: Power curve for quadrotor in edgewise flight and quadrotor biplane

hover and forward flight configurations via differential rotor thrust generated by RPM and pitch control. This mechanism allows for a smooth vehicle transition where forces and moments are in equilibrium throughout all stages. When compared to conventional tailsitter designs (which uses a stall-tumble transition), *AirEZ* boasts a simpler and safer method than conventional tailsitter for transition.

The *AirEZ* vehicle also allows for simple package integration. The space in between the wings and rotors, which already houses the electronics and battery, can be easily used to store packages. On the *AirEZ* vehicle, this payload bay is integrated into a streamlined fuselage which completely houses the parcel and necessary delivery mechanisms. The tailsitter configuration of the quadrotor biplane also provides easy access to the central payload bay when the vehicle is

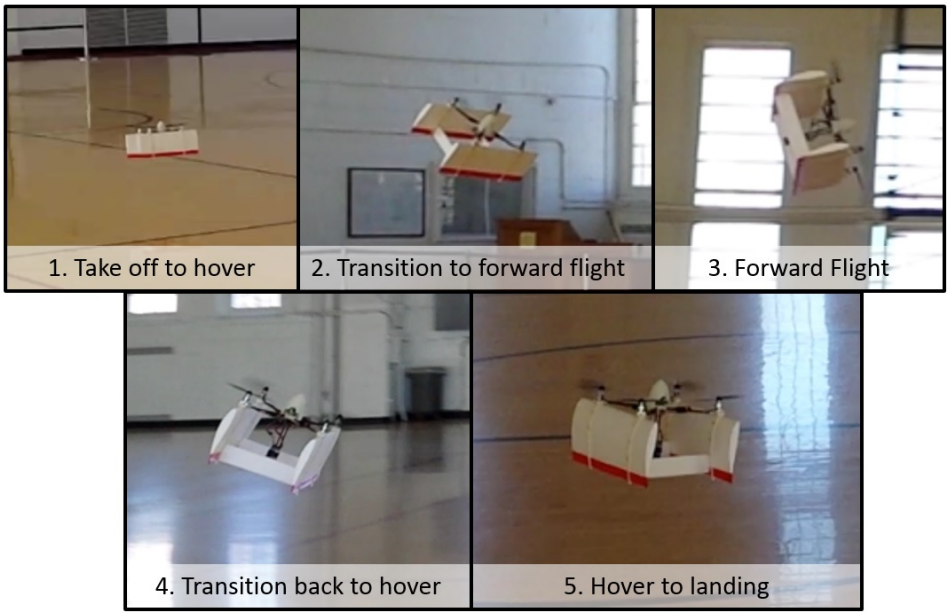

FIGURE 5.6: UMD demonstrator of quadrotor biplane concept (https://www.youtube.com/watch?v=p4jwYW_LV6M)

on the ground. This makes the action of parcel drop-off more simple and does not expose the package to drops from dangerous heights.

In summary, the *AirEZ* vehicle is a unique and efficient aerial vehicle capable of high-speed, long-range parcel delivery.

The *AirEZ-Micro* Vehicle: Proof of Concept

A 1/5th Mach scale model of the *AirEZ* vehicle was **designed**, **constructed**, and **flight tested**; the ***AirEZ Micro***. Stable hover, transition, and high α flights were achieved as shown below.

Vehicle specifications:
- **Weight: 0.67 lbs**
- **Width: 1.36 ft**
- **Length: 1.31 ft**

High $c_{l\,max}$ airfoils for low stall speed

Streamlined vehicle struts

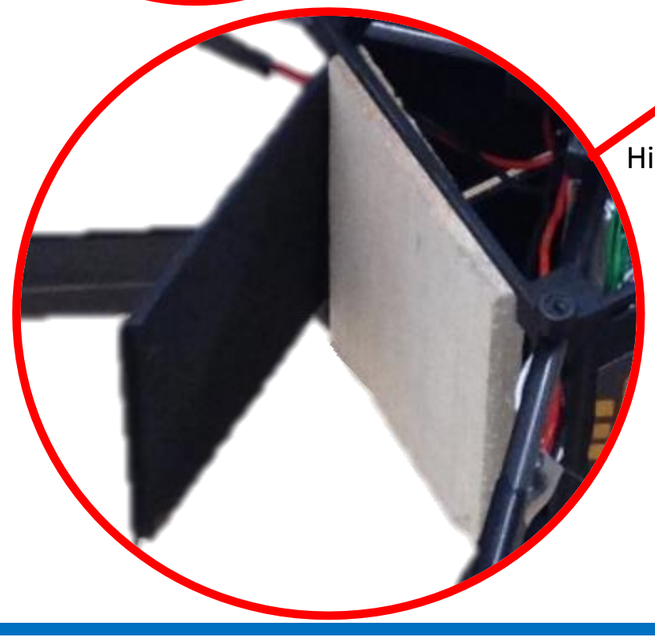

Hinging bay door for payload integration

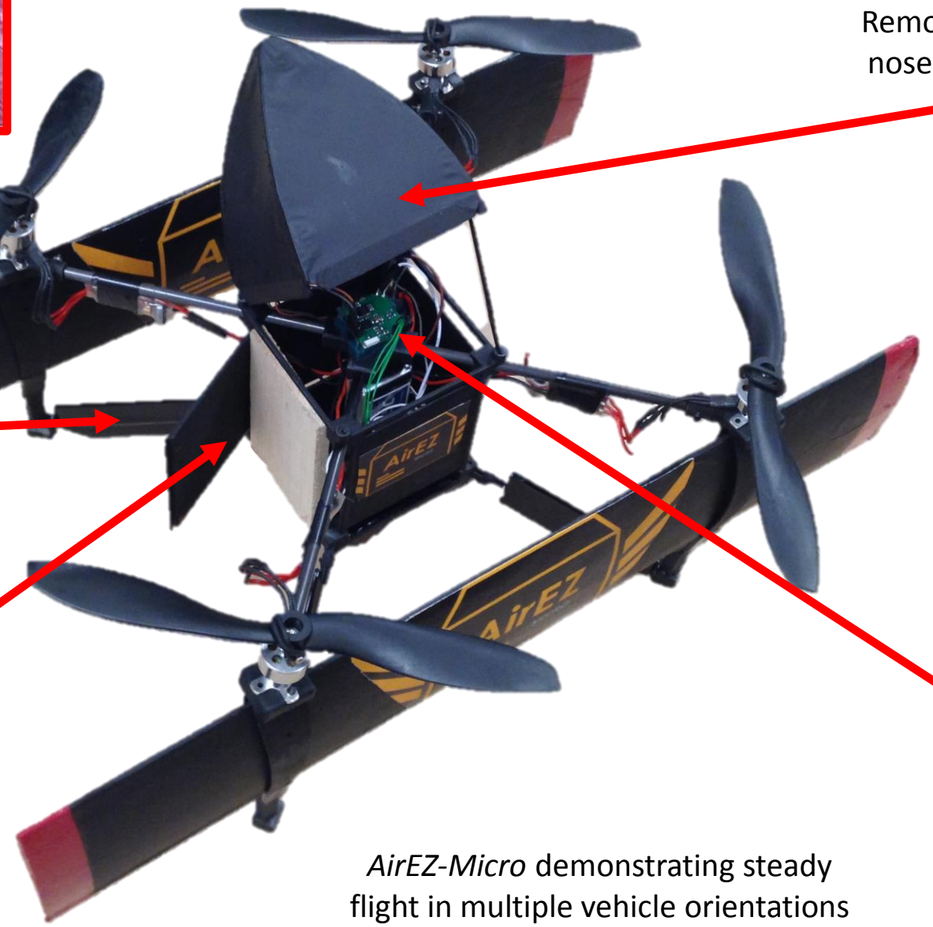

Removable nose cone

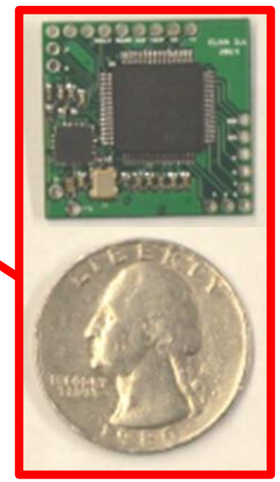

ELKA-R Board (Developed in-house)
- Microprocessor: Cortex-M4
- IMU: MPU-9150
- 2.4 GHz wireless transceiver
- Loop rate: 1000 Hz
- Mass: 1.7 g
- Thickness: 1 mm

AirEZ-Micro demonstrating steady flight in multiple vehicle orientations

6 Preliminary Vehicle Sizing

The *AirEZ* vehicle is designed to be a high-speed, long-range hybrid quadrotor with substantially lower power requirements compared to other multi-rotor vehicles of its size. Once the quadrotor biplane vehicle configuration had been settled upon, an initial vehicle sizing based on the methodology of Tishchenko [2] was conducted. The in-house sizing code was modified to include the capability to perform analyses for multiple fuel sources (including batteries and fuel cells), as well as drive systems. Estimates of vehicle empty weight, motor size, disk area, rotor solidity, tip speed, energy consumed during delivery missions, and other vehicle characteristics were determined as a result of the preliminary sizing. Physics based optimization was then performed to select vehicle aspects such as number of blades, main rotor tip speed, blade loading, and type of fuel source used on the *AirEZ* vehicle. Each parameter has an effect on the overall sizing and, therefore, trade studies were conducted to examine the benefits of varying these vehicle parameters.

Based on mission analyses, the design drivers were: (1) The vehicle must have suitable performance in hover, (2) Travel quickly and efficiently in forward flight, (3) Carry a sizeable payload, and (4) Have a reasonably small footprint while delivering packages on the ground. Some of the key parameters that were taken into account when sizing the *AirEZ* vehicle included gross takeoff weight (GTOW), power and energy required, stall margins, and cost.

6.1 Sizing Mission

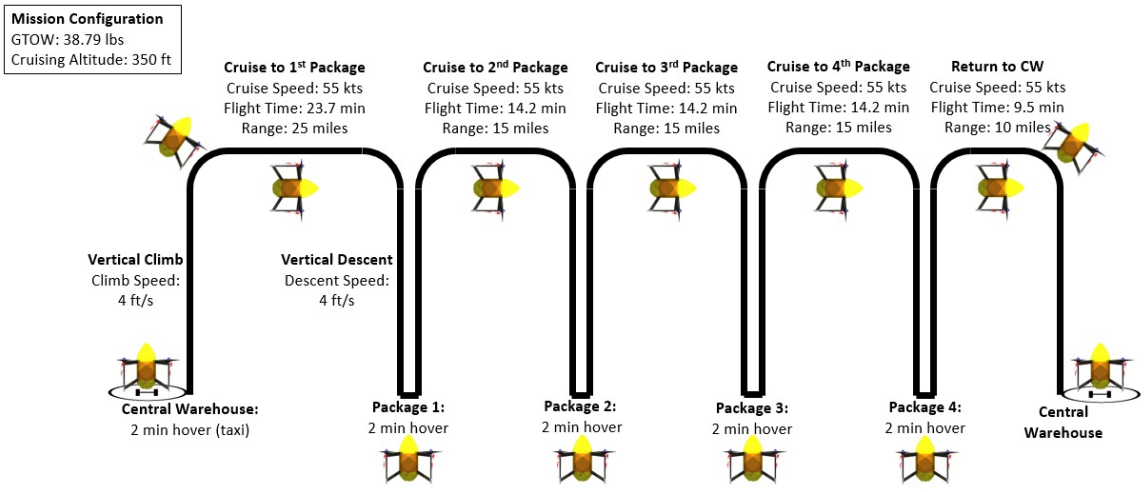

FIGURE 6.1: Mission profile detailing a 4 package delivery

To properly conduct the sizing process, special care was taken to ensure that the correct sizing mission was designed and selected. The goal of the study was to determine the sized vehicle capable of handling a worst-case delivery scenario. Multiple mission profiles were generated based on a varying number of package delivered per trip. Each package delivery involves a vertical takeoff, transition to forward flight, cruise segment, transition back to hover, and a vertical landing. This procedure is repeated for multiple packages. As theoretically there is no upper limit on the design packages per trip, simulations were conducted to determine useful package numbers. From these simulations, it was found that 1 and 2 package trips are very typical, 3

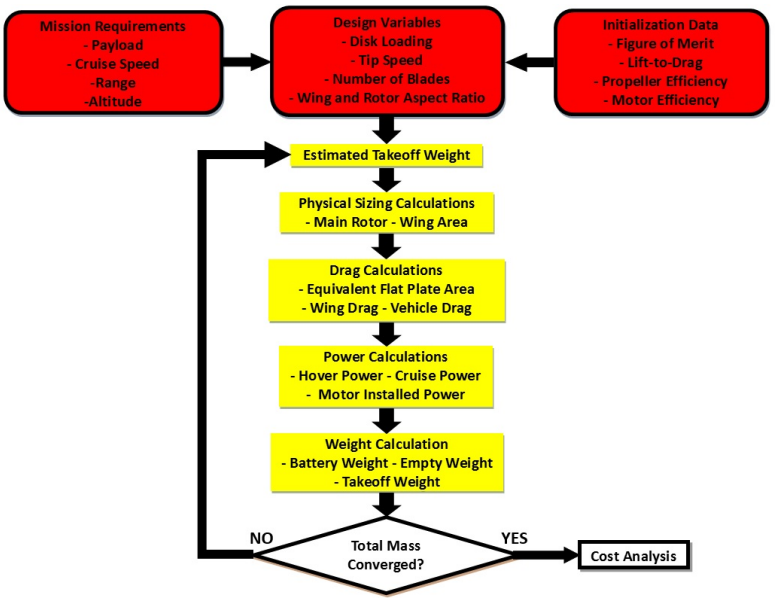

FIGURE 6.2: Block diagram of sizing methodology.

package trips occur less often, and 4 package trips are flown very rarely. Trips delivering package numbers great than 4 almost never occur. As a result, mission profiles representing 1 to 4 package trips were created. Additional simulations were performed to determine which number of packages, and therefore the resulting mission profile, would require the largest battery life and hence largest vehicle. As a result of these studies, it was found that a 4 package mission profile required the heaviest vehicle and was therefore deemed the sizing mission. This mission profile can be seen in Fig. 6.1 and was used in all subsequent vehicle sizing calculations.

6.2 Description of Sizing Procedure

The sizing method takes in several user-defined inputs and then provides the gross takeoff weight of the helicopter as an output. To generate results for the *AirEZ* compound vehicle configuration, the sizing methodology was modified to include the effects of adding wings and multiple proprotors. The equations for fuselage weight and propeller weight were based on in-house completed surveys of small scale uninhabited aerial vehicle weight breakdowns. A flowchart of the sizing algorithm used for the quadrotor biplane is shown in Fig. 6.2.

This procedure contains the following steps:

1. The mission flight profile and all initial vehicle data are user based inputs. Mission data includes flight ceiling, payload weight, number of packages delivered, cruise speed, and vertical ascent and descent speeds. Initial vehicle data includes the performance characteristics of the wing and proprotors.
2. Obtain initial estimate for takeoff weight based on a desirable payload weight fraction.
3. Rotor disk size calculated from takeoff weight, maximum rotor thrust, and disk loading.
4. Wing surface area calculated from takeoff weight, attainable wing $C_{l_{\max}}$, and design load factor.
5. An initial approximation is made for the equivalent parasitic drag area of both the vehicle fuselage and the proprotor hubs.

6. Vehicle drag at the desired cruise and maneuver speeds is calculated, which is the sum of the parasitic drag of the fuselage and hubs, wing profile and induced drag. Interference drag is calculated and added to the total drag force of the *AirEZ* vehicle.
7. The power required is calculated for hover, cruise, and all climb and descent phases, with and without headwind interference. From these measurements, the highest power requirement determines the installed power of the vehicle's motors.
8. The battery weight is estimated based on the energy requirements of the entire mission.
9. Vehicle structure and rotor weights based on survey data for modern small-scale UAVs.
10. Takeoff weight is calculated from the vehicle's empty weight as well as the weights of the batteries and payload. If the weight has converged according to the criteria of less than a 0.01% change in takeoff weight between successive iterations, then the procedure ends and the gross takeoff weight is output. If not, then a new iteration begins with a more appropriate guess for takeoff weight.

Later in the design process, higher fidelity and detailed analyses were conducted to determine wing characteristics, proprotor characteristics (see Chapter 9), parasitic drag area (see Chapter 13), and installed power (see Chapters 15 and 8). These values were used in conjunction with the sizing methodology to obtain improved vehicle weight and size estimates.

6.3 Design Considerations

As the *AirEZ* vehicle is a novel and revolutionary design, comparisons to preexisting aircraft were carried out to better understand the design and operational envelope. The class of fixed wing aircraft which operates most closely to the regime of the *AirEZ* vehicle is the ultralight aircraft class. These vehicles weigh less than 254 lbs, typically operate only during the day, and cannot exceed a flight speed of 55 kts. While these vehicles have an FAA regulated ceiling of 18,000 ft, these are often used as observatory aircraft and flown at altitudes below 1,000 ft, similar to the *AirEZ* limit of 500 ft. Ultralights must also have a stall speed no greater than 24 kts.

When designing the *AirEZ* vehicle, constraints were implemented based on these design criteria to help design a safer vehicle, that operates similarly to well-known aircraft. Based on existing data, a 55 kts cruise speed constraint was enforced on the *AirEZ* vehicle. While a faster vehicle cruise time leads to more timely package deliveries, it also drives up vehicle power required and size. 55 kts represents an efficient compromise between vehicle size and speed. Similarly, a 24 kts stall speed was enforced. These conditions helped to drive the size of the wings installed on the *AirEZ* vehicle, as shown in the following section.

6.4 Parametric Trade Studies

To optimize the proposed vehicle, the in-house *AirEZ* vehicle sizing algorithm was used to determine the ideal combination of proprotor diameter, number of blades, and wing aspect ratio, among other variables. Specifically, the effects of these design parameters on vehicle takeoff weight and wing span for a given tip speed and C_T/σ were taken into account. These parameters were determined using the sizing methodology described earlier while performing a more detailed analysis of the effects of the aforementioned variables. Other vehicle sizing

parameters, including strut sizing, are analyzed in Chapter 11 and are sized to bear vehicle internal loads and provide efficient load paths.

6.4.1 Wing Studies

During wing sizing, key emphasis was stressed on achieving a low span and low stall speed. This conditions helped restrict the vehicle ground footprint to within a reasonable limit and ensure a large stall margin for safety purposes. A wing which expands far beyond the tips of the installed rotor blades would increase overall vehicle size, making for an unwieldy and intimidating delivery vehicle, especially in proximity to customers. A smaller wing kept entirely within the downwash of the proprotors also has the added benefit of decreased gust sensitivity [3, 4]. Therefore, care was taken to design a wing that allows for efficient cruise performance and other desirable vehicle attributes while keeping wing tips within the tip dimensions of the rotor blades.

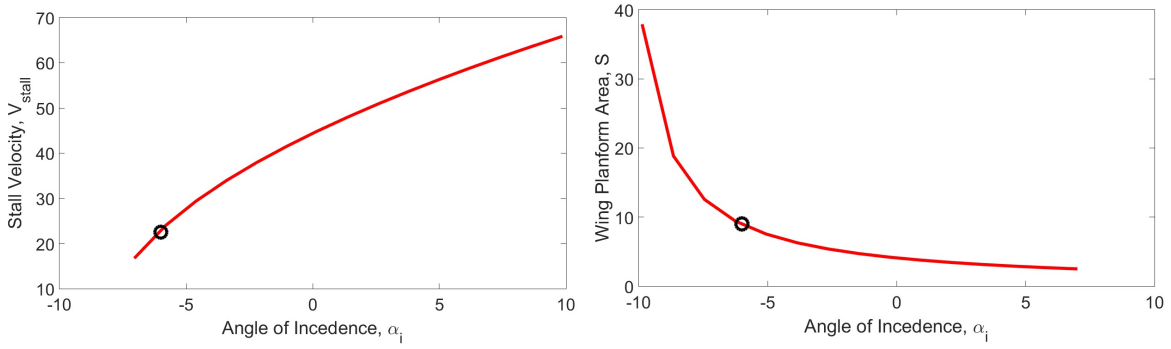

(a) Stall speed versus angle of incidence

(b) Wing planform area versus angle of incidence

FIGURE 6.3: Angle of incidence parameter sweep

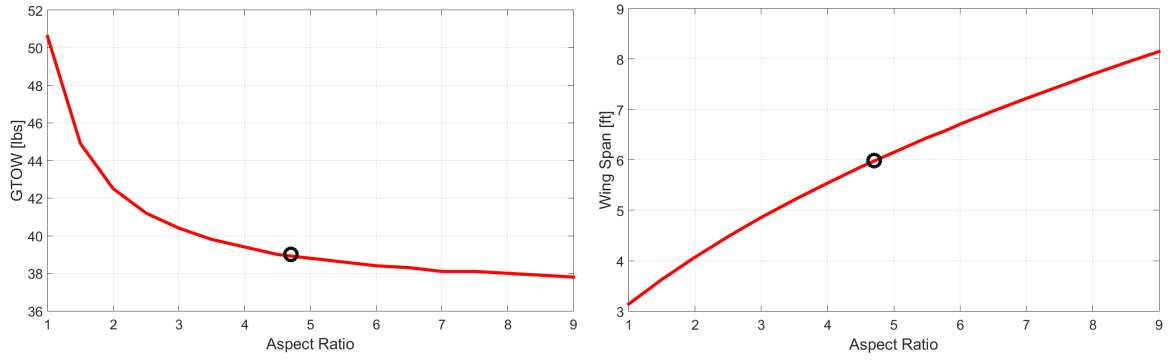

(a) GTOW versus AR

(b) Wing span versus AR

FIGURE 6.4: Aspect ratio parameter sweep

To lower wing stall speed, various angles of incidence were utilized on the wing of the aircraft. While a larger operating C_l allows for a smaller and more compact wing, it decreases the wing stall margin, enforcing a higher stall speed. Figure 6.3 shows the studies conducted on vehicle angle of incidence. An angle of incidence of -6° was selected. While this drove up the wing planform area to a value of 7.5 ft^2, constraints on span can help prevent this from increasing vehicle ground footprint. Therefore, a large stall margin on the wing was achieved with the

airfoil operating at a high wing lift to drag ratio of 14.

The vehicle's wings were sized to carry the full weight of the vehicle during its cruise velocity of 55 knots, completely offloading the proprotors. Therefore, the area of the wing is fixed while leaving the aspect ratio up to the discretion of the designer. For an efficient fixed wing vehicle in forward flight, a large aspect ratio wing is desirable, as it decreases induced drag. However, as mentioned earlier, a constraint was placed on wing span, forcing it to remain completely within the tips of adjacent rotors. Figures 6.4(a) and 6.4(b) show a trade study of wing aspect ratio with respect to vehicle weight and wing span. It can be seen that marginal weight savings are attainable at wing aspect ratios beyond 3 but that wing span increases well beyond the desired constraint length. Therefore, the vehicle wing was driven to have an aspect ratio of 4.7.

6.4.2 Rotor Studies

To arrive at the most suitable design choices for the *AirEZ* vehicle, several configurations were considered based on the variation of four critical parameters affecting the main rotor; blade loading ($BL = C_T/\sigma$), the number of rotor blades (N_b), rotor solidity (σ), and hover tip speed (V_{tip}).

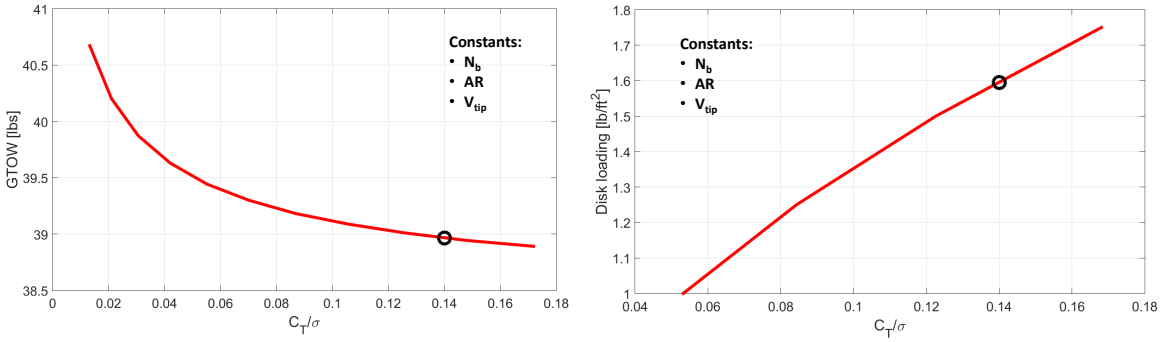

(a) GTOW versus C_T/σ

(b) Disk loading versus C_T/σ

FIGURE 6.5: C_T/σ parameter studies

In the blade loading trade studies, the most important considerations were the stall margin and high-altitude HOGE performance. As the quadrotor is not required to be highly maneuverable, some sacrifices to the stall margin levels were deemed acceptable. A blade loading of 0.14 was selected for the *AirEZ* vehicle. This blade loading satisfies both the conditions of adequate stall margin as well as high-altitude performance (see Fig. 13.1(a) in Chapter 13) which is sufficiently lower than the rotor stall limit. For a BL of 0.14, the corresponding disk loading was 1.47, as shown in Fig. 6.5(b).

Trade studies were performed to decide upon the total number of blades for the *AirEZ* vehicle. In this study, the aspect ratio, blade loading and main rotor hover tip speed were kept constant. With these constraints enforced, an increase in N_b results in an increase in rotor solidity. This increases the disk loading (DL), resulting in a reduction of the main rotor diameter. Increases in DL increase the power required by the rotors, which in turn increases motor and battery weights and consequently, the GTOW. Conversely, an increase in N_b results in a reduction of rotor diameter, which reduces vehicle ground footprint and weight per rotor blade. Therefore,

the empty weight, and hence total weight of the *AirEZ* vehicle, is a balance between DL and N_b.

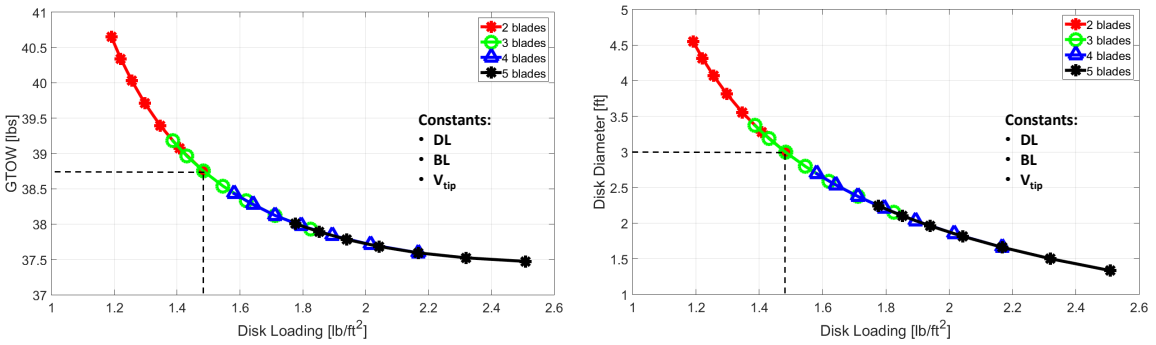

(a) GTOW versus disk loading

(b) Disk diameter versus disk loading

FIGURE 6.6: Blade number and aspect ratio parametric sweep represented as disk loading

The effect of varying rotor aspect ratio and number of blades was studied in detail to determine an optimized configuration for the desired vehicle capabilities. Figures 6.6(a) and 6.6(b) show the effects of these variables on vehicle weight, wing span, and rotor disk loading. It can be seen that as blade number is increased, both GTOW and rotor diameter decrease, which is desirable. However, as detailed in Chapter 9, a variable collective pitch system was implemented in the rotor system to significantly improve hover and forward flight performance. As a result, a low blade number would aid in design feasibility and simplicity. Figures 6.6(a) and 6.6(b) show that significant weight and size reductions can be achieved by decreasing rotor aspect ratio for a constant number of blades. As a compromise between vehicle size and rotor complexity, two low aspect ratio ($AR = 7.69$) blades were selected.

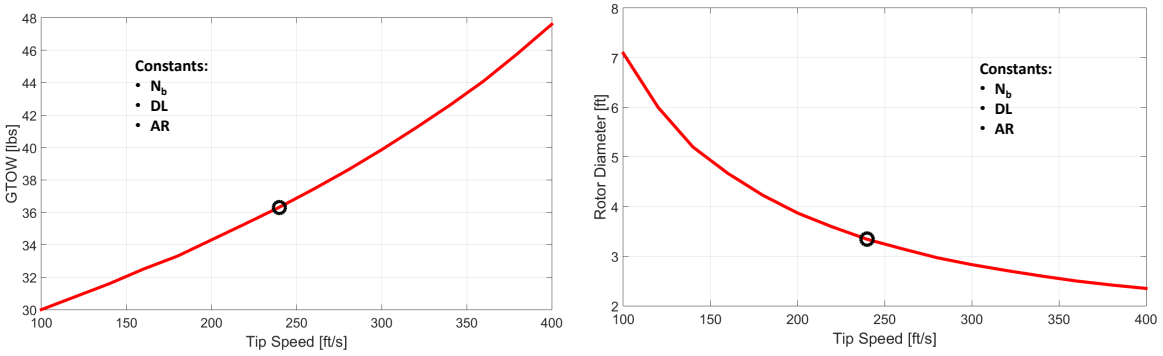

(a) GTOW versus rotor tip speed

(b) Disk diameter versus rotor tip speed

FIGURE 6.7: Tip speed parametric sweep represented as disk loading

Finally, in an attempt to further drive down vehicle power required, total weight, and rotor diameter, parametric studies were done to choose an optimum design tip speed for the *AirEZ* vehicle. Different rotor configurations were considered for a fixed N_b (2-bladed rotor), AR (7.69), solidity (0.0745), and C_T/σ (0.14) with tip speeds varying from 100 ft/s to 400 ft/s. A reduction

in tip speed at a constant C_T/σ results in lower disk loading, which decreases the power required. Reductions in power requirements lead to reduced energy requirements and hence, lower battery weights. Figure 6.7(a) shows that GTOW decreases sharply with tip speed because of the resulting power savings. Although as shown in Fig. 6.7(b), large increases in rotor diameter occur at tip speeds below 250 ft/s. Therefore, a tip speed limit of 250 ft/s was enforced on the *AirEZ* vehicle design.

6.5 Initial Vehicle Sizing

The results of the preliminary sizing resulted in the preliminary vehicle design which can be seen below in Fig. 6.8. All future design adjustments stemmed from this initial design. As the design process progressed, the *AirEZ* vehicle changed drastically, resulting in a small-scale, high-speed quadrotor biplane, capable of multiple package delivery.

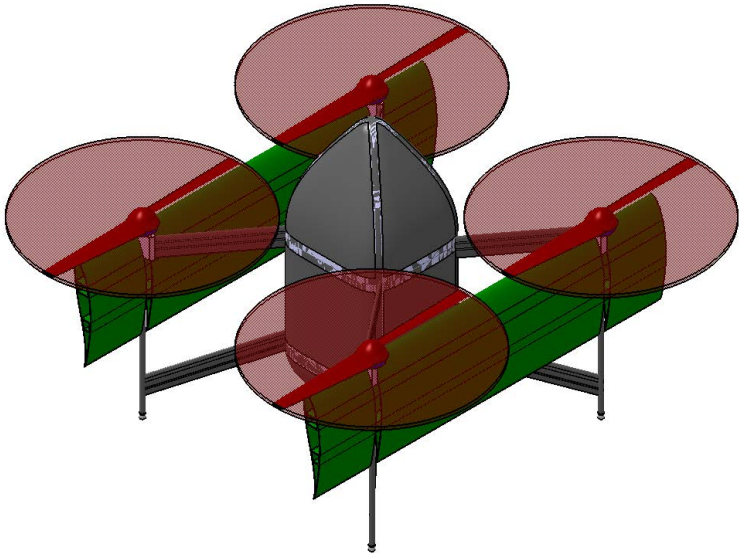

FIGURE 6.8: Vehicle design after initial parametric studies.

7 Vehicle Specifications

Vehicle Dimensions	
MGTOW	38.42 lb (17.49 kg)
Total vehicle length	6.27 ft (1.91 m)
Total vehicle width	6.56 ft (2.00 m)
Total vehicle height	3.60 ft (1.10 m)
Fuselage length	1.33 ft (0.41 m)
Fuselage width	1.33 ft (0.41 m)
Fuselage height	3.42 ft (1.04 m)
Motor Specifications	
Number of motors	4
Max rated power	2.68 hp (2.0 kW)
Max continuous power	2.01 hp (1.5 kW)
Operating RPM	800–1750
Proprotor Specifications	
Number of proprotors	4
Blade diameter	2.95 ft (0.90 m)
Number of blades	2
Blade chord	0.19 ft (0.06 m)
RPM, hover	1,950
RPM, forward flight	850
Blade taper tatio	4:1
Twist (inboard)	19.8°
Twist (outboard)	9°
Twist transition	$0.87R$
Airfoil	SD7032
Wing Specifications	
Span	6.56 ft (2.00 m)
Chord	1.37 ft (0.42 m)
Aspect ratio	4.79
$C_{L,max}$	1.5
Taper ratio	0
Sweep	0 °
Incidence angle	-6°
Max vertical load factor	$3g$
Airfoil	FX 63-137
Performance	
Cruise speed	55.0 kts
Maximum speed	87.7 kts
Best endurance speed	24.3 kts
Best range speed	32.1 kts
Max vertical load factor	$3.0g$
Max endurance	7.2 hr
Max range	210.0 mi
Figure of merit (Hover)	0.74
Prop efficiency, η_p	0.85

8 Power System

8.1 Power Plant Selection

For a vehicle at the scale of *AirEZ* there are a large number of options for the power system, including internal combustion engines and fuel cells, and energy storage devices such as batteries and super capacitors. The options for drive systems include mechanical and magnetic gear trains, and electric options such as brushed and brushless AC and DC motors. In addition, the option of hybridization between two or more of these technologies need to be considered. The following section describes the relative strengths and weaknesses of the available power plant options.

8.1.1 Power Supply Options

The power supply for the *AirEZ* vehicle was selected based on the Measures of Effectiveness (MoEs) in the RFP for reducing CO_2 emissions and yearly operating cost, while maintaining a high specific power and specific energy. Low acoustic signature was also a driving factor since the *AirEZ* vehicles are operating in close proximity to customers' homes.

8.1.1.1 Small-Scale Internal Combustion (IC) Engine

IC engines such as gas or diesel, and turbine, were investigated as options for powering the *AirEZ* vehicle due to the relatively high energy density of hydrocarbon fuels when compared to batteries. However, the cost and CO_2 emissions of burning fuel were also considered in the power plant selection. While IC engines have been widely used on single-prop, fixed wind UAVs (e.g. Boeing Scan Eagle, GTOW: 39.6 lbs) for high speed and endurance, the quadrotor tailsitter configuration of the *AirEZ* vehicle complicates integration of the IC engines and fuel supply lines.

8.1.1.2 Batteries

Lithium batteries are used extensively in many mobile, electric-based applications such as phones, electric cars, and small UAVs. Three types of lithium batteries are examined: lithium ion (Li-ion), lithium polymer (Li-poly), and lithium sulfur (Li-S) that has the highest theoretical specific energy and specific power of any rechargeable battery chemistry [5]. Note that while Li-S batteries typically have poorer cycle life compared to Li-ion batteries, some Li-S batteries have demonstrated higher mid-life specific energy than state-of-the-art Li-ion batteries even after 1500 charge and discharge cycles [6].

8.1.1.3 Fuel Cells

Fuel cells offer the advantage of processing high specific energy (33.3 kWh/kg) hydrogen fuel. Although the weight of the actual hydrogen fuel is negligible, a fuel cell power plant requires a number of components including a fuel tank, fuel cell stack, and additional "balance of plant" (BoP) accessories. These BoP accessories usually include a water management system, air blower, fuel management system, cooling pumps, start-up battery, and electronic components needed for operating the system and managing the power generated by the fuel cell.

Fuel cell power systems are classified primarily by the materials used for the electrodes and electrolytes. Alkaline fuel cells (AFCs), direct methanol fuel cells (DMFCs), molten carbonate fuel cells (MCFCs) and solid oxide fuel cells (SOFCs) were rejected due to their very high operating temperatures (more than 212°F). Phosphoric acid fuel cells (PAFCs) were also not

considered due to the danger posed by the highly acid electrolyte. For use in a small UAV, proton exchange membrane fuel cells (PEMFC) were determined to be the most viable option.

8.1.2 Power Supply Trade Studies

8.1.2.1 Ragone Chart

A Ragone chart shows the specific power versus specific energy for the various power supply options in Figure 8.1. Specific power is an important measure of vehicle performance in terms of hover capability and max cruise speed. Specific energy is a measure of power supply capacity which translates to the maximum endurance and range of the vehicle. The long range and short delivery window of the *AirEZ* mission requires both high specific power and specific energy. Although Figure 8.1 shows small-scale IC engines have superior specific energy and specific power, considerations against IC engines are:

(i) Four independent, coupled engines and gear boxes would be needed on the *AirEZ* vehicle

(ii) Reliable fuel supply to the engine is difficult in a tilt-body configuration in all flight phases

(iii) Fuel flow control for RPM control is slow to respond compared to electrical systems, resulting in decreased maneuverability

(iv) The acoustic signature is much higher than that of electric options

For these reasons, a battery or fuel cell option with high specific power and energy is more desirable for the *AirEZ* vehicle than IC engines.

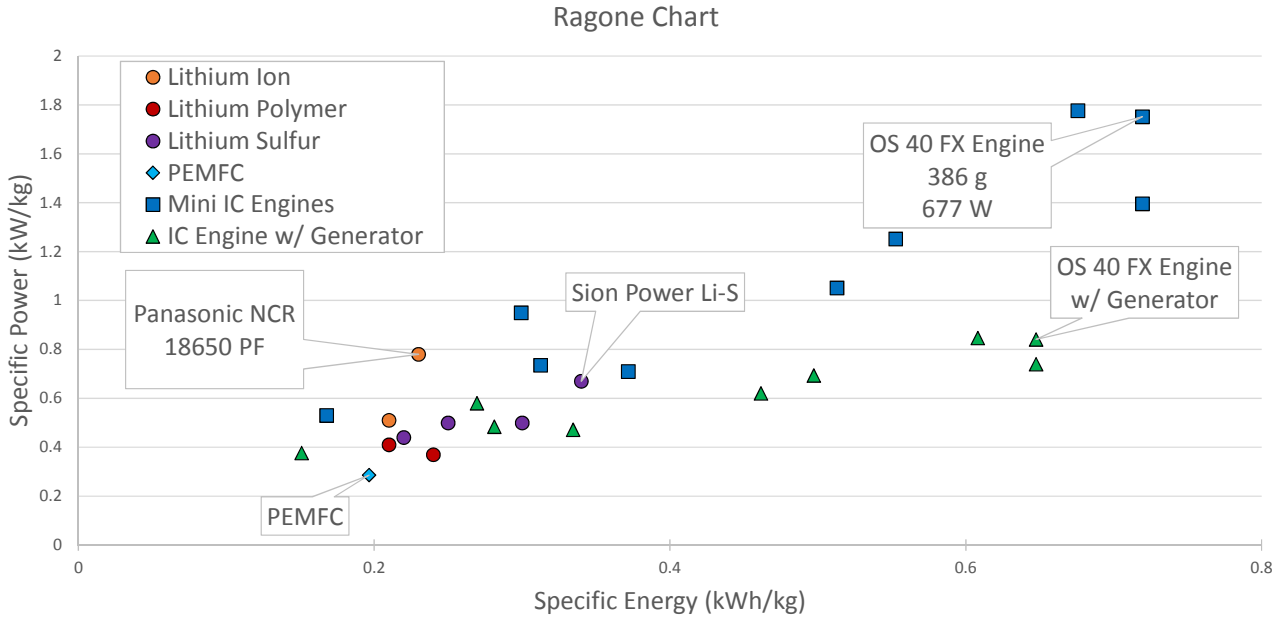

FIGURE 8.1: Ragone Chart for Power Supply Options

Current hydrogen PEMFC stacks have low specific fuel consumption (0.055 kg/kWh) [7] but the overall fuel cell system is shown to have poor specific energy and specific power. The weight of the system: stack, BoP, fuel tank, and accessories, does not scale down well for portable use. This was a major consideration when choosing a battery option over the fuel cell option.

Specifically, the Sion Power Li-S battery was selected, as it showed the best combination of power and energy density.

8.1.2.2 Cost and CO_2 Emissions

In addition to specific energy and specific power, the different power supply options were also evaluated based on the cost and CO_2 Measures of Effectiveness (MoE) given in the RFP. Table 8.1 shows the parameters and assumptions used to generate the MoE comparisons in Figure 8.2.

TABLE 8.1: Power Source Parameters and Assumptions [8–10]

Energy Source	Usage Cost	CO_2 Emissions
Battery (Li-S)	\$0.18/kWh (charging) \$0.17/kWh/life cycle	1.2lb/kWh
Gasoline (OS 40FX)	\$5/gal	3.33lb/ gal
Hydrogen (PEMFC)	\$1.85/kWh	0 lb
Sizing Calculations	2.04kWh/flight	80 mi. range
Other Assumptions	5,000 flights/day	1,500,000 flights/year

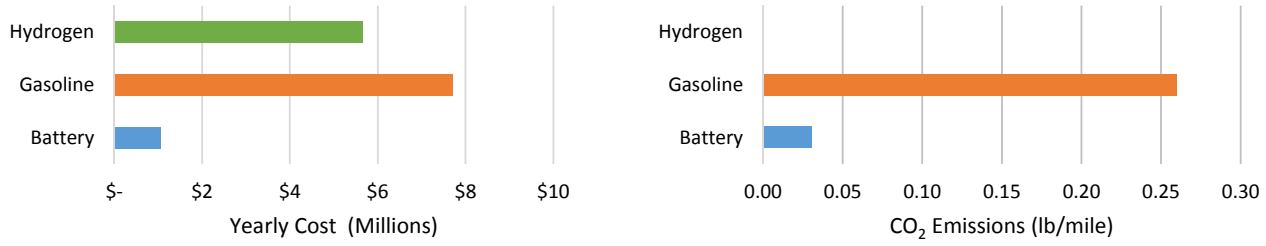

(a) Cost Over One Year

(b) CO_2 Emissions Per Delivery Mile

FIGURE 8.2: Preliminary Comparison of Energy Usage

Figure 8.2 shows the comparison of the various power supply options in terms of usage cost and pounds of CO_2 emissions per delivery mile. Gasoline powered IC engines were determined to be the most expensive and largest CO_2 producer. Though Hydrogen PEMFC systems produce virtually no CO_2, they are more expensive to operate than Li-S batteries. The Li-S battery is the most cost effective and produces small amounts of CO_2. These are the reasons for selecting the Sion Power Li-S battery for the *AirEZ* power supply.

8.2 Motor Selection

There are a large number of possible motors types to be used on the *AirEZ* vehicle. However, the motor selection was narrowed down to motors that are widely used in electric automobiles. Both electric automobiles and the *AirEZ* vehicle have similar criteria for motor selection: power-to-weight ratio, high specific torque, and high torque at low RPM. The most widely used motors in electric vehicles are switched reluctance, brushed DC, AC induction, and brushless DC.

8.2.1 Motor Types

Switched reluctance motors have the advantage of programmable torque-speed characteristics, enabling efficiencies greater than 90%, especially at low speeds. However, switched reluctance motors are not self-starting and cannot be started under load, which is not feasible for the *AirEZ* vehicle which frequently stops and starts its rotors for landings.

Brushed DC motors are simple designs since electric current is conducted through mechanical commutators and brushes. However, the friction due to the brushes results in low efficiency and high maintenance, which is not suitable with the large number of *AirEZ* vehicles.

AC induction motors induce currents in the rotor via an air gap between the fixed stator and rotor, so there is no electrical connection between the two. Therefore, the absence of brush friction allows these motors to achieve high speed and power output. However, the stator has a three-phase winding powered by a three-phase supply, making the speed control difficult since they need expensive variable frequency drives.

Brushless DC motors (BLDC) are similar to AC induction motors in that there is no brush friction between the stator and rotor. However, a BLDC uses permanent magnets and does not need to expend energy to create magnetic dipoles, resulting in high efficiency and power densities. The disadvantage is that BLDC motors have a higher upfront cost due to the cost of the permanent magnets.

Table 8.2: Comparison of Different Motor Options [11]

	Brushed DC	BLDC	AC Induction
Peak efficiency (%)	85-89	95-97	94-95
Max. RPM	4,000-6,000	4,000-10,000	9,000-15,000
Cost per shaft Hp	$100-150	$100-130	$50-75
Relative Cost of Controller to Brushed DC	1	3-5	6-8

Table 8.2 shows the trade-offs in terms of efficiency, RPM, and cost between the available motor options. The high rotation rates of AC induction motors (15,000 RPM), are not necessary on the *AirEZ* vehicle where the rotor speed is approximately 1,750 RPM and would require the added complexity of gearboxes. Furthermore, the peak efficiency of AC induction motors is less than that of BLDC motors, and the cost of AC motor systems with a speed controller factored in are higher. Therefore, a BLDC motor system was selected due to its high peak efficiency and moderate cost.

8.2.1.1 Motor and Controller Specifications

The specific BLDC motor choice for the *AirEZ* vehicle was based on the preliminary sizing (installed power requirement): 6.24 hp (4.65 kW), or 1.6 hp (1.2 kW) for each motor. A 2 hp (1.5 kW) BLDC motor was selected from a survey of motors to provide a 25% safety factor. The U-10 KV100 BLDC motor manufactured by T-Motor was chosen to power the *AirEZ* vehicle. This motor weighs 0.88 lbs (0.4 kg) and has a specific power of 2.3 hp/lb (3.8 kW/kg). The motor electronic speed controller (ESC) was sized by the max power and current (35 A) specifications of the U-10 KV100 motor. Therefore, the Phoenix EDGE LITE HV40 controller with with 40 A current and 50V voltage ratings was selected. The U-10 motor and HV40 ESC were also selected since they are commercial off-the-shelf (COTS) technology.

9 Proprotor Design

The *AirEZ* design presents a unique set of aerodynamic and structural challenges. The vehicle operates in aerodynamic environments that have dissimilar design drivers, i.e., operates as a helicopter during takeoff and/or deliveries and as a propeller driven craft during cruise. Beyond these aerodynamic challenges the prop-rotor also features an adjustable root pitch mechanism and variable RPM control, allowing the vehicle to achieve the highest possible aerodynamic performance. However, these systems have to seamlessly operate at a high level of reliability, structural efficiency and dynamic stability over the entire operation range while keeping low the design complexity and cost.

9.1 Aerodynamic Design

One of the key challenges associated with the design of the prop-rotor blades is to obtain a combination of design parameters, such as blade twist, taper and rotor solidity that allows for efficient operation as both a rotor and propeller. A well-validated method based on blade element momentum theory (BEMT) was configured specifically for this prop-rotor design task [12]. The tool was developed in-house at the University of Maryland and used to determine the prop-rotor configuration that achieves the optimal combination of hover and forward flight efficiency. The methodology neglected small angle assumptions inherent to typical BEMT codes and included the effect of swirl velocities. For the purposes of this study, efficiencies were quantified using the rotor figure of merit (FM) for hover and the propulsive efficiency (η_p) for forward flight. These metrics are defined as

$$FM = \frac{P_{\text{ideal}}}{P_{\text{actual}}} = \frac{C_T^{3/2}/\sqrt{2}}{C_P}$$

$$\eta_P = \frac{\text{thrust} \times \text{true airspeed}}{\text{power required}} = \frac{TV_\infty}{P_{\text{req}}} = \frac{C_T \mu}{C_P}$$

Considering the *AirEZ* vehicle is operating primarily in forward flight over most phases of the delivery mission, it is imperative that the designed vehicle have high propulsive efficiency. Therefore, a benchmark for the prop-rotor design was set at $FM = 0.6$ and $\eta_P = 0.85$. The final design of the prop-rotor is summarized in Table 9.1.

9.1.1 Methodology

The steps used in the stage of proprotor design were as follows:

1. Preliminary parametric study of twist, blade taper, shaft RPM and rotor solidity was performed to identify the optimized design for a pure rotor and a pure propeller and the driving parameters.
2. A combination factor was introduced, which weights the design between the hover optimum and forward flight optimum to arrive at the most efficient compromised proprotor design.
3. Figure of merit and forward flight efficiency was used as a metric to determine if there is a need for a variable blade pitch design.
4. Trade studies were conduction with multiple airfoil shapes to arrive at an airfoil that has superior performance in low Reynolds number flows.

Global Properties	
Radius (ft)	1.32
Root cut out	10%R
Number of blades	2
Solidity	0.0745
Taper ratio	0.25
Inboard twist	19.8°
Outboard twist	9°
Twist transition (r/R)	0.87
Average chord (ft)	0.172

Hover/Cruise Performance	
Hover	
Pitch setting	33.36°
RPM	1750
Thrust coefficient, C_T	0.0106
Disk Loading (lb/ft^2)	1.47
C_T/σ	0.142
FM	0.7308
Cruise	
Pitch setting	70.34°
RPM	750
Cruise efficiency	0.8501

TABLE 9.1: Geometric properties of the designed proprotor with hover and cruise performance.

5. Extended parametric studies were performed by introducing variations in rotor solidity and taper were introduced to further optimize the proprotor.

9.1.2 Preliminary Parametric Study

The design of a rotor or propeller involves finding the chord and twist distributions along the blade span, the blade collective and the RPM settings that maximize the performance metrics ,i.e., FM and η_p. As part of preliminary aerodynamic design, two sets of parametric studies were performed:

1. Obtain a pure propeller design, with propeller efficiency in cruise as the target function.
2. Obtain a pure rotor design, with FM in hover as the target function.

Table 9.2 lists the parameters of interest for this initial study, specifically the fixed inputs, the parameters that were varied, and the resulting output values. During the parameter sweep, RPM, linear twist rate, average chord length and taper ratio were varied one at a time. For each variable value, the required thrust was set (from sizing considerations), and the pitch setting and efficiency metric were calculated using the afore mentioned modified-BEMT methodology. After one variable was swept through its range of interest, the value of that parameter that produced the best efficiency was used for the subsequent set of variables.

Fixed inputs	**Variable parameters**	**Output values**
Rotor radius	RPM	Collective setting
Hovering thrust	Linear twist rate	Figure of merit
Cruising thrust	Average chord length	Propeller efficiency
Cruising speed	Taper ratio	
Blade number		

TABLE 9.2: List of inputs, outputs and variable parameters for the preliminary parametric study.

Figure 9.1 presents the results of this preliminary study, showing the effects of RPM, twist, chord, and taper on the efficiencies of both a pure rotor and pure propeller in terms of the % variation of FM and η_p over the range of the parameter studied. It was observed that the efficiency metrics were most sensitive to the rotor RPM and blade twist. In contrast the rotor solidity and taper ratio resulted in a maximum of 3% change in the efficiency metrics. Therefore a good understanding of the rotor of RPM and blade twist is key to obtaining an efficient proprotor design.

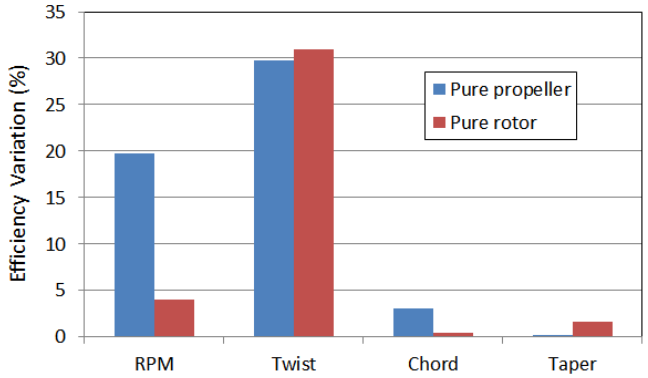

FIGURE 9.1: Effects of RPM, twist, chord, and taper on proprotor efficiency

9.1.3 Combining a Rotor and Propeller

With the best rotor and best propeller design achieved, the next step involved the combination of these two design states. Simultaneously, the merits of a fixed versus adjustable pitch mechanism were also studied. This combination process was achieved using a so-called combination factor, α, that indicates where the design is on the spectrum between a pure rotor and pure propeller. It was used according to the equation: $X_{\text{proprotor}} = \alpha X_{\text{rotor}} + (1-\alpha)X_{\text{rotor}}$, where X identifies a blade geometry variable such as twist/taper and α varied between 0 to 1, with $\alpha = 0$ representing a pure rotor design and $\alpha = 1$ is a pure propeller design.

For a fixed pitch design, the geometric parameters that can be changed are twist rate, chord, taper, and root pitch. For each value of α, the hovering and cruising RPMs that match the respective required thrusts are determined, while returning the best respective efficiencies. For an adjustable pitch design, a similar process was used, except that the root pitch is now an additional variable that was allowed to vary along with the RPM. Figure 9.2 shows the results of this study, illustrating the best rotor and propeller performance for a range of combination factors.According to the results, when the propeller efficiency approaches 0.85, the figure of merit of the fixed pitch design is extremely low at approximately 0.1. The physical reasoning behind this poor efficiency is that the forward flight optimized prop-rotor has excessive root pitch and twist, and therefore needs to operate at a high RPM to prevent blade stall. However, with the inclusion of the adjustable pitch design, the figure of merit is not increased to 0.7 when the propeller efficiency is at 0.85. The huge performance improvement makes the adjustable pitch design more favorable than the fixed pitch counterpart with the aerodynamic advantage gained making up for the increased complexity of the rotor hub design.

Therefore, this preliminary study provides insight into the basic physics behind the proprotor design, i.e., the rotor RPM and blade twist significantly impact the proprotor performance, and

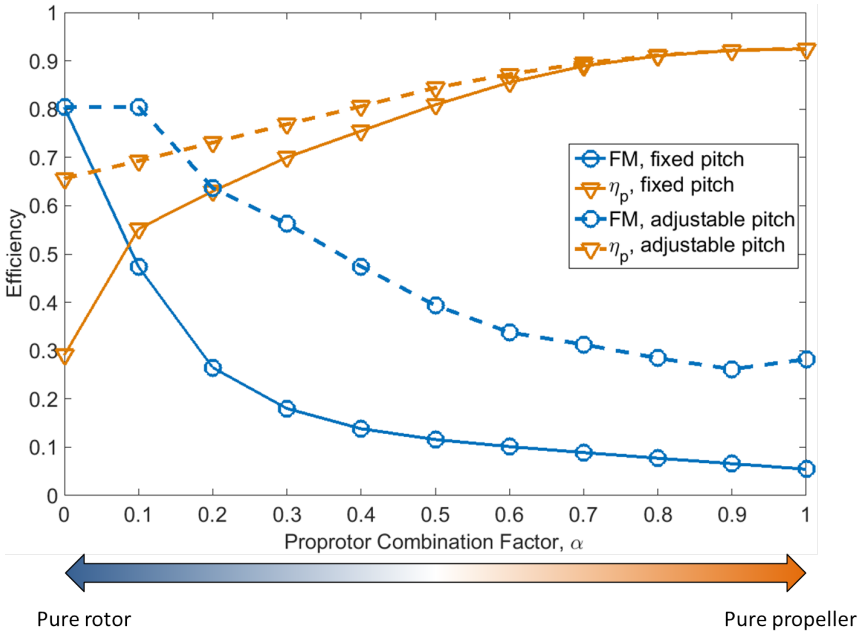

FIGURE 9.2: Comparison between fixed and adjustable pitch proprotor

have to be designed with care. Furthermore, to achieve a high figure of merit and propeller efficiency simultaneously, an adjustable pitch structure must be implemented.

9.1.4 Airfoil Selection

The physical dimensions of the *AirEZ* vehicle and operating conditions results in the airfoil operating largely in the low Mach number and low Reynolds number regimes. The desirable characteristics for such an airfoil are:

- High $C_{L,max}$ that is insensitive to Reynolds number
- Gentle stall characteristics
- Airfoil camber of less than 5% to prevent excessive moment about the aerodynamic center
- Thickness-to-chord greater than 10% to provide the necessary structural strength

The preliminary study used a NACA0012 airfoil baseline blade [13]. Although this airfoil has been well studied and is a natural choice for helicopter blades, it is a poor choice for the *AirEZ* proprotor blades. To this end, various low Reynolds number airfoils were studied, typical of those used in rotorcraft, windturbine and micro air-vehicle applications. The chosen airfoil for the *AirEZ* proprotor is the SD7032 [14]. This airfoil has a thickness of 10%, a 3.4% camber, $C_{L,max} = 1.36$ and a maximum lift-to-drag ratio of 51.3.

9.2 Extended Parametric Study

With the identification of the dominant design variables (RPM and twist) and a good airfoil (SD7032), an extended parametric study was performed to further optimize the existing design. This extended study focused on RPM variations and multiple twist distribution, wherein a bilinear twist distribution was considered. It should be noted that the proprotor optimization

was performed in tandem with the sizing code to ensure the most accurate values of the vehicle design.

Similar to the previously conducted preliminary study, the best pure rotor and pure propeller were determined for the extended parametric study. The variation now considered included a series of iterations with RPM, inboard/outboard twist rates and transition radius as variables. At each stage of the iterations the combination of variables with the best performance was determined, refining the range of the variables for the next iteration. After three iterations, the variables had more or less converged to the best rotor and propeller design, respectively.

Combining the best rotor and propeller designs was done in a similar manner to that described in the preliminary parametric study. A more rigorous combination can be done with 3 combine factors, each for one variable (inboard twist, outboard twist, and transition radius). Utilizing a step size of 0.1 for each combination factor from 0 to 1 yields $11^3 = 1331$ total possible designs. All of these design points can be seen in Figure 9.3.

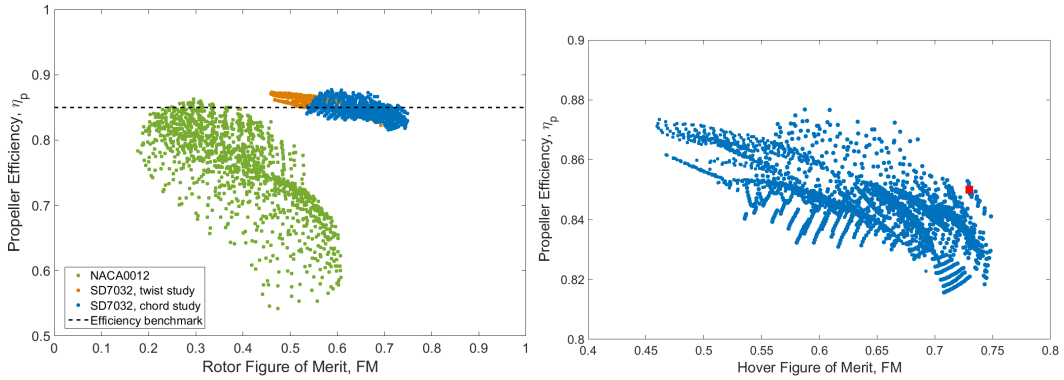

(a) Full rotor design space

(b) *AirEZ* proprotor design point

FIGURE 9.3: Hover and cruise efficiencies for all proprotor designs considered

As stated before, a major part of *AirEZ* operational time is spent in cruising flight, so sufficient propeller efficiency must be guaranteed. A benchmark was set for the propeller efficiency to be no less than 0.85. Among the designs that satisfied the threshold propeller efficiency, the design with the best figure of merit was chosen. Care was also taken to ensure that the blade operating conditions at the design point (in both hover and forward flight) were away from any stall limited boundaries. Geometrically, an inboard twist of 19.8°, and an outboard twist of 9°, with the change in twist occurring at $0.87R$ was determined. This design provided a figure of merit of 0.65 at 2,000 rpm in hover and a propeller efficiency of 0.85 at 900 rpm in cruise.

9.3 Optimization and Final Results

The final step in the proprotor design process was to optimize the average chord length and taper ratio. The objective of the optimization was hovering figure of merit, with the constraint that the propulsive efficiency be greater than 0.85. From these conditions, a final design was chosen with an average chord length of 0.172 ft and a taper ratio of 0.25. Therefore, the completed proprotor design achieves a figure of merit of 0.73 at 1,750 RPM in hover and a propeller efficiency of 0.8501 at 750 RPM in cruise. The wide range in operating RPM must be noted between hover and forward flight conditions. This aerodynamic requirement in varying RPM along with requirements of controllability were the design drivers for choosing a variable RPM based design. The final blade design is shown in Figure 9.4.

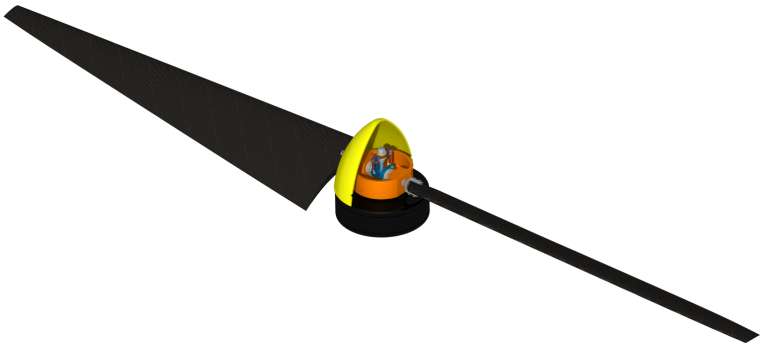

FIGURE 9.4: Final proprotor blade design

9.4 Proprotor Blade Structural Design

The proprotor structured is primarily comprises three components: 1. A foam core that defines the shape of a blade, 2. A carbon fiber spar along the length of the blade that provides axial and bending stiffness, and 3. A carbon fiber sleeve on the surface of the core that protects the foam from external influences and provides torsional stiffness. The spar is made of uniaxial carbon fiber strips and a root insert. The root insert is a slender aluminum piece with two 1/16 in holes through which the blade are attached to the hub. The carbon fiber strips around the root insert wrap it smoothly to balance the radially outward centrifugal forces on the blade, as shown in Fig. 9.5(b). The spar was designed with a uniform rectangular cross section except the blade

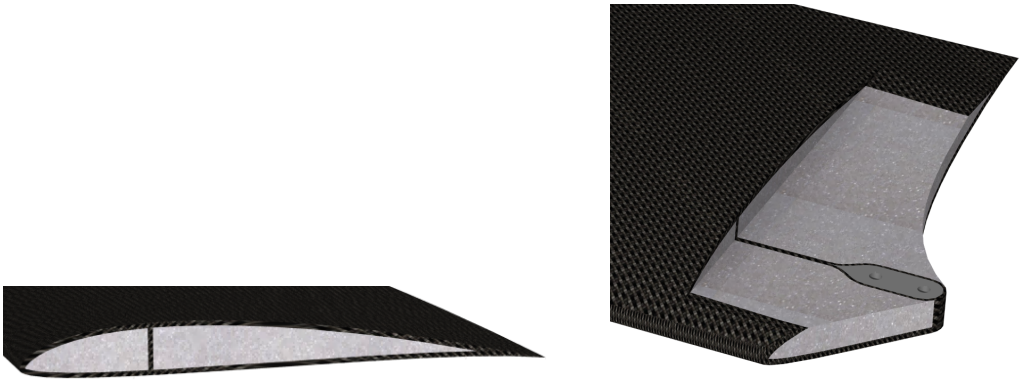

(a) Proprotor Blade Cross Section

(b) Proprotor blade root design

FIGURE 9.5: Proprotor design: (a) Blade cross section, (b) blade root section

root section, which contains the insert. The dimensions of the rectangular spar is designed to carry: 1. The total blade centrifugal force at the maximum RPM setting, and 2. The bending moment at the maximum thrust condition. To maximize bending stiffness, the spar dimension along the blade thickness direction should be as large as possible. For the SD7032 airfoil, the maximum thickness is 10% chord at 26.6% along the chord. Therefore, it is reasonable to assume that the spar dimension along the thickness is 9.5% chord at the 25% chord position along the span after taking into account skin thickness.

Engineering margins are assumed to design the axial and bending stiffness. For the axial load caused by centrifugal force, the axial strain should not exceed 0.0001 anywhere along the blade

span at 2,000 RPM, and for bending moments caused by the thrust, the tip deflection of the blade should be less than 5% rotor radius when the thrust level is 1.2 times hover thrust at 2,000 RPM. As a result, the constraint on axial load is considerably more stringent and the minimum spar dimension along the chord can be calculated, as shown in Figure 9.6.

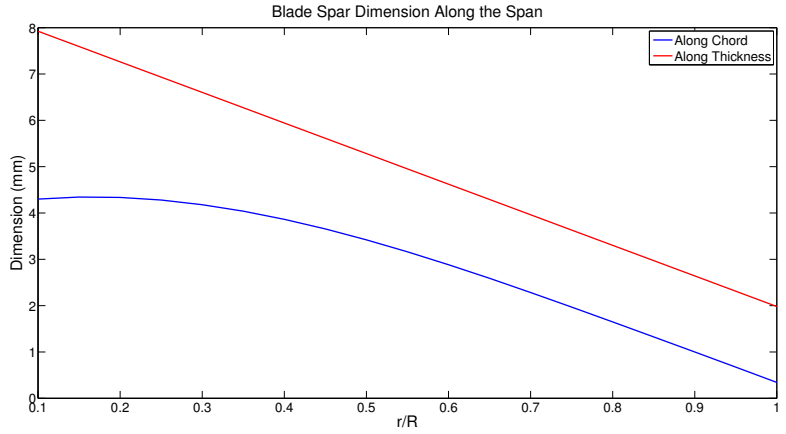

FIGURE 9.6: The dimensions of the spar cross section on the span. The dimension along the thickness is defined by the blade thickness, and the dimension along the chord is defined by the axial load constraint

The carbon fiber sleeve is made of +/-45 interwoven carbon fiber sheet with 60% fiber volume and a thickness of 0.004 in. The foam core is made of Rohacell 71 SL foam, which is used only for maintaining the airfoil shape and takes no significant load. To adjust the center of gravity to 25% chord, tungsten carbide rods (1/8 in diameter near the root, 1/16 in diameter near the tip) are placed at the leading edge of the foam core. After all the structural properties are determined, the total weight of a blade is 0.154 lb.

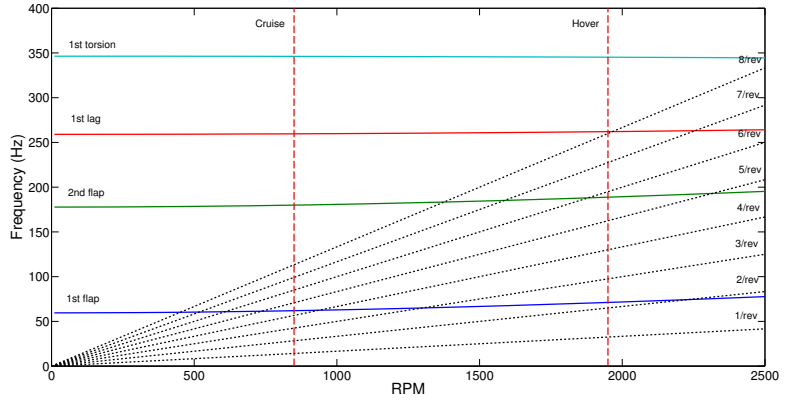

FIGURE 9.7: The fan plot of the prop-rotor shows the first two flap modes, the first lag mode and the first torsional mode, and 1 8/rev curves. The two red dashed lines are cruising RPM (900) and hovering RPM (1750)

The rotor fan plot for the current design is shown in Fig. 9.7. The fan plot shows that at the two distinct operating RPMs in helicopter and airplane mode, the 1–8/rev harmonics of the rotor will not excite the second flap, first lag and torsional mode of the blades. The 4/rev harmonics is close to the first flap mode at airplane mode (900 RPM; however, the first flap mode is highly aerodynamic damped and therefore it does not pose a problem for structural instabilities. It is worth noting that the blade stiffness is extremely high compared to a blade of conventional

helicopter with a maximum deflection under its own weight being onlt 0.005 in. The flap natural frequencies at different RPMs are verified using Timoshenko beam theory for a rotating beam [15], and the results agree well.

9.5 Hub Design

The proprotor hub is designed as a rigid hub with root pitch collective control. A collective control rod is attached to the pitch link crossbar and goes through the motor and motor mount to a linear actuator attached to the landing stilt. The linear actuator is used to push and pull the collective control rod to vary the root collective from 33.4° to 75.2° through a 0.26 in. stroke. Turnbuckles on pitch links allow tracking and balancing of rotors when produced at the factory and when HUMS detects an issue. Optional sleeves over the blade grips allow for balancing centrifugal forces to account for any weight difference from manufacturing or wear. The three bearings required for the hub were each selected based on their unique loading case.

A rigid hub design enables a very mechanically simple package that requires low maintenance. A rigid hub is acceptable for our design because the the quadrotor-biplane-tailsitter's unique control ability and relatively low hub loads (9.74 lb. lift, 2.78 lb. drag, 9.63 ft-lb. flap moment, 3.12 ft-lb. lag moment).

- Blade grip to hub base bearing - PTFE plain bearing is used for simplicity and low friction since this joint sees both low rotation speeds and low loads
- Pitch actuator rod to pitch link crossbar bearing - Bronze SAE 841 plain bearing is used since this joint sees high rotation speeds (up to 1800 RPM) and low loads.
- Centrifugal bearing - Steel ball bearings selected since this joint sees high loads from the centrifugal forces (and low rotation speeds)
- All other components made of Aluminum 6061-T6 for it's high strength-to-weight, easy machinability, and good corrosive resistance

9.6 Rotor Dynamic Stability

As in a conventional helicopter, flap-lag and pitch-flap coupling on rotor blades may cause flutter. However, the blades of the current design are very unlikely to flutter because they are hingeless and are designed to be very stiff. A simple eigenvalue study is done on flap-lag and pitch-flap flutters in both hovering and cruising, which shows no risk of rotor flutter, see Figure 9.9.

There are other types of dynamic instabilities, such as pitch divergence and ground resonance. The pitch divergence instability can be avoided by placing the the gravity center of the blade quarter chord position, where the aerodynamic center lies. On the other hand, the design rotor is stiff in-plane, so the ground resonance instability is irrelevant.

10 Wing Design

When designing the wings of the *AirEZ* vehicle, performance requirements and structural loads were kept in mind. Some characteristics which dictated wing sizing included low stall speed, high lift to drag ratio, and gentle stall. Internal structure was highly influenced by maximum loading and Section 13.3 shows this to be 3 g's. The final design of the *AirEZ* vehicle wing includes an FX 63-137 airfoil profile, two wings of aspect ratio 4.7, and an easily attachable configuration.

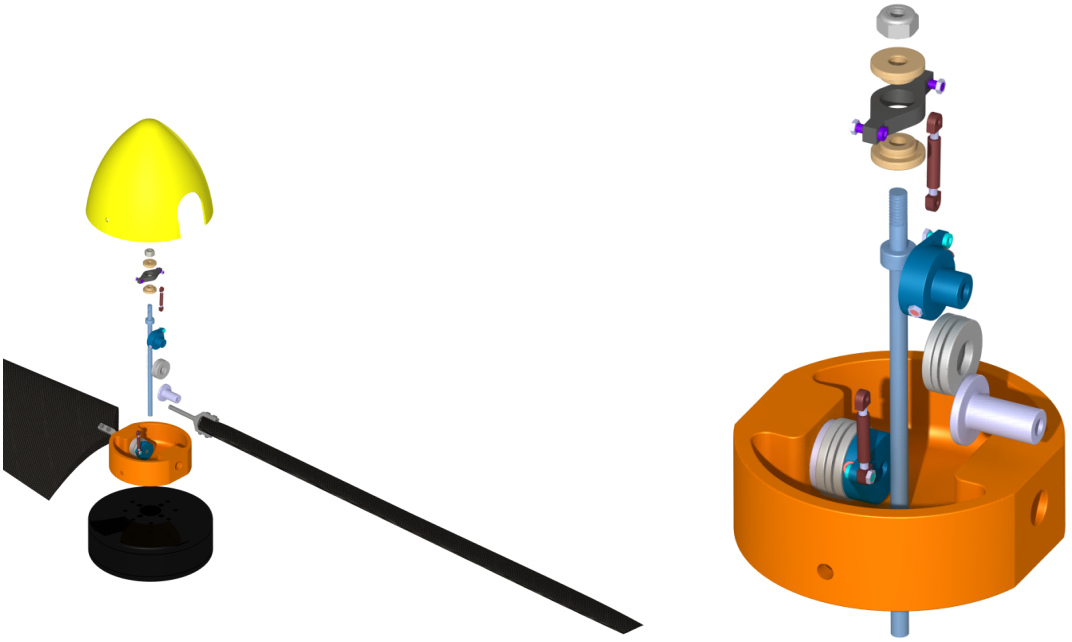

(a) Blade and motor (b) Exploded hub

FIGURE 9.8: Detailed assembly of the hub design: (a) Blade and motor, (b) Exploded view.

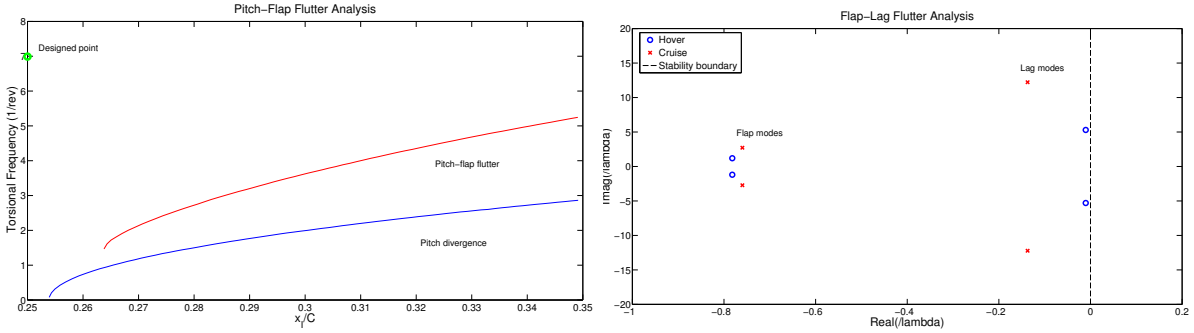

FIGURE 9.9: The results of flap-lag and pitch-flap flutter eigenvalue analysis. None of them occurs during operating

10.1 Wing Geometry

The wings of the *AirEZ* vehicle are sized to carry the entire weight of the vehicle during the designated 55 kts cruise. This performance requirement, used in accordance with the vehicle sizing algorithm determined that the wing of the *AirEZ* vehicle has a 78.7 in. span and an aspect ratio of 4.7 (Section 6.4.1). It is unswept and untapered. No sweep was used because of the low free-stream Mach numbers that are encountered. The wing incidence was fixed to -6° relative to the body center line; this angle was chosen to generate sufficient lift across the range of operating airspeeds and provide a large stall margin to allow for transition to cruise at low speeds (see Section 6.4.1).

10.2 Airfoil Selection

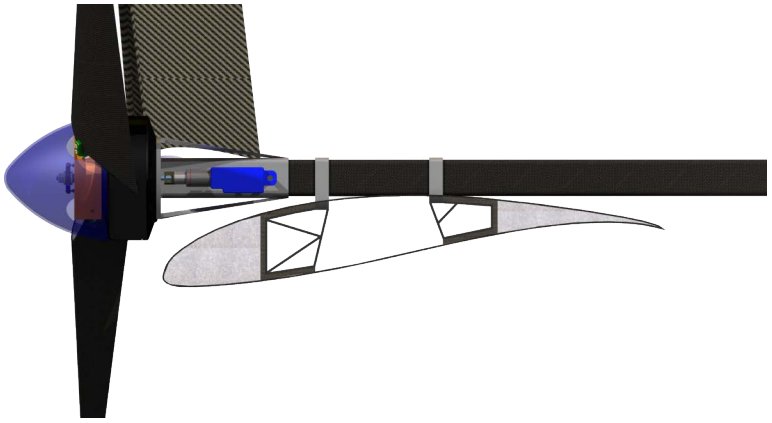

FIGURE 10.1: Wing Connection to Landing Leg Side View

To perform transition maneuvers, it was necessary to use an airfoil with a high maximum lift coefficient and benign stall characteristics. It was also important that the chosen airfoil have a wide drag bucket with a low drag coefficient. The vehicle was sized to fly at 55 kts in cruise, which is relatively low as compared to larger scale fixed wing aircraft. This combination of wing geometric design and flight conditions resulted the wings of the quad-rotor biplane to operate at low Reynolds numbers close to 677,000.

TABLE 10.1: Effect of airfoil on vehicle weight

Airfoil	Vehicle GTOW [lbs]
FX 63-137	38.79
SH3055	40.13
E387	42.49

Therefore, a study was conducted on airfoils designed with high performance at low Reynolds numbers. Over 35 airfoils were studied, with design purposes ranging from model aircraft to sailplanes [16, 17]. Most high performance airfoils with high maximum lift coefficients were discarded because their drag characteristics were unsuitable, i.e., these airfoils provided relatively high coefficients of drag ($C_{d_0} > 0.02$) when exhibiting high coefficients of lift ($C_l > 1.0$). The FX 63-137 airfoil was selected because of its good maximum lift coefficient ($C_{l_{\max}} = 1.5$), high maximum lift-to-drag ratio ($C_l/C_{d_0} = 21.3$), gentle stall characteristic, and large drag bucket ($C_{d_0} = 0.012$ from -6^o to 0^o) in the required range of Reynolds number (around 677,000).

The relatively large thickness-to-chord ratio (13.7%) of the wing has adequate room for structural material to provide higher bending and torsional stiffness. Table 10.1 shows a comparison of the effect of the airfoil choice on vehicle weight.

10.3 Wing Structural Design

The wing box is made of two C-channel spars located at 25% and 61%, respectively, of the chord. The skin completes the torque box providing necessary torsional stiffness. Two metal inserts are positioned along the wing span to allow connection to the landing stilt as seen in Fig. 10.1. A graphite/epoxy composite structure was chosen for the wing box because of the low weight and good fatigue strength. Each spar is constructed with plies oriented at 0°/90°. This arrangement helps keep manufacturing relatively simple, while providing the adequate bending stiffness. The skin was designed to provide sufficient torsional stiffness to the wing; it is made of ±45° fabric.

10.4 Wing to Airframe Attachments

The wing loads are transferred to two landing gear stilts. Each wing has four aluminum machined spar inserts, which feature four connection points to the landing stilts, as shown in Fig. 10.2(a). These provide two chordwise location points and two spanwise connection points. During assembly the spar inserts slide onto the landing gear stilt and are then bolted in place. The landing gear stilts are then attached to four struts with aluminum bolts. The struts in turn are bolted to the aluminum corners of the airframe bulkheads. The struts utilize a NACA 0024 cross section with a 3 in. chord for minimum drag and to add to passive stabilization while still allowing enough internal space to hold wires. The struts have a graphite/epoxy skin and a hollow core to allow wires to run through them to the electronic speed controller and sensors near the hub.

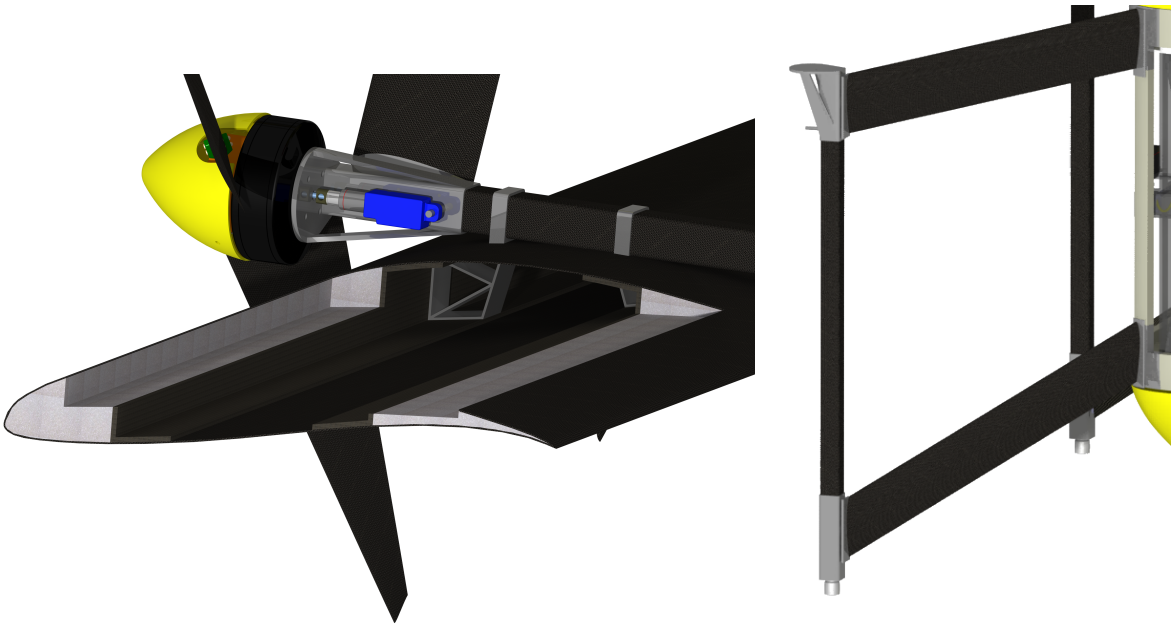

(a) Wing connection to landing stilt

(b) Strut connection to landing stilt and fuselage

10.5 Whirl Flutter Analysis

In cruising condition, the vehicle works as a multiple-engine propeller aircraft. Thus, whirl flutter instability may happen on the proprotor nacelle mounted on the wing. A whirl flutter code developed in the University of Maryland based on a tilt-rotor vehicle study is used to inspect any potential whirl flutter [18]. In the study, the inner part of a wing is modeled as a cantilevered beam with 4 finite elements, and the motor-proprotor assembly is attached to its tip. The shape and eigenvalue of all vibration modes are calculated, and the damping factors of each mode at different cruising speeds are plotted in (Figure 10.2. All the damping factors are positive, indicating whirl flutter does not pose a problem for the current design.

11 Structural Design

A unique feature of the *AirEZ* design is the integration of the package bay into the fuselage. Such a design has multiple advantages; 1. The package is stored internally and is therefore shielded from elements such as rain, dust and snow, 2. The dimensions of the fuselage are fixed

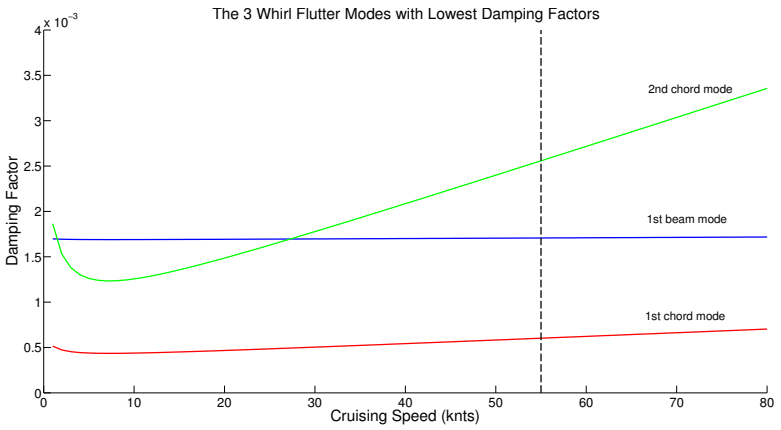

FIGURE 10.2: The 3 modes with lowest damping factors at different cruising speedsspeeds. None of them is negative on the speed range anywhere

irrespective of the packages carried within, which results in predictable flow patterns around the fuselage and therefore allows for predictable handling characteristics.

The *AirEZ* vehicle has a three part airframe design, which is essentially a semi-monocoque design composed of graphite/epoxy foam core sandwich beam frames with a load bearing composite skin. As the aircraft was sized to carry a 12x12x16 in. payload, the largest interior component of the vehicle is the package compartment. The fuselage was sized around the package compartment, while maintaining space and positioning for the battery system, sensors, and package dropoff mechanism. Therefore, the fuselage of the *AirEZ* vehicle measures 16x17 in. across at its widest point to account for the space occupied by the packages and dropoff mechanism. The overall height of the fuselage is 41.2 in., allowing enough vertical space to fit the packages in the center, the battery system on top, and the electronics suite on the bottom. The major dimensions of the vehicle are listed in Table 11.1 and is highlighted in Fig. 11.1.

TABLE 11.1: Notable dimensions

	Distance (in)
Wingspan	78.7
Rotor tip to tip	75.4
Landing gear to nose	42.49
Rotor diameter	35.4

To eliminate the risk of the rotors striking each other, the wings are positioned 40 in. apart from each other to provide proprotors with a 4.6 in. clearance from each other. The stilt landing gear of the vehicle are positioned directly beneath the rotor motors and extends downward 2.4 in. from the lowest point of the fuselage, allowing the fuselage to clear the ground by 2 in. if the elastomeric landing springs compress all the way. The wide spacing of the landing struts gives the vehicle a tipover angle of 51° and a pitch over angle of 50° (Figure 11.7). The battery system of the *AirEZ* vehicle is attached in the nosecone of the fuselage. By designing a simple and easy to maintain airframe with lightweight materials, the development, manufacturing time, and maintenance costs can be reduced.

11.1 Airframe Material Selection

The varying flight conditions of the vehicle flight environment implies that the airframe of the *AirEZ* vehicle must be capable of withstanding winds, gusts, rain, and snow. When considering materials, cost, density, strength, stiffness, manufacturability, fatigue characteristics, and

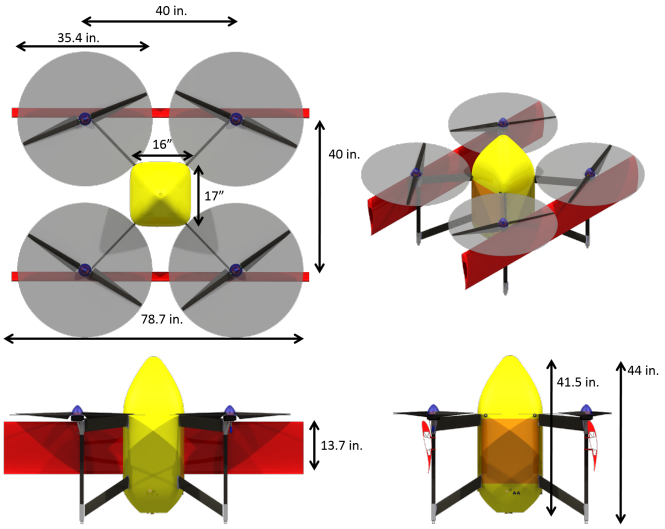

FIGURE 11.1: Vehicle Dimensions.

environmental reactiveness were identified as key properties. A wide range of materials were considered:

- **Plastics:** Ultra High Molecular Weight (UHMW) Polyethelene (PE), Polycarbonate, Acrylonitrile butadiene styrene (ABS), Polytetrafluoroethylene (PTFE), Polyether ether ketone (PEEK), Nylon, Acetal, Rulon, Vespel Polyimide
- **Metals:** Steel, Titanium, Aluminum, Aluminum-Lithium
- **Composite Fiber Materials:** Graphite (IM-7), Aramid (Kevlar-49), E-Glass, S-Glass, R-Glass, Polyethelene (Spectre HT 240)
- **Composite Core Materials:** Honeycomb, Balsa Wood, Cork Wood, Extruded Polystyrene (XPS), Expanded Polystyrene (EPS), polyvinyl chloride (PVC), polyurethane (PU), polymethacrylamide (PMI), polyetherimide (PEI), styreneacrylonitrile (SAN)
- **Composite Resin Materials:** Epoxy, Thermoplastics, Ceramics

The package delivery mechanism is a novel screw conveyor based design and is extensively discussed in Chapter 12. When considering materials for the package cage and auger, the coefficient of friction was an additional key material property because the mechanism depends on sliding the packages along the supporting structure.

During preliminary design stages plastics were considered as a favorable choice for many of the components because of the cheap cost and easy manufacturing processes. However, if plastics were used for key load bearing components, the structure would be excessively heavy owing to the relatively low strength to weight and stiffness-to-weight ratios of plastics. Therefore, as an alternative to plastics, the primary load bearing members were chosen to be made of graphite/epoxy composites with Aluminum 6061-T6 joints. The graphite/epoxy composite material decreased the weight of the structure while the aluminum joints allowed for easy assembly and maintenance. Composites are also used for the fuselage skin where continuous panels can contribute to stiffness and crash-worthiness, as well as having low weight.

The bulkheads are primarily composed of graphite/epoxy sandwich structure beams with Rohacell 71 SL foam core, with the intersection of the bulkheads and longitudinal beams using an aluminum 6061-T6 core. A carbon fiber and extruded polystyrene composite sandwich skin is used for the fuselage. Carbon fiber composites allow for high stiffness with low weight, and can utilize a sandwich structure to greatly increase resistance to buckling loads. Composite construction also has the benefit of allowing the bulkheads, beams, and skin to be manufactured as a single unit, increasing strength and lowering the number of manufacturing steps and lowering the number of parts in the vehicle. The bulkheads, beams, and skin can be manufactured with pre-pregs using a co-curing vacuum process in an autoclave since they are relatively small parts. This procedure eliminates the need for expensive automated fiber placement machines and slow debulking cycles typical of an out of autoclave curing process.

Intermediate modulus graphite was chosen as the fiber material because of its higher strength-to-weight and stiffness-to-weight properties compared to E-Glass, S-Glass, or R-Glass. Aramid and polyethylene fibers were initially favored for their lower density, but were ultimately decided against because of their poor compression and UV degradation properties. The better properties of high strength or high modulus graphite fiber were not necessary because of the relatively low loading of the structure, so intermediate modulus carbon fiber was chosen to reduce costs. Rohacell 71 SL foam was decided as the core material because of its combination of high compression strength, low density, and high working temperatures. Epoxy was chosen as the resin material because of its low cost and adequate strength compared to thermoplastics or ceramics. Aluminum 6061-T6 was chosen as the material for the joints because of its low density, high strength and ease of machining the components. While Aluminum-lithium alloys posses lower density and greater fatigue properties, the increase in cost incurred makes Aluminum-lithium as an undesirable option. All of the composite layups consist of layers of $\pm 45°$ and $0/90°$ fibers to handle the multiple load paths in hover and cruise.

The package enclosure, auger, hinges, and electronics mounting points were chosen to be manufactured out of UHMW polyethylene because to its low density, low coefficient of friction, low water absorption, excellent chemical resistance, and good wear resistance. Compared to UHMW polyethylene, PTFE's lower friction coefficient was desirable, but the increase in density and decrease in strength makes it an undesirable choice. An exploded view of some of the key fuselage components is shown in Figure 11.6.

11.2 Primary Load Paths

During the most intense maneuver, i.e., the transition, there is a load factor of $3g$ on the wing and fuselage. The airframe was designed with a safety factor of 1.5. Most of these loads are transmitted from the wings through the structs to the remainder of the airframe by the two main bulkheads. The primary load paths in cruise and hover are highlighted in Figs 11.3 and 11.2, respectively.

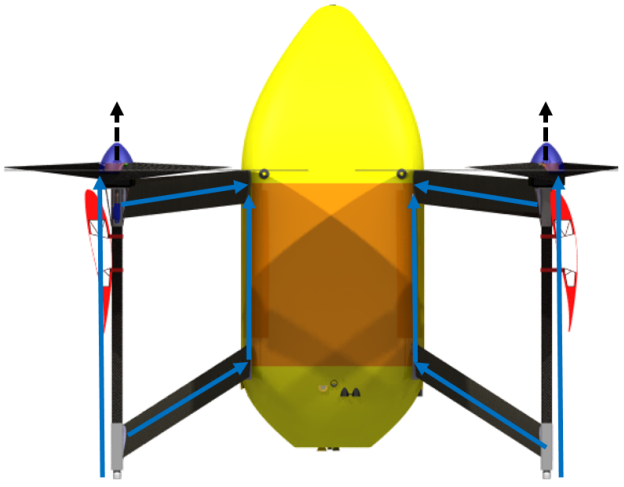

FIGURE 11.2: Hover Load paths viewed from the side

At the top of the fuselage, these bulkheads react the bending loads on the mast as they are passed through the standpipe. The rotor

thrust is carried by a thrust bearing from the
main gear box carrier through the transmission case and into the standpipe. From the standpipe, the load is transmitted by means of four struts to the longitudinal beams supporting the engine deck. A reinforcing band is fastened around the four strut connection points to react the bending moments. The longitudinal deck beams for the engine are fastened directly to the main fuselage keel beams, which carry the thrust load to the remainder of the airframe, including the main bulkheads.

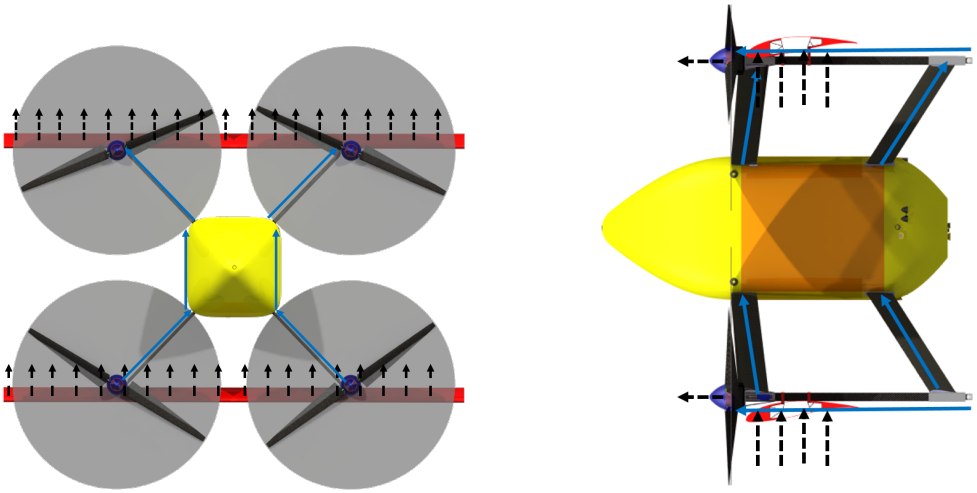

(a) Front view (b) Side view

FIGURE 11.3: Load paths for vehicle in cruise

11.3 Fuselage Structure

11.3.1 Forward Structure

The forward section of the fuselage is designed to minimize drag and allow space for the mounting of the camera, transceiver, GPS, and parachute system. The skin covering the parachute opening is designed with failure points to allow the parachute to deploy with minimal obstruction. The beams that support the skin are attached to a UHMW polyethylene hinge on one end and on the opposite end have pins that fit into a cam lock system internal to the top main bulkhead. The cam lock system provides a detent and positive stop for consistent positioning and vibration-resistant performance. The cam lock system provides quick access to the battery and quicker turn around time of the vehicles compared to threaded fasteners. This hinge system allows for the fore section to easily and quickly be opened up when replacing the battery yet still remain secure in flight. As the hinge and cam lock system were not designed to

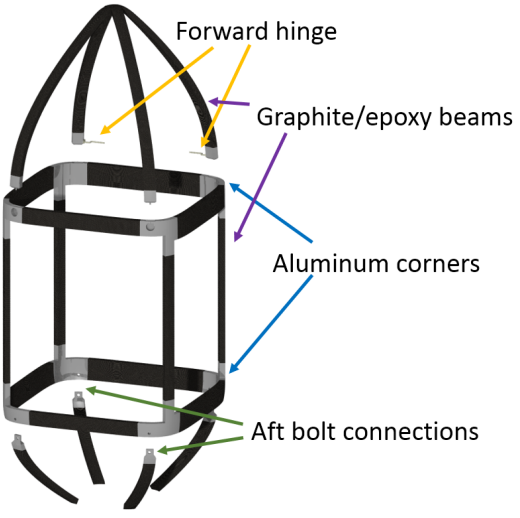

FIGURE 11.4: Exploded fuselage skeleton

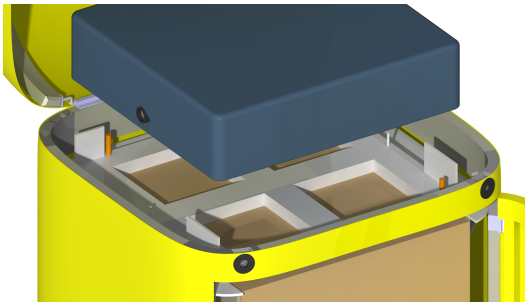

FIGURE 11.5: Battery Slots

hold the entire weight of the aircraft, the parachute system is secured to the top main bulkhead with Spectra HT 240 polyethylene string.

11.3.2 Battery Mount Structure

The top shelf in the *AirEZ* vehicle is bolted to the top bulkhead in four locations. The shelf acts to both secure the packages during flight and act as the battery mounting point. The battery is mounted by sliding the battery pack onto the guide rails, bus rails, and locking pins built into the top shelf. The guide rails are designed asymmetrically so the battery can not be attached backwards, thereby preventing reverse polarity problems thus preventing human error. The cam locking system built into the battery pack can then lock the battery in place to prevent any motion during flight and secure the electrical connection.

11.3.3 Package Compartment Structure

The primary purpose of the center section of the fuselage is to carry the packages. The top and bottom shelf secure the package in hover while the side walls carry the package weight while cruising. The side walls have a rectangular track along the middle to support and protect the auger and package tabs.

11.3.4 Aft Structure

The aft section of the fuselage houses most of the electronics required by the avionics, sensors and communications suite. The flat back profile of the aft structure allows for shorter package dropping height with ample room for the sensors. In the case of emergency landings, this section is designed to behave as a crumple zone. The beams supporting the skin and electronics in this section have tabs that extend into the bottom bulkhead for secure bolting.

11.4 Landing Gear

The *AirEZ* vehicle uses a quad stilt landing gear configuration that allows for good roll over angles when on the ground, which is deemed necessary when landing is mostly unprepared surfaces in an urban environment. The landing legs are connected to the wing spar and two struts which make a strong truss like structure that distributes the load and provides high rigidity. At the bottom of each carbon fiber landing leg a polyester based elastomeric spring is attached to absorb shock loads when landing. The wide spacing of the landing stilts gives the

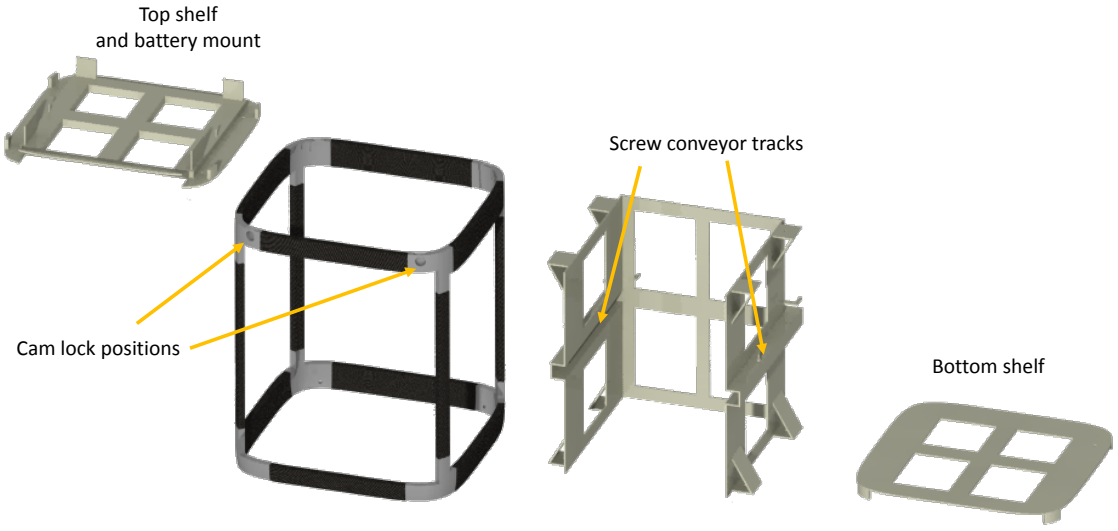

FIGURE 11.6: Package Compartment Exploded View

vehicle a tipover angle of 51° and a pitch over angle of 50°, as shown in Fig. 11.7.

(a) Pitch Rollover Angle

(b) Tip over Angle

FIGURE 11.7: Rollover Angles

11.5 Maintainability and Modular Assembly

As the number of vehicles in a fleet for the *AirEZ* system is relatively high (480 vehicles), consideration was given to design replaceable components that would decrease repair and maintenance time. The proprotor hub comes as one package and the same package is used for both clockwise and counterclockwise rotors. The blade grips are direction dependent and come as a package with the blade. The pitch links in the hub have a turnbuckle mechanism so the rotor can be rebalanced when the health monitoring system detects excessive vibrations. The hub is easily

detached from the motor with 4 studs. Similarly the motor can be detached from the structure by removing four studs. The wings, struts, and landing legs are each individual components that can be replaced by unbolting them. The fuselage skeleton can come apart as the fore, center, and aft section, allowing easy access to components in each section. Once the center section has been detached from the fore and aft, the shelves and package retainment walls can slide out. This design allows for swapping these components and easy access to the package dropoff mechanism. Since all of the structural components are detachable, spare part storage will be compact.

12 Delivery Mechanism

For a complete aerial delivery system, the mechanism for package delivery is critical. This chapter presents the criteria used in selecting the delivery method, the alternatives that were considered, as well as the final design for the *AirEZ* vehicle.

12.1 Delivery Method Selection Criteria

In selecting a delivery method, a variety of factors were considered in terms of how the methods would affect the performance of the overall system of systems.

- **Adaptability to multiple packages**: Simulation results show that the ability to deliver multiple packages per vehicle significantly reduces the number of vehicles needed to complete one day of deliveries. This results in an increase in vehicle productivity as measured by the number of packages delivered per vehicle per day. Therefore, it is very important that the delivery method be flexible enough to allow for delivery of multiple, different-sized packages in a single trip.
- **Integration into fuselage:** Any sort of box, especially one as large as the 12x12x16 inch dimensions given in the RFP, will introduce a large parasitic drag penalty to the vehicle. Such drag increases the necessary power, and as a result, the weight of the vehicle. It also greatly impedes the ability to achieve the high speeds necessary to satisfy the 2-hour delivery requirement. For these reasons, a delivery mechanism must be compatible with the packages being housed in an aerodynamic fuselage. Additionally, a closed fuselage allows the packages to be protected from the elements.
- **C.G. Shift:** Although the ability to deliver multiple, different-sized packages per trip was deemed a necessity for *AirEZ* , the vehicle's tailsitter design makes c.g. shift an important consideration. A delivery mechanism that would allow the remaining package(s) to be shifted after one or more is delivered was desirable.
- **Number of Actuators Needed:** To keep the weight and power requirements of the vehicle as low as possible, a simple mechanism with a limited number of actuators is desired. In addition, the number of actuators needed should be independent of the number of packages being delivered, allowing for the maximum flexibility.

12.2 Delivery Options

A number of options were considered when selecting a delivery mechanism and some of the initial concepts are shown in Figure 12.1. The delivery method hinges completely on the a decision about whether or not the vehicle will land. Both options are considered in the following sections.

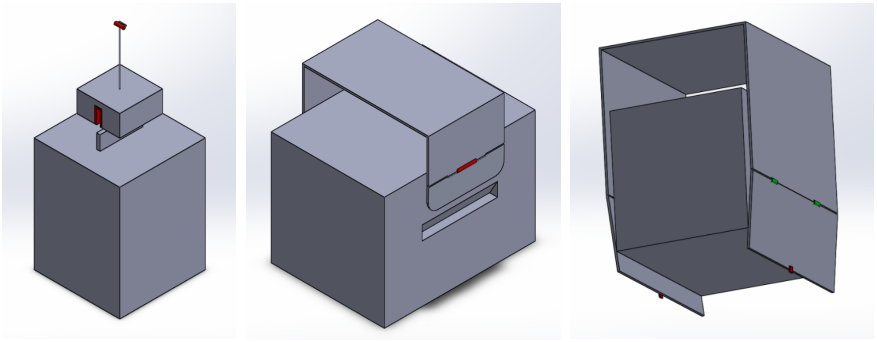

(a) Winch (b) Clasp (c) Hatch

FIGURE 12.1: Initial delivery method concepts

12.2.1 Option 1: Hovering Delivery

With a VTOL vehicle, a hovering delivery mechanism is an obvious option. Hovering keeps the vehicle from having to land at the delivery location, reducing the need for complicated sense-and-avoid schemes while simultaneously reducing the risk of injury to the customer from the vehicle itself. A hovering delivery is essentially limited to two options, dropping or winching.

- **Drop**: The vehicle hovers above the ground at some predetermined altitude and drops the package, with or without a parachute. However, a parachute is highly susceptible to even slight winds, which dramatically decreases the accuracy of the drop. Without a parachute, customer safety is compromised by packages falling through the air. Also, minimizing risk of damage to the package requires hovering closer to the ground, thus almost eliminating any of the benefits of hovering a hovering delivery.
- **Winch**: In this system, the package is winched to the ground using a thin rope cable. This is the method is shown schematically in Figure 12.1(a). This method offers a slight benefit over dropping in that there is almost no risk of damage to the package. However, the customer is likely to reach for it before it has been released and this action increases the risk of customer injury or damage to the vehicle. Furthermore, a winch system has the added complication of releasing the package, requiring additional actuators.

12.2.2 Option 2: Landing Delivery

Landing the vehicle to deliver the package presents a number of challenges, including avoiding the possibly numerous ground obstacles. Additionally, the vehicle will have to operate in much closer proximity to the customer, bringing about possible concerns for customer safety. However, landing the vehicle offers decreased energy consumption during the delivery. Since the vehicle can rest on the ground of the specified package location, it does not waste as much energy during the actual parcel drop. This also eliminates the need for a complicated winching system, which can make multiple package deliveries much more complex.

- **Clasp and Release:** Many modern day delivery UAVs has been shown to have a mechanism in which the package is held by a kind of clasp, similar to what is shown in Figure 12.1(b), which is opened to release the package upon landing. While such a mechanism is relatively simple and seems reliable, it does not easily allow for delivery of multiple, different-sized packages.

- **Automatic Door:**A final option for landing delivery involves packages leaving the vehicle through some manner of door, as shown in Figure 12.1(c). This sort of method has the advantage of enclosing the packages, allowing for an aerodynamic package housing. Furthermore, such a method seemed most adaptable to delivery of multiple packages, though the mechanism for pushing packages out was a separate consideration.

12.3 *AirEZ* Delivery Procedure

Detailed drawings of the *AirEZ* delivery mechanism can be seen in Figure 12.2 and a schematic of the delivery process is shown in Figure 12.3. Upon landing, the side door opens using a servo. Two more servos mounted at the rear of the payload bay are used to turn augers (screws) on either side of the package, similar to those found in many vending machines. The augers are aligned with tabs built in to the packing boxes, and when they rotate, the push against the tabs, forcing the package laterally out the side door. After a package has been dropped, the servos can be run in reverse so the remaining packages are shifted backward, allowing the c.g. to remain as close to the center of the vehicle as possible. Package loading can be done quickly by running the servos in the opposite direction to feed in packages in the reverse order of delivery.

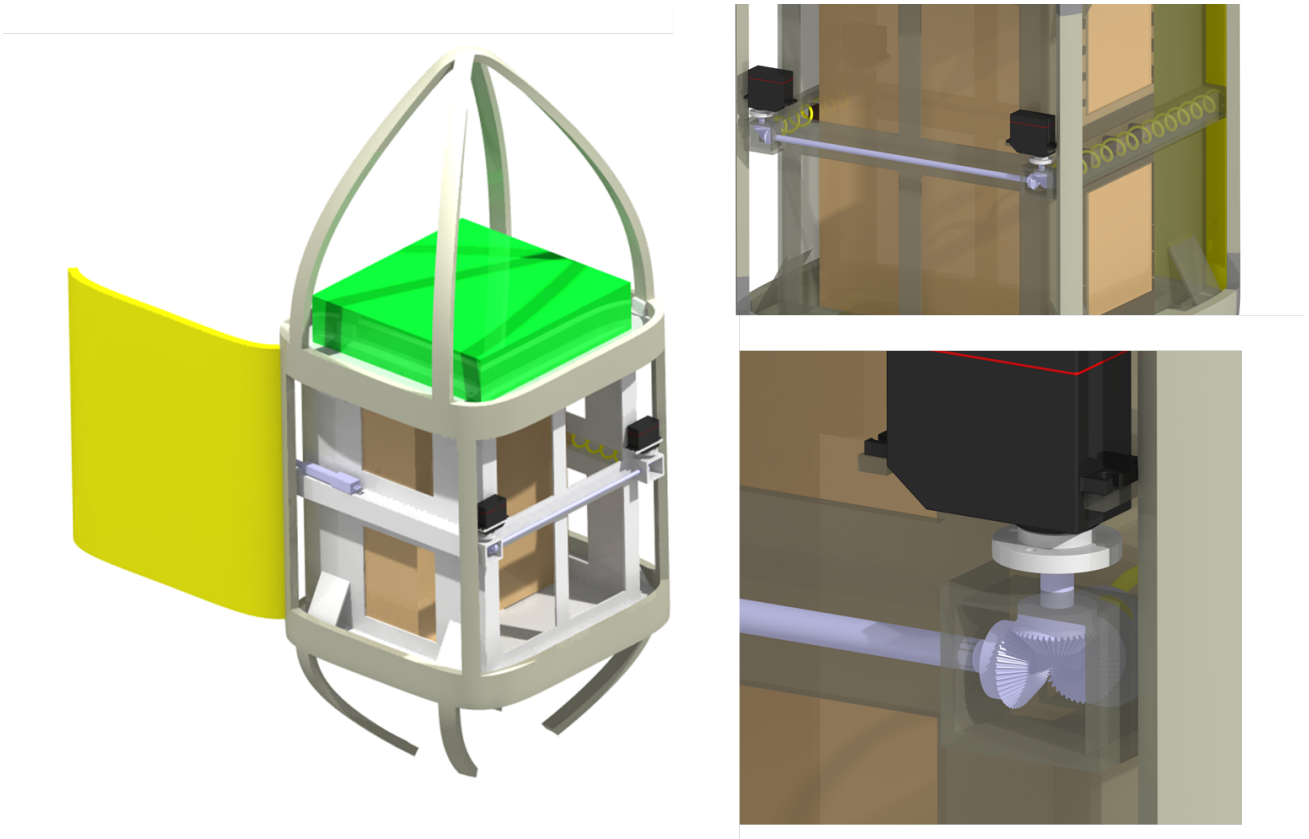

FIGURE 12.2: Delivery mechanism

12.3.1 Reliability Considerations

In order to ensure that packages are reliably delivered, some redundancies were added and small adjustments to the vehicle were made. First, the servos are back-drivable upon failure, meaning they are free to turn in the absence of power. They are also sized with enough power that, in

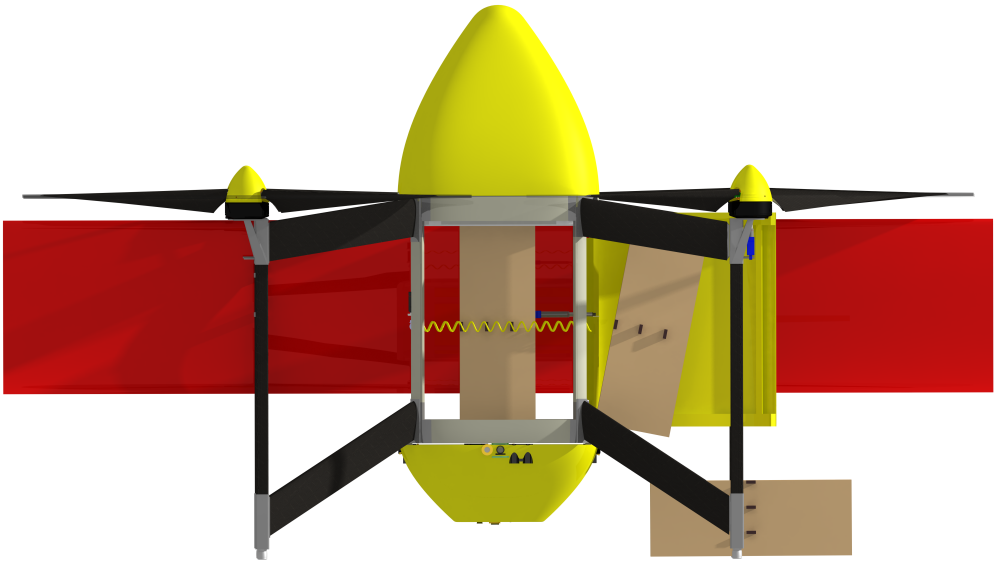

FIGURE 12.3: Delivery method

the unlikely event that one fails, the other can still operate the entire mechanism. In addition, the opening through which the packages are pushed is angled at the top to ensure parcels do not get wedged into the opening before dropping to the ground.

There was initially some concern about dropping the package from any height. However, a study in which mid-size (about 13 x 13 x 13 in), lightweight (15 lbs) packages were instrumented with sensors for measuring shock, orientation, and vibration showed that for three major carriers (UPS, FedEx, and DHL), 95% of all package drops were between 18 and 34 inches [19] during express or 2-day deliveries. Furthermore, smaller and lighter packages generally experienced higher drops. The floor of the *AirEZ* vehicle is situated 10.5 in above the ground, and since the study showed that packages routinely experience higher drops from major delivery companies, this was not seen to be an issue.

12.4 Slung Load Capability

The cargo bay dimensions for the *AirEZ* vehicle are 12x12x16 inches, sized for 90% of the packages requested, as stated in the RFP. It was desired that packages not fitting these dimensions be carried as a slung load.

Though the *AirEZ* vehicle was designed for high cruise speeds, the addition of the slung load inhibits the vehicle's ability to transition from hover to the attitude necessary for high speed flight. As a result, slung loads can only be delivered in edgewise flight. The drag penalty from the wings, the profile drag of the rotors, as well as the drag from the slung load itself, limits the maximum vehicle cruise speed to 40 knots. This speed limit will limit the allowable delivery range for the oversized packages.

The *AirEZ* system has the capability for delivering slung loads by attaching a slung load module to the landing gear and using four vehicles to jointly carry oversized packages. The slung load module would include:

- a hook to carry and release the slung load

- a servo to actuate the hook
- a transceiver to receive commands for servo actuation
- a CPU to manage all components
- a 0.1 kW-hr battery to power the components

For specified slung load delivery missions, the module is rigidly attached to each of the four landing gear stilts, where the lower struts meet the stilts, via aluminum bolts. Since it is oriented below the fuselage, the slung load module is designed to be small enough so as not to interfere with downward facing sensors. This module is installed onto four vehicles which will each help to lift the package. The oversized package is attached to each of the slung load modules with Spectra polyethylene string. The package would have mounting for the string built directly into the package box. Since the package is carried between four vehicles, it is suspended directly between the vehicles and does not obstruct the sensors, regardless of size.

As stated in item number 18 of the AHS response to questions issued on 11 March 2015, all slung load packages contribute a 2 ft^2 equivalent flat plate area to the vehicle system [20]. The inclusion of a slung load delivery module further increases the fuselage flat plate area of the vehicle by 20%. Utilizing the delivery strategy outlined above, an additional 25% of total drag is considered in order to account for interference effects. This drastic increase in vehicle drag area leads to a decrease in achievable maximum speed. Therefore, to reach delivery destinations, the vehicles, flying in edge-wise flight, must travel at low speeds. To reach a destination in gang-delivery mode, the vehicles fly at the speed for best range under these conditions, 19.5 kts. Upon delivery, the vehicles return at their design speed for best range, 32.1 kts. This mission profile allows for a maximum slung load delivery range of 30.5 miles.

Table 12.1 shows a performance and cost comparison between a system which uses this slung load delivery strategy and one that does not. Both systems are under the simple assumption that any package weight up to 20 lbs can be delivered. The simulation also sets a constraint that all that packages which are able to be delivered must reach their destination within 90 minutes.The metrics used to compare these methods are number of vehicles required (Nvehicles), percentage of packages successfully delivered, and total 3-year lifespan cost. It can be seen from the data shown that a system without slung load capability is substantially more cost efficient. While a system with slung load capabilities can increase the number of successful deliveries, it drives up the vehicle number and total system cost. For a 9% increase in success rate, the system using 4 vehicle slung load delivery requires 40% more vehicles and costs 37% more. While the consideration of slung load delivery can be beneficial in some regards, this study shows that it is not necessarily worth the trouble. Therefore, this study discourages the inclusion of such a system and will run delivery simulations without this design consideration.

TABLE 12.1: System performance comparison

System	N_{vehicles}	Success rate	Cost ($ million)
4 vehicle slung load	560	95%	151.2
No slung load	400	86%	109.8

13 Vehicle Performance Analysis

The *AirEZ* vehicle was designed to deliver packages under demanding time constraints in expansive urban environments around the globe. Since the vehicle is of a unique configuration that operates similarly to an edge-wise quad-copter and a fixed wing propeller aircraft depending on its flight mode, great care was taken to ensure that the *AirEZ* vehicle is highly efficient during both hover and forward flight. The vehicle was designed to provide desirable performance capabilities while reducing fuel consumption as compared to modern day multi-rotors. The low flat plate area of the *AirEZ* vehicle was an outcome of many innovative decisions made in its design process, notably the streamlined fuselage and low drag wings. The proprotors give superior cruise capabilities with high, responsive translational acceleration.

By offloading the lift onto the wing during transition and using the proprotors for only forward thrust, the *AirEZ* vehicle significantly decreases its power requirements in forward flight compared to a conventional quadrotor. This design feature enables it to reach a maximum airspeed of 87 kts in MSL ISA conditions. Performance calculations were conducted to determine hover ceilings for different payload weights and environmental conditions. It can be seen from these studies that the *AirEZ* vehicle has excellent performance capabilities in hover in both high altitude and high temperature environments, making the *AirEZ* delivery system deployable to numerous geographical settings. Forward flight performance calculations were carried out taking into consideration propeller and electric motor efficiencies as well as power required for avionics and sensor actuation. The calculations showed that the *AirEZ* vehicle has highly desirable performance capabilities, making it the ideal rotorcraft for large-scale urban environment package delivery.

13.1 Drag Estimation

To minimize the fuel requirements of the *AirEZ* vehicle during package delivery, significant attention was given to reducing the drag of the entire vehicle. This section discusses the necessary modifications implemented on the *AirEZ* as a result. The preliminary sizing of the *AirEZ* vehicle was performed using a relatively large parasitic drag area of 0.75 ft^2, estimated for a quadrotor biplane with a rounded fuselage carrying a payload of the 90^{th} percentile package volume. To minimize the drag of the *AirEZ* vehicle, a streamlined fuselage design was designed. Chapter 11 describes the *AirEZ* vehicle fuselage shape in more detail, which allows for a reduction in the overall vehicle drag. The aerodynamic fuselage design made carrying such a large payload bay feasible thus making the *AirEZ* vehicle a revolutionary unmanned aerial vehicle.

The parasitic drag of separate vehicle components was estimated using methods presented by Raymer [21]. The total parasitic drag was determined by considering each component separately and later aggregating the drag calculations. The equivalent drag area of each component was calculated as the product of its wetted area, skin friction coefficient, interference factor, and form factor. The values for component skin friction coefficients, which are functions of both Reynolds and Mach numbers, were calculated at MSL ISA conditions and a cruising airspeed of 55 kts. Table 13.1 shows the component breakdown of the equivalent parasitic drag area for the *AirEZ* vehicle. Equivalent areas for the multiple components were calculated from vehicle drawings used in conjunction with formulas from Raymer. An additional factor of 20% was then added to the total as recommended by Prouty [22] to account for the interaction effects between different constituents of the vehicle body. Table 13.1 shows that the predicted flat plate area

of the *AirEZ* vehicle is 0.62 ft^2, which is 34% lower than the initial highly conservative sizing assumption, allowing for far greater vehicle cruising speeds. From the table, it can be seen that the fuselage is the main contributor to vehicle drag and as such, special care was taken to reduce this drag through its aerodynamic design.

TABLE 13.1: Vehicle Component Equivalent Flat Plate Areas

Component	Flate Plate Area (ft^2)	Percentage%
Fuselage	0.444	86.05
Wings	0.003	0.58
Landing Gear	0.016	3.10
Struts	0.009	1.74
Nacelles	0.045	8.72
Total	0.516	100.00
120%	0.619	–

13.1.1 Fuselage Drag Calculations

To properly size the vehicle's drive and power systems, the drag calculations over the entire body in flight and individual constituents were critically analyzed. As shown above in Table 13.1, the vehicle fuselage was a main concern for drag estimates, as it comprised the largest flat plate and wetted areas of the entire *AirEZ* vehicle. Using the prescribed areas based on the fuselage design and CAD drawings, an accurate drag calculation was made. The Raymer [21] build-up method was utilized to determine the skin friction drag coefficient of the fuselage. This was then used in conjunction with a Hoerner form factor [23] to determine the parasitic drag on the vehicle fuselage.

The analysis led to a C_{d_0} of 0.244 for the fuselage, which is equivalent to a 5% reduction from the initial sizing guess, which results in a superior performance throughout the entire mission profile. This decrease in drag was achieved via the design detailed in Chapter 11, which included increasing fineness ratio and decreasing fuselage cross sectional area.

13.2 Hover Performance

The *AirEZ* vehicle, which is designed for high-speed and long-range flight, requires only 33% of its installed power to hover out of ground effect at MSL ISA. This significant hover power margin implies that the *AirEZ* vehicle is capable of hovering at high density altitudes or while carrying heavy payloads. Figure 13.1(a) shows a maximum hover ceiling of 8,300 ft at MSL ISA conditions. A high ceiling of this magnitude proves that even operating at maximum height as specified by the FAA (500 ft above ground level), such a vehicle would be deployable in any urban environment across the United States. The ISA+40° C condition corresponds to 135° F at sea level. Although the capability to hover at high altitudes and high temperatures does not necessarily apply to the *AirEZ* vehicle intended usage for package delivery in many US markets, it highlights the versatility of the aircraft. These vehicle abilities allow for operations at high-altitudes in mountainous regions or high-temperatures in hot regions. This also makes the *AirEZ* vehicle ideal for deployment as an emergency payload delivery system in hot, high-altitude, and dangerous environments for both civil and military applications. The maximum hover ceiling as a function of gross weight is shown in Fig. 13.1(b). This shows that the *AirEZ* vehicle is capable of operating at gross weights higher than its design takeoff weight. At MSL

ISA conditions, the *AirEZ* vehicle's proprotors are fully capable of lifting the GTOW of the vehicle plus an additional payload of 16 lbs.

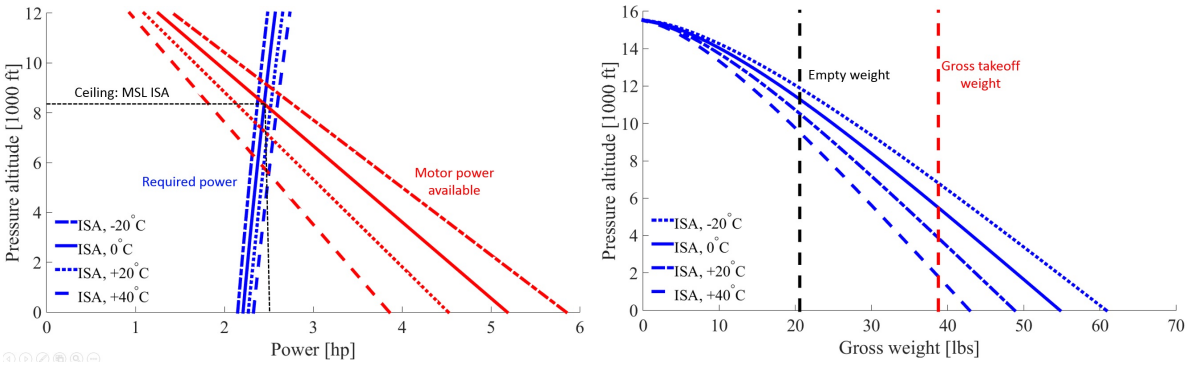

(a) Hover ceiling

(b) Hover power at design takeoff weights

FIGURE 13.1: Hover performance

13.3 Forward Flight Performance

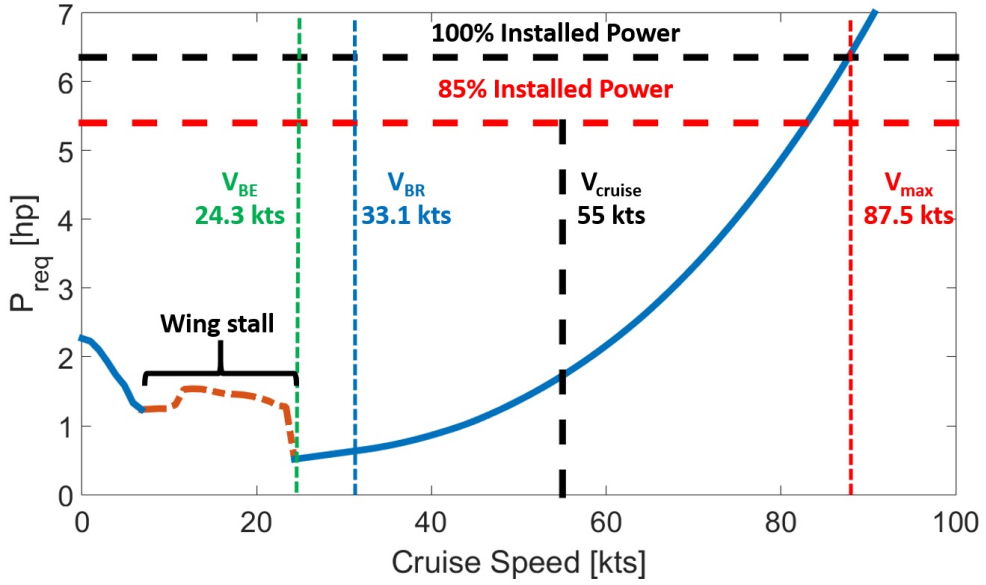

FIGURE 13.2: Vehicle power curve

One of the merits of the *AirEZ* vehicle is its lift augmentation system. Figure 13.2 shows the power required by the *AirEZ* vehicle as a function of airspeed. For a large range of forward flight speeds the proprotors require less power than they do in hover due to the lift from the wings of the vehicle. The wings have been sized to carry the entire weight of the vehicle during cruise, and therefore, the proprotors must simply overcome vehicle drag during this flight mode. This requires a lower thrust than hovering which allows the vehicle to fly faster than an edge-wise flying multi-rotor vehicle.

The power curve shown in Fig. 13.2 was generated by considering the equations of motion from full nonlinear vehicle dynamics. These motion equations were evaluated for the trim condition

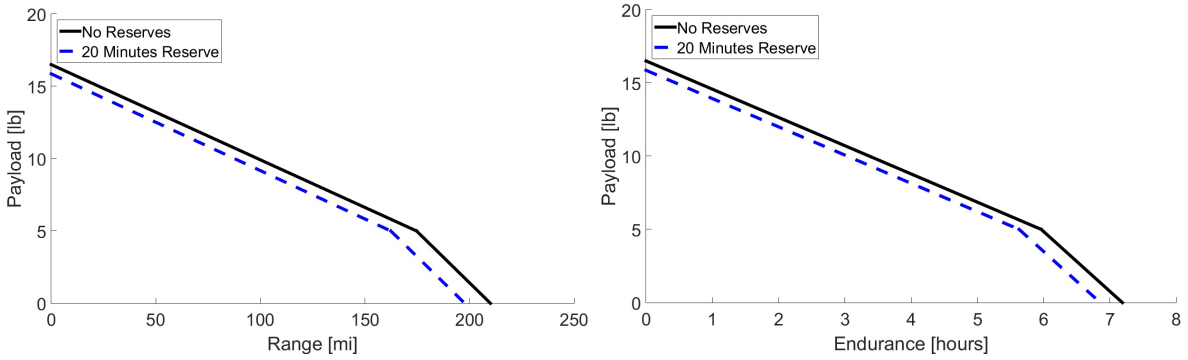

(a) Range versus payload weight

(b) Endurance versus payload weight

FIGURE 13.3: Range and endurance plots

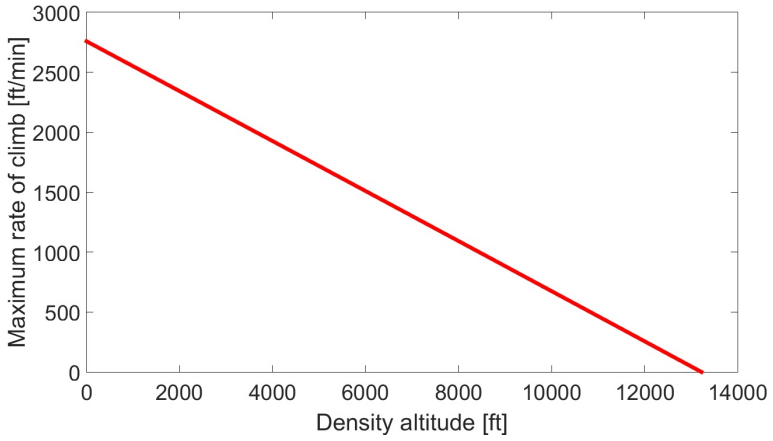

FIGURE 13.4: Max climb rate versus altitude

in every state of transition to output rotor RPM and vehicle power required for every climb angle. More details can be found regarding the power curve in Section 15.1.2. As shown in Fig. 13.2, the *AirEZ* vehicle can reach a forward speed of 83.0 kts at 85% maximum power, which it reaches when flying through heavy headwinds of 30 kts. At maximum installed power, the vehicle can achieve an airspeed of 87.5 kts; although this speed is not expected to be reached during the mission profile, the extra power margin improves the aircraft's maneuverability and heavy gust tolerance. As shown by the curve in Fig. 13.2, the speed for best endurance is 24.3 kts and the speed for best range is obtained at 32.1 kts. The maximum range and endurance of the *AirEZ* vehicle on a 12 lb battery pack in MSL ISA conditions, as shown in Fig. 13.3, are 210 miles and 7.2 hours respectively. With 20 minutes of reserve battery life accounted, those values fall to 198 miles maximum range and 6.9 hours maximum endurance.

The vehicle climb rate as a function of altitude can be seen in Fig. 13.4. A maximum value of 2,750 ft/min can be achieved at sea level in ISA conditions due to the high installed power on the vehicle. The service ceiling is shown to be12,700 ft while the vehicle's absolute ceiling is found at 13,200 ft. Figure 13.5 shows the load factor versus flight speed for the *AirEZ* vehicle in fixed wing mode. The vehicle can endure a maximum load of 3 g's when pulling maneuvers, which is an outcome of the sizing of the wings.

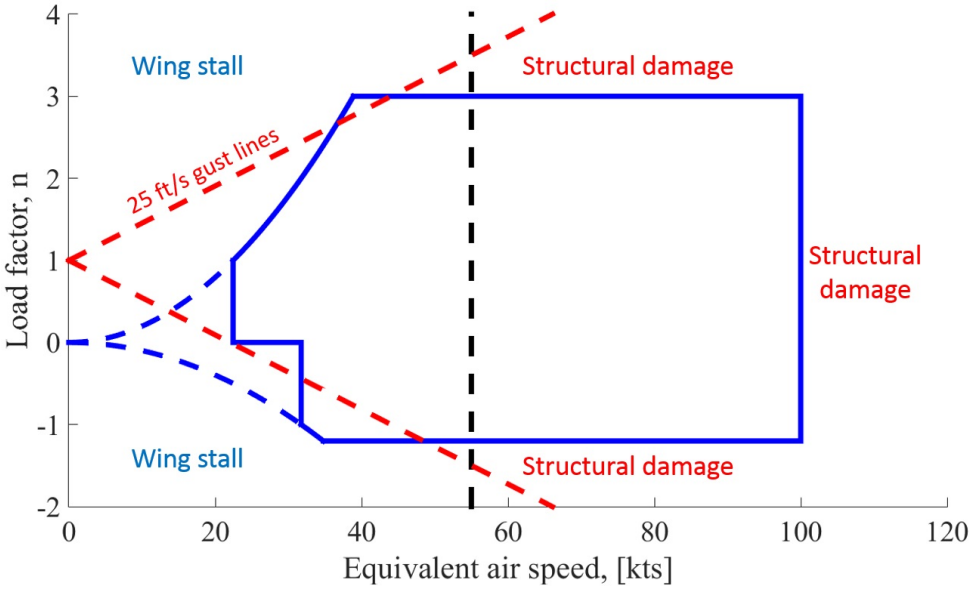

FIGURE 13.5: Forward flight V-n diagram

13.4 Autorotative Capability

A vehicle's ability to autorotate is affected by many variables, including vehicle lift to drag ratio and total kinetic energy stored in the rotor. A variety of autorotational indices (AI) have been quantified in an effort to compare the ability to perform an autorotational maneuver. The Sikorsky autorotative index (AI), represented as $AI = I_R\Omega^2/(2WDL)$ [24], is a ratio between the kinetic energy ($I_R\Omega^2$) stored in the rotor, the weight of the helicopter (W), and the rotor disk loading (DL). Multi-engine helicopters with an AI of 10 or above have been proven to have acceptable autorotational characteristics, with an AI of 5 being unacceptable. The *AirEZ* vehicle has an AI of 10.2, which is far above the lower boundary of 5.

14 Avionics and Sensors

The main goal of the sensors and avionics suite is to support robust autonomy for each vehicle within the system of systems. By expanding the autonomy of each vehicle, the delivery system will be faster, safer, more reliable, and less expensive to operate. A fully autonomous aerial vehicle demands a state-of-the-art sensor system to support delivery missions in a variety of uncertain environments with minimal human interaction. The avionics and sensor system on board the *AirEZ* vehicle is designed to provide a full situational awareness in these situations while minimizing power, weight, and cost.

14.1 Sensor Mission Requirements

The delivery mission introduces a series of challenges for delivering a package from the central warehouse to the customer such as: long travel distances, narrow urban canyons to navigate, possible loss of GPS signal, and a variety of ground obstacles including powerlines. The mission is divided into two key phases with unique sensor requirements

1. Navigating to the customer in cruise phase

2. Sense-and-Avoid during landing and take-off phase

In high speed cruise, the *AirEZ* vehicle needs a deployment strategy and sensor system that can support localization in the global frame while enabling efficient collision avoidance. The second mission phase occurs near the ground in cluttered urban environments, requiring a comprehensive sensor suite that can provide simultaneous spatial mapping of the surroundings.

A survey of current state-of-the-art sensor systems has been conducted and each technology has been evaluated against the specific requirements of the *AirEZ* vehicle. By selecting a complementary combination of technologies, the inherent strengths of individual components have been used to form a mutually supportive system with enhanced capabilities and built-in redundancies. The resulting sensor suite is a comprehensive and versatile system that is ready to meet the challenges of long-distance flight and urban operations.

14.2 Sensor Technology Overview

In developing the *AirEZ* avionics package, a study of the state-of-the art was conducted and relevant technologies reviewed based on the unique requirements of the delivery mission.

Global Positioning Systems have formed the mainstay of navigation systems since their development. Using time and location information from orbiting satellites, GPS receivers provide position estimates within 10 ft on the Earth's surface. GPS based systems play a key role in the cruise phase of the *AirEZ* mission as will be described in a following section.

Monocular Vision, IMU Fusion was selected as one of two primary obstacle sensing and avoidance methods during low-level operations. It offers the best sensing advantages with low vehicle weight and system acquisition cost. Monocular vision, IMU sensor fusion is a state-of-the-art SLAM technique which uses a single camera and the motion of the vehicle to generate depth maps as depicted in Figure 14.1 [25]. As the vehicle moves, motion data from the IMU is used to track features between camera frames. Since the vehicle distance traveled between frames can be measured, the locations of features between multiple images can be triangulated. This is an effective and computationally efficient SLAM method that has been proven through autonomous quadrotor landings using only a smartphone processor [25].

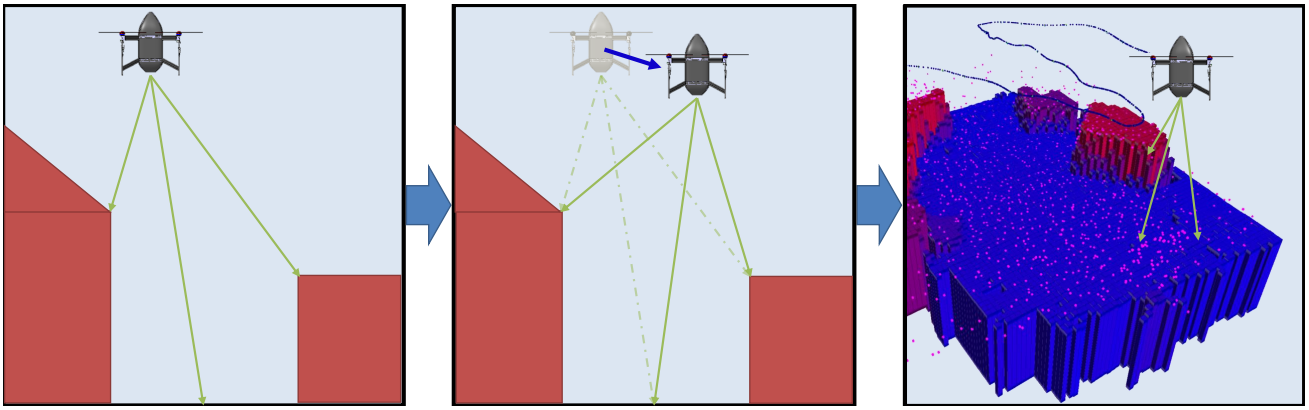

FIGURE 14.1: Monocular-IMU Operational Concept. Features are tracked in the camera frame as vehicle motion is tracked by the IMU. The location of the features in the frame are compared to the distance traveled by the camera and a depth map is computed.

However, visual-based obstacle avoidance requires sufficient ambient lighting. As the delivery time period is assumed to be between 9 am and 7 pm each day, the *AirEZ* system will need to operate in darkness, requiring the strengths of multiple sensor types have to be combined within the sensor package.

Infrared "Time-of-Flight" (ToF) Sensors utilize a combination of infrared cameras and infrared pattern projectors and are chosen as the second main obstacle sensing system. Pulses of IR light are generated and the time taken to reflect back to each individual pixel is measured. Since the resolution is based on the number of pixels in the camera, spatially dense maps can be generated. ToF depth sensors can also filter out ambient IR light between light pulses and are effective in both daytime and low-light conditions. Furthermore, depth is computed using time rather than stereo triangulation so IR camera and emitter pairs can be positioned close together. These factors make ToF sensors versatile, compact and lightweight solutions but with limited ranges of approximately 15 ft, other sensing modalities are still needed in the package.

Thermal Imagers detect long-wave infrared heat signatures. While this is a useful capability for detecting warm bodies in reduced visual scenarios, thermal imagers offer poor resolution. Additionally, if the thermal signature of an obstacle is not significantly different than the background, then it cannot be detected.

Ultrasound Sensors were considered for the main sensor suite since they are inexpensive, lightweight, and simple to implement. They also work regardless of lighting conditions and can penetrate rain and fog. However, they have limited range (10 ft) and only one object can be detected for each ultrasonic range finder. Alone, ultrasonic sensors, would not be able to provide the detailed mapping needed in complex environments but are useful when augmenting other higher resolution systems.

LiDAR systems traditionally use a rotating laser rangefinder to measures depth at multiple points in a disk around the sensor. Laser rangefinders have long detection ranges (90 - 210 ft) but very limited fields of view, requiring additional mechanisms to sweep the module to generate 3-dimensional maps. As such, LiDAR systems commonly used in ground robotics are heavy (approx. 1 lb), expensive ($4,000 - $8,000) [26, 27], and power intensive (12 W) compared to emerging visual SLAM techniques. By using a simple and lightweight non-rotating *LiDAR Lite* system on the *AirEZ* , long-range detection capability of laser rangefinders is leveraged to augment other sensor types without the associated disadvantages of traditional rotating systems.

Structured Light Depth Sensors (e.g. Microsoft Kinect and Asus Xtion) [*rejected for size and poor sunlight tolerance*] use infrared cameras and pattern projectors. Instead of pulsing IR light, the cameras are spaced apart like stereo cameras in order to generate a depth map. The distorted dot pattern is reflected off of objects and captured by the IR camera. By comparing the captured pattern to the projected pattern, a depth map can be obtained. This type of sensor cannot function outdoors as sunlight obscures the IR pattern. The effective resolution of structured light sensors is also relatively low since it depends on the number of dots used in the emitted pattern.Furthermore, these sensors tend to be large and bulky due to the spacing of the IR projector and camera which could complicate integration in to the vehicle.

Stereo Visual [*rejected for high processor bandwidth requirements*] cameras determine the distance to objects similarly to human vision in which features in the the left and right camera image are matched and triangulated. The advantage of stereo cameras is that each camera is less expensive ($50) and lighter-weight (<1.4 oz) compared to other sensors. However, stereo vision mapping is computationally expensive since two images need to be digitally processed

simultaneously. This issue is exacerbated by the need for multiple stereo sensor heads on the sides of the vehicle to sense incoming obstacles from multiple directions.

Qualitative results of relevant sensor technologies are summarized in Table 14.1 as a Pugh Decision Matrix that evaluates the relative strengths and weaknesses of each sensor system and weights each option using an overall metric.

Criteria	Weight	Meaning	Ultrasound	Structured Light	Infrared "ToF"	Thermal Imager	LiDAR	Stereo Visual	Mono-Visual, IMU Fusion
Resolution	10	How small of an object can be seen at a given range	1	3	3	2	5	3	3
Range	10	How far away can an object be detected	2	1	2	5	3	5	5
Weight	9	Less is better	5	2	4	5	1	4	4
Cost	8	Monetary Cost	5	2	2	1	1	2	3
Customer Recognition	7	Can the delivery zone be recognized	1	2	2	2	2	5	5
Environmental Tolerance	6	How well it works in different lighting, rain, fog, snow	5	1	4	3	2	2	2
Implementation Complexity	6	Ease of integration into the vehicle	4	2	3	4	2	2	3
Computational Complexity	5	Algorithm complexity and power consumption	5	3	3	4	3	3	4
Total			**201**	**121**	**173**	**199**	**150**	**206**	**225**

TABLE 14.1: Pugh Matrix of Different Sensor Options (5 is Most Effective, 1 is Least Effective)

14.3 Final Sensor Package

As discussed in the previous section, no single sensor can can provide complete situational awareness in every environment and in every scenario. To meet the requirements of the *AirEZ* vehicle, a sensor suite which fuses the strengths of visual, infrared, laser, and ultrasonic sensors was designed. Figures 14.2(a) and 14.2(b) provides an overview of the sensor configuration and placement.

A pair of Odroid-XU3 Lite computers serve as flight managers while also executing computationally intensive tasks such as running visual SLAM and path-planning algorithms for navigation. These are full-scale PC grade computers each with two quad-core processors (1.8 and 1.3 Ghz) but scaled down to only 3.7in x 2.8in x 0.7in and 2.3 oz. The main computers provide USB connections to interface with the monocular cameras.

Matrix Vision mvBlueFOX Cameras are used to implement the vision based obstacle avoidance technique described in the previous section. The mvBlueFOX is an Aptina MT9V034 sensor-based camera with a global shutter rather than a rolling shutter. This allows it to capture the entire frame at once, avoiding motion blur that creates erroneous depth maps. The camera combines a high frame rate (90 fps) with high resolution (752x480-pixel) for quickly and accurately mapping the area within its field of view. Four cameras surround the vehicle while one faces forward from the nose and another one is oriented downwards towards the landing gear.

A SoftKinetic DS536A "Time-of-Flight" (ToF) IR depth sensor was selected to supplement the mapping and data collected by the vision-based system. The ToF depth sensor lacks the long range of the visual system but is critical at night since it operates well in low-light conditions.

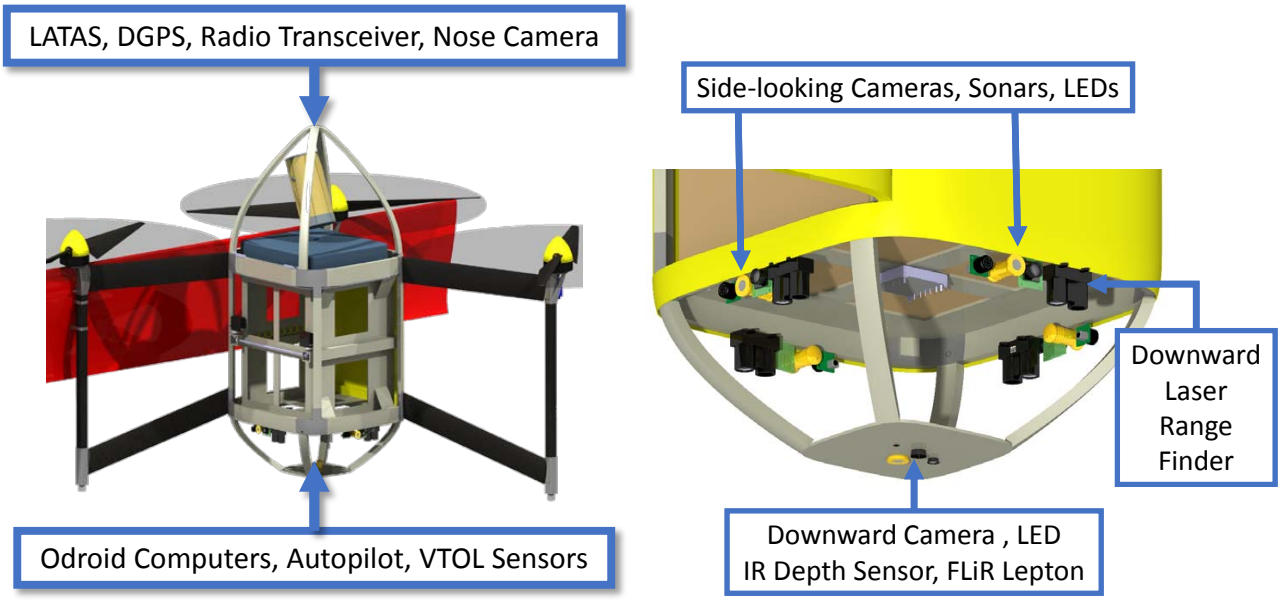

(a) Sensor layout in helicopter mode

(b) Bottom view of sensor layout

FIGURE 14.2: General Sensor Layout

A FLiR Lepton thermal imager is integrated into the bottom of the *AirEZ* vehicle to aid in the detection of heat signatures from warm bodies at night. The FliR Lepton was chosen for its small size (0.5" x 0.5") and light weight (0.1 oz). The thermal signatures captured by the FLiR Lepton are fused with the local depth map on the landing manger to provide an additional modality that senses obstacles such as people or animals.

LiDAR-Lite Laser range finders with a 130 ft detection range are positioned on the bottom of the *AirEZ* vehicle pointing downward. By spacing 4 laser range finders around the periphery of the fuselage, the landing manager can estimate a ground slope based on the difference in range readings between each of the range finders. Furthermore, the range finders serve as a backup for emergency landings if both the visual camera and ToF depth sensor malfunction or become occluded and cannot resolve height above obstacles.

LVMaxSonarEZ0 ultrasonic range finders were integrated into the *AirEZ* vehicle next to each side camera to add an additional sensing modality. that is particularly important in poor visual conditions.

Fenix E35UE high intensity LED lights were selected for the *AirEZ* vehicle due to their small size and weight. Each provides 900 lumens and approximately 160 ft effective range (as reference, low beams on a car are typically 880 lumens and 150 ft [28, 29]). The downward camera and side cameras are each paired with LED (total of 5) to support visual detection in low-light conditions. The lights will also allow the *AirEZ* vehicles to be easily seen by other *AirEZ* vehicles and people on the ground

NASA / PrecisionHawk LATAS is a small (3x2x1 inch), lightweight (3.9 oz) cellular network (GSM) based communications device which allows for real-time location tracking of each vehicle. This system is described in a following section.

A MicroPilot MP2128^{g2} autopilot is used for low-level flight control and provides velocity, altitude, position and attitude data at a rate of 200 Hz for sensor fusion.

14.4 Navigation During Cruise

In forward flight, the *AirEZ* vehicle uses precise localization and path planning to navigate to a specific customer while avoiding obstacles.

14.4.1 Altitude Segregation Strategy

The vehicle cruises at approximately 55 knots, making flight near ground level impractical in urban environments. A safer strategy is to cruise only at a defined altitude above the majority of buildings. Since the delivery area can be mapped a priori, tall buildings and obstacles can be designated as no-fly-zones which all path planners can avoid.

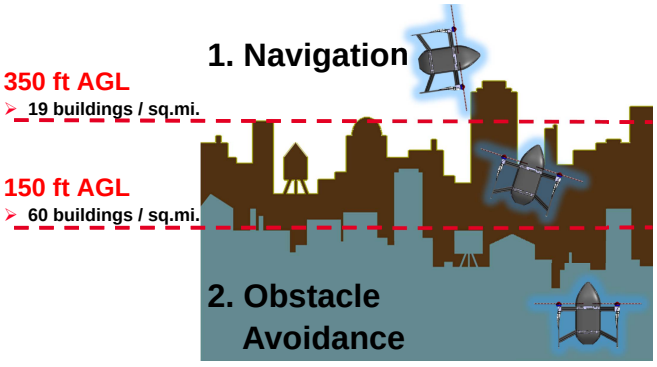

FIGURE 14.3: Representation of Altitude Segregation Strategy

This strategy was developed using urban building height distribution data from an MIT study [30]. Building height distributions in the densest parts of three representative cities (Los Angeles, Phoenix, and Salt Lake City) were categorized and used to generate worst-case estimates on building height in the *AirEZ* urban delivery environment depicted in Figure 14.3. It was determined that there are approximately 60 buildings/sq. mi. taller than 150 ft and 20 buildings/sq. mi. taller than 350 ft in the city's core. Assuming 2,500 sq. mi. of delivery area, this translates to 150,000 buildings taller than 150 ft and 50,000 buildings taller than 350 ft. Based on these worst-case estimates that do not account for low-rise residential areas, 150,000 still represents a feasible number of data points to be stored as no-fly-zones in a map on each delivery vehicle.

14.4.2 Differential Global Positioning System (DGPS)

In order for the *AirEZ* vehicle to precisely deliver to customers and avoid known obstacles, it must be able to sense its position on the map to within 10 ft. To provide enhanced map awareness, the *AirEZ* vehicle will use the Differential GPS (DGPS) receiver on the Micropilot MP2128^{g2} autopilot. DGPS enhances accuracy by utilizing a nation-wide network of ground stations which correct for satellite errors. With DGPS, the *AirEZ* vehicle can locate its position with an accuracy of 3 ft [31].

14.4.3 Low Altitude Tracking and Avoidance System (LATAS)

To support airspace control and provide a redundant positioning system, the *AirEZ* vehicles will employ the Low Altitude Tracking and Avoidance System (LATAS), in development by NASA and PrecisionHawk [32]. LATAS is a cellular network (GSM) based communications device which provides real-time location tracking of each vehicle. It is a small (3x2x1 inch), lightweight (3.9 oz) module, making it easy to integrate into the avionics suite. To provide positioning redundancy, the LATAS module also has an independent GPS to be used in the event that the autopilot DGPS malfunctions. Additionally, LATAS further enhances vehicle localization accuracy by triangulating between cell towers to correct GPS error. Using cell tower

triangulation in conjunction with GPS, the *AirEZ* vehicles can determine their position with sub-meter accuracy [33]. By providing a form of air traffic control, the LATAS module is crucial for safety and redundancy for the *AirEZ* vehicle in forward flight navigation.

14.4.4 Forward Looking Camera

Though each *AirEZ* vehicle will have a stored map of known obstacles (i.e. buildings over 150 ft.), unmapped obstacles like construction cranes may still exist at cruising altitude. As an added measure for safe navigation in forward flight, a forward-looking, wide angle camera is integrated into the nose cone. This camera will interface with a flight management computer to visually process the images with Canny edge detection and search for large obstacles with efficient Haar classifier algorithms [34]. If there are low-light conditions, the exposure time on the camera is automatically increased to take-in more ambient city lighting for obstacle detection. The the images captured by the forward camera are compared to a database of typical obstacles at cruising altitude. If a large obstacle is detected, the flight manager will issue a turning maneuver to the autopilot and update the path planner with waypoints around the obstacle, represented in Figure 14.4.

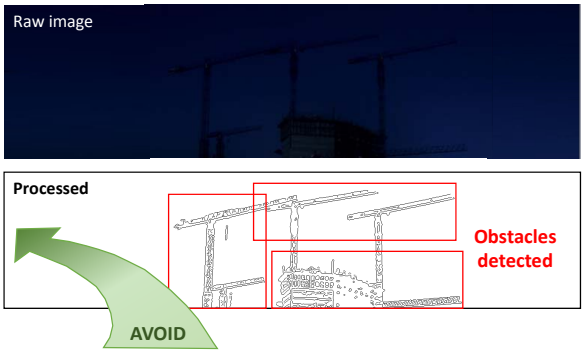

FIGURE 14.4: Forward Flight Obstacle Avoidance with Canny Edge Detection

14.5 Sense-and-Avoid During Landing and Take-Off

During the landing phase, the *AirEZ* vehicle will be descending from approximately 150 ft AGL. Below this altitude, the flight environment becomes cluttered with obstacles and the aircraft may loose GPS reception. At present, it should be noted that Amazon and Google have not released the exact details of how sensors will be integrated into their systems to provide autonomous obstacle avoidance [35, 36].

The *AirEZ* vehicles use separate arrays of side-looking and downward-looking sensors to map the volume around it. Mounting one array on a 2-axis, 360^o rotating gimbal for lateral sensing was investigated but decided against because visual sensing is most accurate when camera is rigidly attached to the airframe. The landing struts and wings would also restrict potential viewing angles and limit the benefits of a mechanically complicated gimbal system.

14.5.1 Finding the Specific Customer

Though the *AirEZ* vehicle can navigate to the GPS location of the customer's home, a safe landing zone needs to be distinguished from roads, yards, and houses. To ensure the *AirEZ* vehicle delivers the package to the correct location, a pre-flight procedure at the warehouse is implemented as follows:

1. The customer order and address is received at the central warehouse.
2. The central management computer references the the address to a GPS location and image of the customer location via a satellite imagery database (Google Earth).

3. The central computer runs image processing algorithms (Canny edge detection and expansion) to determine probable primary and secondary safe landing zones.
4. The reference image (Fig. 14.5) of the customer's home with landing zone identifiers is uploaded to the *AirEZ* vehicle via WiFi as it is being loaded.

Once at the approximate GPS location of the customer, the AirEZ drone will utilize the downward facing sensor system scans the area, capturing visible-light and thermal intensity information. In daytime operations, thermal intensity affords the vehicle more information to help it differentiate between areas of water and areas of grass or tarmac. In night time or low visibility conditions, variations in temperature between buildings and the ground will allow areas of probable landing zones to be identified. The vehicle will compare its own landing map against predictions made by the central computer. Once consensus between both mappings has been reached, the vehicle will guide itself to the largest regions of clear space and begin the landing sequence.

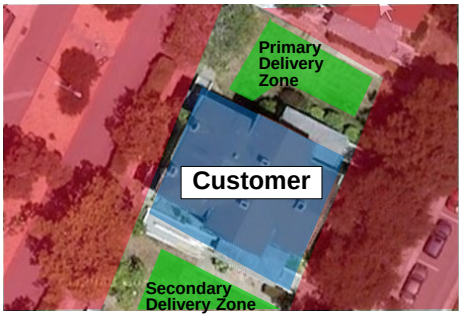

FIGURE 14.5: Example of a delivery zone reference image for specific customer recognition.

14.5.2 Vertical Obstacle Detection

The majority of the sensor package is oriented downwards to support the most challenging phase of the mission. Obstacles such as trees, powerlines, houses, and people will need to be accurately mapped and avoided.

Depth information from the ToF senor is fused with the camera-IMU depth map and the thermal signatures detected by the FliR sensor, generating a comprehensive obstacle map during landing. In good light conditons, these systems can provide high resolution 3D maps over a large volume and support higher descent rates. In poor light conditions, the vehicle will rely on the ToF sensor and descend at a lower rate to compensate for the shorter visual range.

In all lighting conditions, the spatially distributed laser range finder system provides the landing manager with basic altitude estimates. These measurements serve to improve the overall accuracy of the system while providing a fail-safe if the visual sensors fail.

14.5.3 Lateral Obstacle Detection

Side-looking monocular cameras are mounted on each side of the fuselage as seen in Fig. 14.2(b). These provide the *AirEZ* vehicle with sensor coverage on all sides when in helicopter mode. The data from these cameras supplements the local 3D map generated by the downward-facing sensors and enables the detection of moving obstacles which might approach the vehicle from outside of the frame of the downward camera [37]. To compensate for the added computational load of the visual processing from the side cameras, the second Odroid-UX3 Lite computer is used to interface with the cameras.

Each side-looking camera is paired with an Ultrasonic range finder. Since the ultrasonic sensors have limited range ($\tilde{1}0$ ft) they serve as a last resort "bumper" sensor in the event that the an obstacle is not detected by the side cameras due to poor lighting conditions or low visual contrast in poor visual environments.

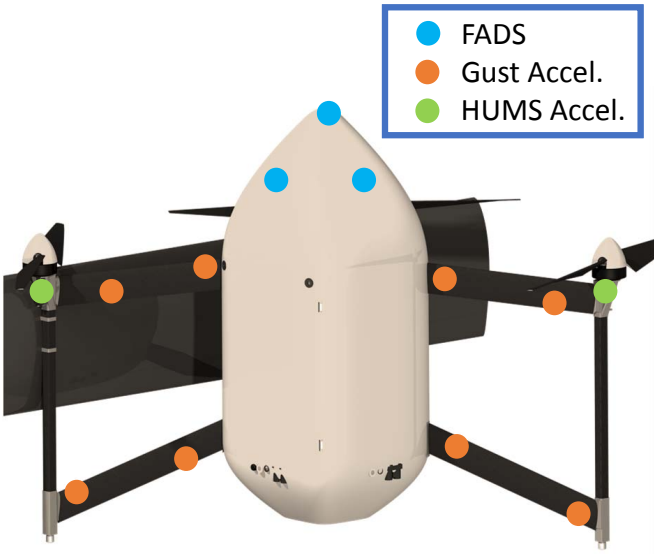

FIGURE 14.6: Layout of Supporting Flight Instrumentation

14.6 Supporting Flight Instrumentation

The *AirEZ* mission requires additional instrumentation to support the autonomy requirements that are unique to the *AirEZ* delivery fleet. An expanded flow-disturbance sensing system supports flight operations in unknown flow environments and an on-board health monitoring system that predicts vehicle failures in between service intervals.

14.6.1 Flow Measurement System

The delivery mission profile requires the *AirEZ* vehicle to cruise, hover and transition in potentially gusty flow environments. External disturbances can severely disrupt operations, requiring additional flow sensing systems to support flight control.

14.6.1.1 Flush Air Data System (FADS)

The *AirEZ* vehicle requires wind-vector information across a wide range of conditions between hover and cruise. Conventional pitot-static and multi-hole probes are effective solutions but protrude from the vehicle and could easily cause disruptions in a busy warehouse during battery changes and cargo loading. Instead, a Flush Air Data System (FADS) is integrated into the nose of the *AirEZ* vehicle. FADS uses distributed, flush pressure ports on the the nose of the *AirEZ* vehicle to measure airspeed as well as angle of attack and sideslip angle. FADS configurations have been successfully implemented on the F-18 for measuring airspeed at up to $\alpha = 80°$ and are also suitable for micro air vehicles[38].

On the *AirEZ* vehicle, five 0.076" diameter pressure ports are distributed around the nose (one close to the nose center and one for each side). The center port is split between four differential pressure transducers and each side port is connected to one transducer. The pressure on the sides is referenced to the center port pressure to determine airspeed and air flow angle. In helicopter mode, the side pressure ports also act as an orthogonal airspeed probe, providing measurements of flow speed in the rotor plane.

14.6.1.2 Gust Rejection Accelerometers

To aid in the bio-inspired gust attenuation (see Stability and Controls Analysis Section), 16 ADXL345 3-axis Digital Tilt Accelerometers are embedded throughout the *AirEZ* vehicle structure. These are small (1" x 0.5") and lightweight (0.05 oz) enough to not affect the structure of the vehicle. The accelerometers are placed at arbitrary, non-collinear locations in the *AirEZ* to enhance gust attenuation.

14.6.2 Health and Usage Monitoring System (HUMS)

The demanding flight hours which the *AirEZ* vehicle is subjected to makes it imperative to diagnose problems before they cause failures in flight. The Health and Usage Monitoring System (HUMS) continuously determines the status of flight critical systems, such as the rotors, to determine the system's overall health.

14.6.2.1 Rotor Track and Balance (RTB)

The HUMS system can perform rotor track and balance to predict rotor failure by analyzing 3-axis accelerometers that are placed on each motor mount. The accelerometers measure the vibration frequencies from the rotors and sends the signal to an ARM Cortex microprocessor. The microprocessor analyzes the vibrations with a fast Fourier transform (FFT) algorithm to determine anomalies in the rotor frequencies. The processed accelerometer data is compared to a database of potential risks and failure modes that is compiled during the flight testing portion of aircraft development. If the measured data matches the recorded failure mode behavior, the HUMS microprocessors can send an alert signal to the on-board flight manager computer. Depending on the severity of the alert, the flight manager can notify the ground crew at the warehouse that maintenance is needed, or it can issue an emergency landing command before the actual failure occurs. This analysis occurs in real-time and has the potential to dramatically improve aircraft safety.

14.6.2.2 Voltage Monitoring

A key feature of the MP2128^{g2} autopilot is its built-in voltage monitoring capability. This allows the autopilot to automatically monitor the battery's health in real-time and calculate estimated remaining flight time. In the rare event that the estimated flight time is less than the predicted time to return to the warehouse, the flight manager computer will issue a return to base command. If the autopilot detects that the voltage has dropped below the minimum critical level, then an emergency landing will be initiated before a complete power failure occurs.

14.6.2.3 Data Recording

The MP2128^{g2} also has a built-in data logger for basic flight information . The data recorder tracks all attitude readings, control outputs, airspeed, flight time, altitude, and battery voltage. These data are then stored and transmitted to the maintenance crew for post-flight analysis at the warehouse. Crews can analyze trending data such as battery discharge rates over multiple flights and diagnose any abnormal flight behavior.

14.7 Communications

The large 50 mi x 50 mi delivery area represents a challenge for maintaining communication links between the *AirEZ* vehicles and central management system. With a maximum possible

distance of 35 mi between an *AirEZ* drone and the central warehouse, a single direct radio communications link to the central management computer is not feasible or reliable. A single link to the central warehouse would require a large satellite or radio transceiver that would be too heavy (6 lbs for Heli-Coder 4 (HC4) COFDM Downlink Transmitter) for the *AirEZ* vehicles to carry efficiently. Fixed ground nodes could be placed throughout the delivery area to relay the signal, but that would incur additional rental and maintenance cost for remote stations. Instead, the *AirEZ* vehicles utilize two redundant, multipoint transmitting systems on-board for vehicle-to-vehicle and vehicle-to-warehouse communications.

14.7.1 Cell Network Communication

By utilizing the cellular network infrastructure already in place in cities, the *AirEZ* vehicles will be able to communicate their relative positions, velocity, and status across any distance within the urban delivery zone. Not only will this data be communicated back to the central warehouse for mission management, but it will also be transmitted between vehicles to increase aerial awareness. The LATAS module will also have the capability to transmit *AirEZ* vehicle position to nearby air traffic control towers, which can then automatically communicate that data to commercial aircraft in the area to create a safe airspace free from aerial collisions.

14.7.2 Radio Transceiver Mesh Network

The *AirEZ* vehicle is equipped with a ultra lightweight (1 oz) RFD-900+ radio transceiver with 25 mi. rated range as a redundant communication option. While this range covers 79% of the delivery area, it can be extended using the transceiver's built-in multi-point mesh network capability. Since each *AirEZ* vehicle is equipped with the RFD radio transponder, each vehicle can communicate its position and velocity directly to others within range. In the event that a vehicle is outside of the range of the central communication station, the signal will be routed to the next closest vehicle until it reaches the central receiver. This mesh networking is more robust for the *AirEZ* vehicle than point-to-point communication since the com-link is extended over multiple nodes and is not dependent on a single point of failure.

14.7.3 WiFi

The *AirEZ* vehicle is also equipped with a dual-band (5GHz and 2.4GHz) WiFi antenna for short range, high bandwidth data transmission with the central management system at the warehouse. The WiFi link is utilized to transmit more data intense digital packages such as recorded flight images, mission plans and delivery zone images, as well as HUMS data for ground maintenance crews.

14.8 Final Avionics Breakdown

A comprehensive table of each avionics component discussed with associated weight, power, and cost estimates is provided in 14.2.

TABLE 14.2: Avionics Weight, Power, and Cost Breakdown

Component	Type	#	Weight (g)	Total Weight	Size	Power (W)	Total Power	Cost ($)	Total Cost
Autopilot	MP2128[g2]	1	1.0 oz	1.0 oz	1.6" x 3.9" x 0.4"	1 W	1 W	$ 1,300	$ 1,300
CPU	ODROID-XU3 Lite	2	2.3 oz	4.7 oz	3.7" x 2.8" x 0.7"	5 W	10 W	$ 95	$ 190
Transceiver	RFD-900+	1	0.5 oz	0.5 oz	1.2" x 2.2" x 0.5"	1 W	1 W	$ 76	$ 76
LATAS		**1**	3.9 oz	3.9 oz	3" x 2" x 1"	1 W	1 W	$ 100	$ 100
Visual Cameras	MatrixVision mvBlueFOX	6	0.6 oz	3.8 oz	1.4" x 1.3" x 1.6"	2 W	12 W	$ 50	$ 300
LED Lights	Fenix E35UE	5	0.5 oz	2.5 oz	0.9" dia x 1.5"	4 W	22 W	$ 15	$ 75
FLiR Camera	FliR Lepton	1	0.1 oz	0.1 oz	0.4" x 0.5" x 0.2"	1 W	1 W	$ 300	$ 300
IR Depth Sensor	Soft Kinetic DS536A	1	1.8 oz	1.8 oz	3.1" x 0.5" x 0.6	2 W	2 W	$ 150	$ 150
Laser Range Finder	LIDAR Lite	4	0.6 oz	2.3 oz	0.8" x 1.9" x 1.4"	0.5 W	2 W	$ 90	$ 360
Ultrasonic Range Finder	LV-MaxSonar-EZ0	4	0.2 oz	0.8 oz	0.6" x 0.8" x 0.8"	0.3 W	1 W	$ 15	$ 60
Solid State Drive	SAMSUNG 500GB USB 3.0 Portable SSD T1	1	1.0 oz	1.0 oz	2.8" x 2.1" x 0.4"	2 W	2 W	$ 200	$ 200
Pressure Transducers	MPX5500DP	4	0.3 oz	1.2 oz	1" x 1" x 0.5"	0.1 W	0 W	$ 7	$ 28
Gust Accelerometers	ADXL345	16	0.05 oz	0.8 oz	1" x 0.5"	0.05 W	1 W	$ 3	$ 48
HUMS	MK20DX256 CPU	4	0.1 oz	0.4 oz	1.4" x 0.7"	1 W	2 W	$ 20	$ 80
Antennas				2.4 oz					$ 39
GPS Antenna	ANN-MS active GPS antenna	1	1.5 oz	1.5 oz	1.9" x 1.6" x 0.5"	0 W	0 W	$ 15	$ 15
Transciever Antennas	2dBi Right Angle Monopole (RPSMA)	2	0.3 oz	0.5 oz	0.4" (Dia.) x 2.1"	0 W	0 W	$ 5	$ 10
WiFi Antenna	IEEE 802.11b/g/n w/ Dual band antenna	1	0.4 oz	0.4 oz	2.7" x 0.9" x 0.3"	0 W	0 W	$ 14	$ 14
Total				27.0 oz			57.2 W		$ 3,306

Transition Maneuvers

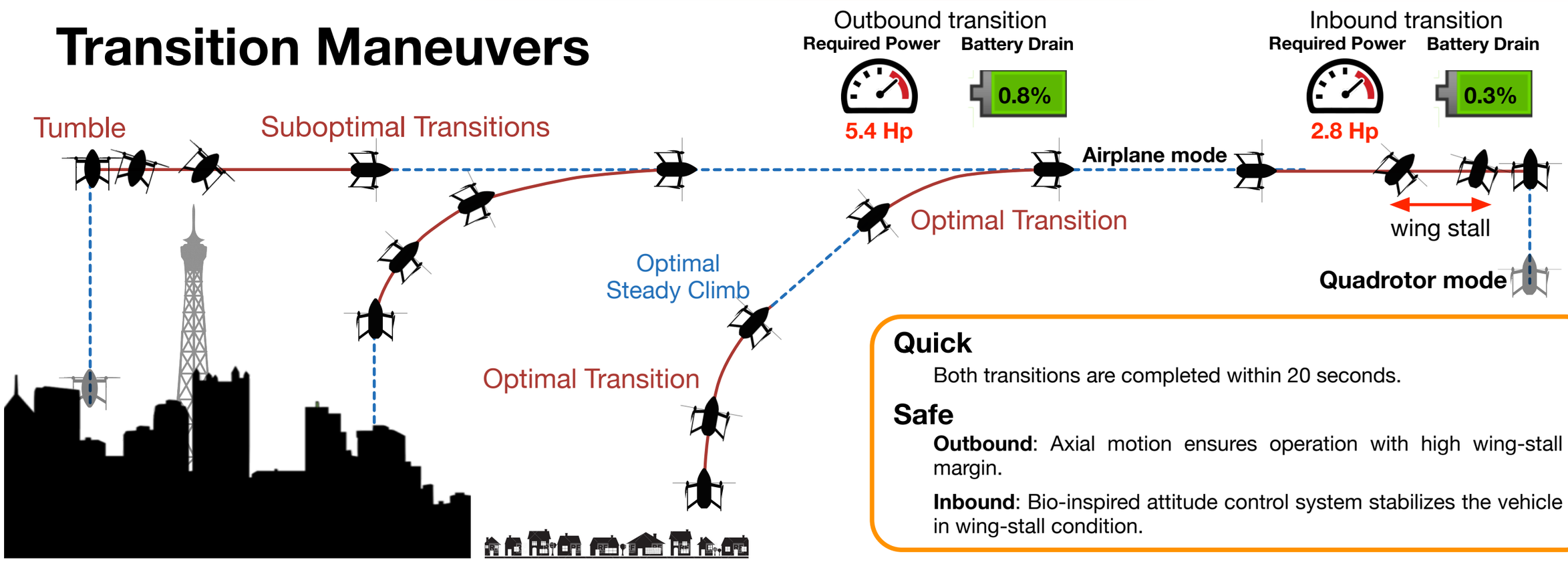

Quick

Both transitions are completed within 20 seconds.

Safe

Outbound: Axial motion ensures operation with high wing-stall margin.

Inbound: Bio-inspired attitude control system stabilizes the vehicle in wing-stall condition.

Efficient

Outbound: Trim analysis was used to find the most efficient velocity and angle to climb.

Inbound: Fuselage flat-plate area is increased by increasing the pitch attitude. Drag force from fuselage as well as stalled wing is used to decelerate.

Collective pitch: Collective is varied with the feedback from airspeed sensors so that power is minimized in each stage.

Autonomous

Maneuver selection: Optimal maneuver is chosen from a set of possible maneuvers depending on the environmental constraints.

Control: A combination of feedforward and feedback controls tracks the desired attitude during the transition.

Validated by Simulation

The designed maneuver and controller were tested using the full nonlinear vehicle dynamics.

Outbound transition: accelerating climb

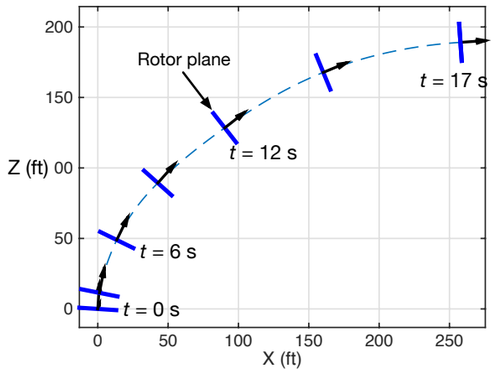

Inbound transition: return to hover

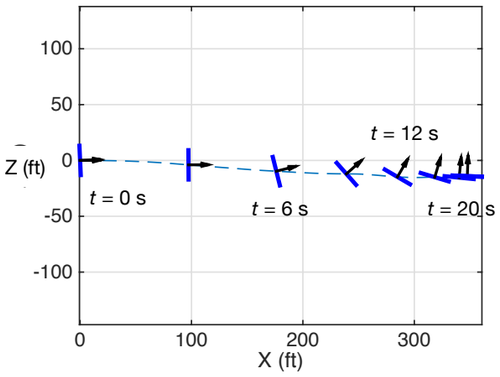

15 Dynamics and Controls

In this chapter, an in-house model developed specifically for the *AirEZ* vehicle is used to evaluate performance, perform stability analysis, and simulate the transition between hover and forward flight. Vehicle dynamics linearized around the trim conditions at different airspeeds are used to synthesize feedback control laws, and the designed controller is evaluated using the simulation with full nonlinear vehicle dynamics.

15.1 Flight Dynamics Model

A nonlinear dynamical model of the *AirEZ* vehicle is used to evaluate vehicle performance, perform stability analysis, and simulate transition maneuvers. The model is based on an in-house analysis developed at the University of Maryland's Alfred Gessow Rotorcraft Center. The *AirEZ* flight dynamics simulation incorporates a variety of physics-based models that include first-order interactions between multiple components. The vehicle free body diagram is shown in Figure 15.1. The vehicle is treated as a rigid body, and equations of motion are

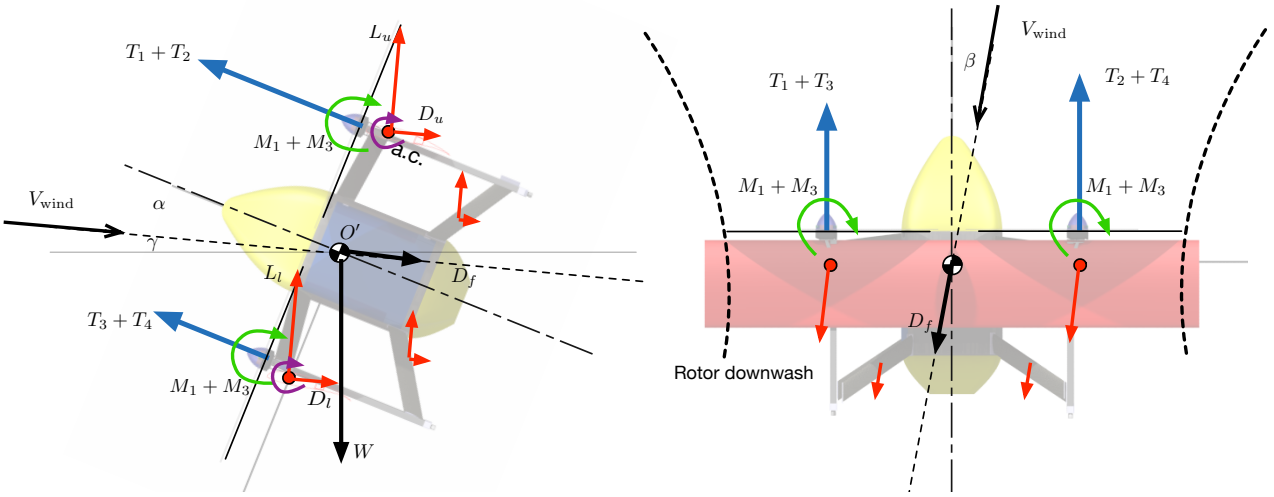

FIGURE 15.1: Dynamical model of *AirEZ* vehicle.

$$\begin{aligned} m\mathbf{a} + m\boldsymbol{\omega} \times \mathbf{v} &= \mathbf{F}_{\text{rotors}} + \mathbf{F}_{\text{wings}} + \mathbf{F}_{\text{g}} + \mathbf{F}_{\text{strut}} \\ \mathbf{I}\dot{\boldsymbol{\omega}} + \boldsymbol{\omega} \times \mathbf{I}\boldsymbol{\omega} &= \mathbf{M}_{\text{rotors}} + \mathbf{M}_{\text{wings}} + \mathbf{M}_{\text{g}} + \mathbf{M}_{\text{strut}} \end{aligned}$$

$m, \mathbf{I}, \mathbf{v}, \mathbf{a}$ and $\boldsymbol{\omega}$ are the mass, moments of inertia, velocity, acceleration and angular velocity, respectively. The right-hand side consists of forces and moments at the center of gravity, generated by the four rotors, wings, struts, fuselage, and gravity.

Rotor model

Multibody kinematics and kinetics are used to incorporate rotor-body couplings. Individual rotor blades are assumed to be rigid structures. Rotor aerodynamic loads are obtained from a blade element analysis. Blade section aerodynamics are modeled using look-up tables with quasi-steady and non-circulatory corrections for airfoil pitch and plunge motions. Look-up tables span over all angles of attack, and a pre-defined Reynolds number range. The Pitt-Peters inflow model has been integrated into the code to compute rotor induced inflow as a function of thrust distribution and flight condition. For the trim solution, the rotor loads are averaged over one revolution and substituted into the vehicle trim equations.

Fixed wings
The rotor downwash and its contraction are incorporated into the calculation of wing aerodynamic loads ($\mathbf{F}_{\text{wing}}$, $\mathbf{M}_{\text{wing}}$). Fixed-wings and struts are treated as low aspect ratio lifting surfaces with aerodynamic lift and drag given by finite wing theory. Due to rotor downwash, wing stall is delayed, and the aerodynamic interactions between the two wings and fuselage are decreased. In the post-stall angle of attack regime, quasi-steady aerodynamic characteristics obtained from wind tunnel tests are used for both rotor blade sections and wing airfoils.

Struts and Fuselage
$\mathbf{F}_{\text{strut}}$ and $\mathbf{M}_{\text{strut}}$ include the contributions from fuselage and the struts connecting the landing gear and airframe. The airframe is modeled as a rigid body that experiences aerodynamic drag acting at the vehicle center of gravity. The struts work both as horizontal and vertical stabilizers and improve the directional stability of the vehicle.

The model was used for the following purposes:

- **Performance:** Propulsive trim is obtained when the system attains zero body-axis linear and angular accelerations, i.e. steady flight condition. A numerical solver (fsolve) was used to find trim conditions. Given the airspeed (V), climb angle (γ), and rotor collective pitch ($\boldsymbol{\theta}_0$), the solver iteratively adjusts the vehicle attitudes and rotor RPM ($\boldsymbol{\Omega}$) to **calculate power required in steady forward flight and steady climbing flight**. The trim analysis was used to obtain vehicle performance and **guide the formulation of the transition maneuver** (see Section 15.2).
- **Stability analysis:** For each trim condition, linearized vehicle dynamics are obtained. These linearized dynamic models are used in the stability analysis and **controller design**.
- **Maneuver simulation:** A numerical integrator (ode15i) was used to simulate the vehicle motion for given control inputs. Once the desired vehicle maneuver and control law were designed, the controller synthesized based on the linearized dynamics was tested using the full nonlinear vehicle dynamics.

Vehicle attitude and control using differential rotor RPM is described in the next section.

15.1.1 Differential RPM

There are two methods available to regulate individual rotor thrusts in a quadrotor configuration. The first method is to change the individual collective pitch angles ($\boldsymbol{\theta}_0$) at fixed RPM, used in traditional helicopters. The second method is to change the individual rotor RPMs at fixed collective. To achieve high cruise efficiency and hover figure of merit with the same rotor (see Section 9), it is necessary to employ a combination of collective and RPM changes. The control variables chosen for feedback are the rotation speeds ($\boldsymbol{\Omega}$) of the individual rotors. Collective pitch angles ($\boldsymbol{\theta}_0$) are fixed at hover and cruise, and changed at the transition for efficiency. Thrust and torque from the four rotors are manipulated by the RPM control, $\boldsymbol{\Omega}$. The control scheme is summarized in Figure 15.2. One of the main benefits of this scheme is that **existing and proven quadrotor control methodology can be used in both hover and forward flight modes without additional weight penalties**.

Results for pitch attitude are presented using Euler angles throughout this chapter for simplicity. However, for the actual implementation, the controller is formulated with quaternions to avoid singularities (gimbal-lock) that occur in cruise and transition.

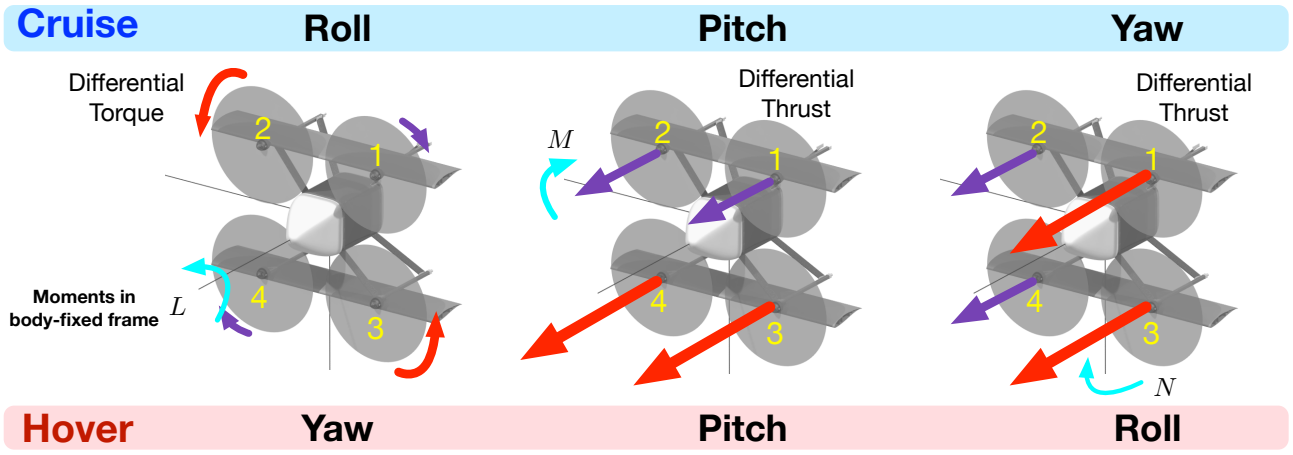

FIGURE 15.2: Attitude control by differential RPM.

The synthesis of the closed loop controller to ensure vehicle stability using rotor RPM is described in Section 15.3

15.1.2 Performance

The strength of the *AirEZ* vehicle lies in simultaneous achievement of high hover and cruise efficiency. This superior performance is enabled by the combination of fixed-wing and quadrotor, optimized blade design (see Section 7), the variable-pitch proprotor and a BLDC motor capable of 50% RPM variation with less than 1% drop in efficiency. Figure 15.3 shows the mechanical power required in steady level flight.

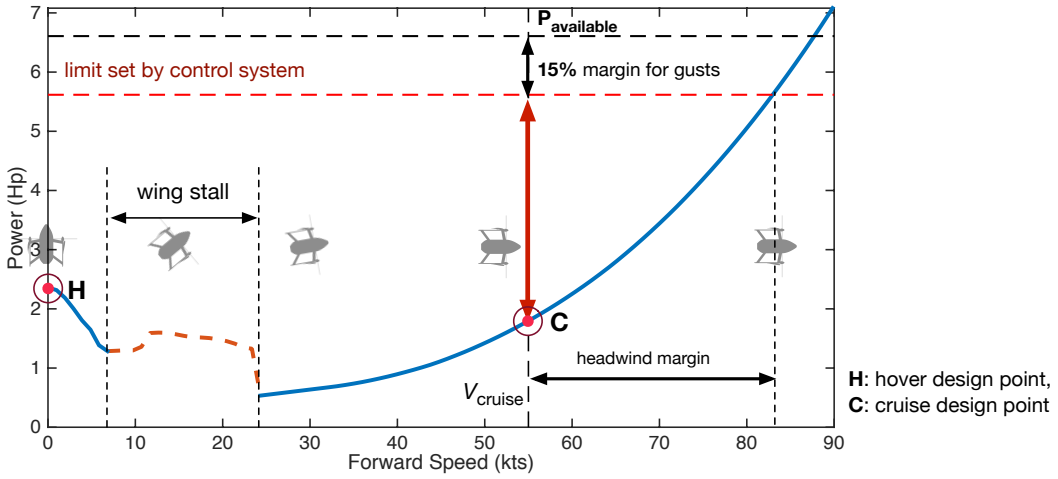

FIGURE 15.3: Power curve for transition.

The available power ($2.8P_{\text{hover}} = 6.62$ Hp) is designed for flight safety in one engine inoperative (OEI) case. This available power enables the *AirEZ* vehicle to fly into 30 kts headwind intermittently and still maintain 55 kts ground speed. To accommodate corrections for gust rejection, a 15% power margin limit is imposed by the control system. This power limit is taken into account in the design of transition maneuvers presented in the following section.

The collective pitch angle is changed at 23 kts, which is a key factor to ensure good proprotor propulsive efficiency. If a fixed collective angle is used, the power penalty is 500 % of the optimized values shown in Figure 15.3.

Wing stall does not occur in low speed edge-wise flight because of the downwash from the rotors. For forward speed between 8 and 23 kts, the wing experiences static stall. Therefore, the drag from the stalled wing increases the power required to fly forwards. When the fixed wings start to generate lift for forward speeds greater than 23 kts, efficient forward flight is achieved.

15.2 Transitional Maneuvers

For each package delivery, the vehicle must fly through the following phases of flight 1. Outbound transition (from hover in helicopter mode to cruise in airplane mode, increasing attitude and forward speed), 2. Cruise in fixed-wing mode, and 3. Inbound transition (decrease speed while returning to hover).

It is essential to design robust transitional maneuvers that are safe and efficient, for which the following issues are considered: 1. Wing angle of attack and stall margin, 2. Required power and power margin, 3. Maximum acceleration (g-force), 4. Maneuver time, 5. Energy consumption, 6. Horizontal and vertical displacements. With all these considerations, a set of maneuver options depending on the environmental conditions is selected. A computationally inexpensive switching algorithm on the vehicle uses sensor information to decide the appropriate maneuver based on available space and designated no-fly zones. The feasibility of these maneuvers are validated by the in-house flight simulation that includes full nonlinear vehicle dynamics (see Section 15.1).

15.2.1 Transition Maneuver Formulation

Following the work by Kubo et al. [39], trim conditions (obtained in Section 15.1) are utilized as reference points to construct a transition maneuver. For example, Figure 15.4 shows the contour plot of the trimmed wing angle of attack. Four different trim conditions are shown, corresponding to hover, vertical climb, cruise, and steady climbing flight.

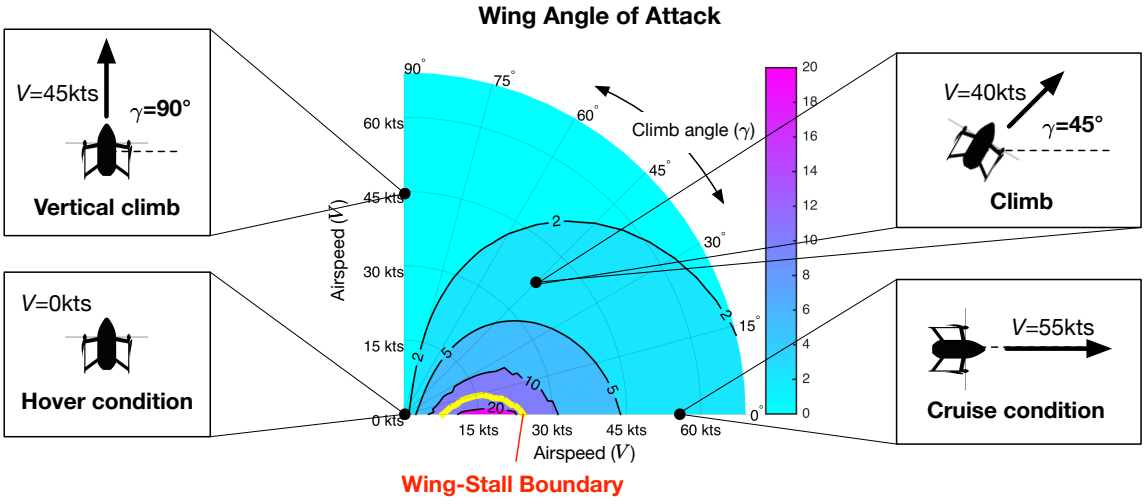

FIGURE 15.4: Distribution of body pitch attitude and wing operating angle of attack.

The goal is to design a trajectory using this diagram that connects any two flight conditions using a specific "path". For outbound transition, the path starts at hover and ends at cruise, and vice-versa for inbound transition. By specifying the desired time to change from one condition to the next, a candidate transition maneuver is obtained. The reference states are tracked by a feedback controller, detailed in Section 15.3. Important points that are considered in the design of the maneuver are: 1. Wing stall (buffeting affects package integrity), 2. Power limit (motor burnout), and 3. Thrust limit (rotor stall and loss of control).

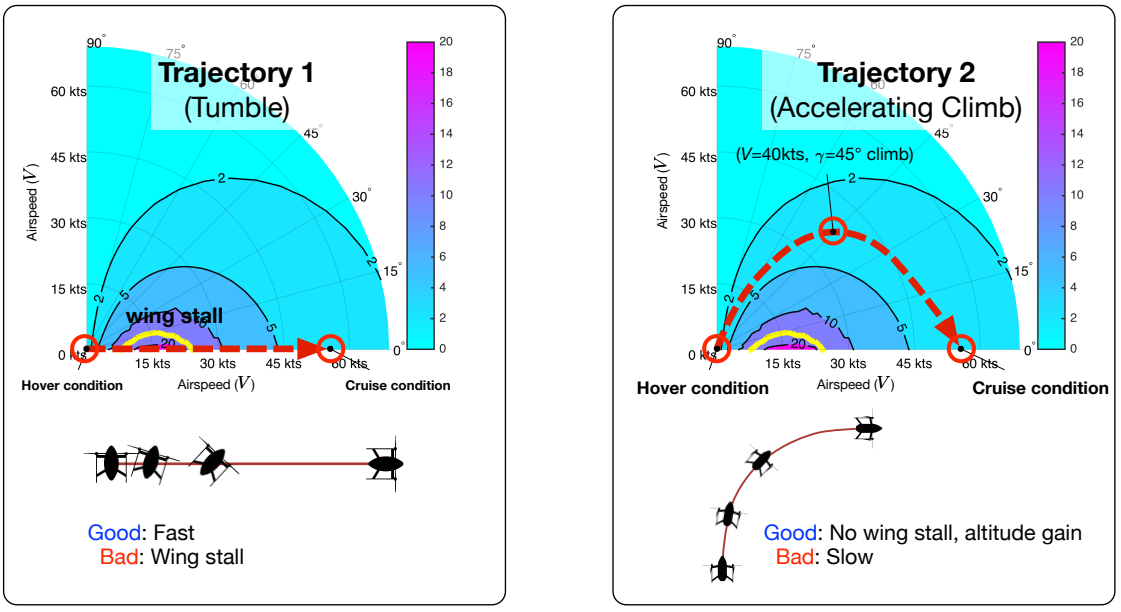

FIGURE 15.5: Candidate outbound transitions.

Candidate Outbound Transitions: Two candidate outbound trajectories are shown in Figure 15.5. The first case called a "tumble" is one in which the vehicle experiences wing stall at low flight speeds. Wing stall is less problematic during outbound transition because higher downwash from the rotors during the maneuver induces flow reattachment over the wing, even more so than during steady flight. The second option, called "accelerating climb", avoids this issue by choosing a flight profile where the vehicle is mostly in axial flight.

The next section details the methodology used to identify the optimal trajectory out from infinitely many choices, using the available trim condition data.

15.2.2 Optimal Outbound Transition: Efficiency Metrics

Delivery drones may be required to clear a minimum height in vertical climb before transitioning to cruise for safety reasons and to comply with federal, state or city-specified regulation. Different ways of climbing are parametrized by the airspeed V and the climb angle γ.

The battery drain to gain the same height (100 ft) is used to rank different outbound transition strategies. The condition $V = 40$ kts and $\gamma = 45°$ consumes minimum electrical energy while adhering to the motor power limit shown in Figure 15.6.

Figure 15.6 shows the distribution of energy required to climb (E_{climb}) and the curve indicating the power limit 5.4 Hp. The limitation on the power is set to be 5.4 Hp to provide margins for gust rejection. Although the global optimum exists at $V = 45$ kts vertical climb as shown in

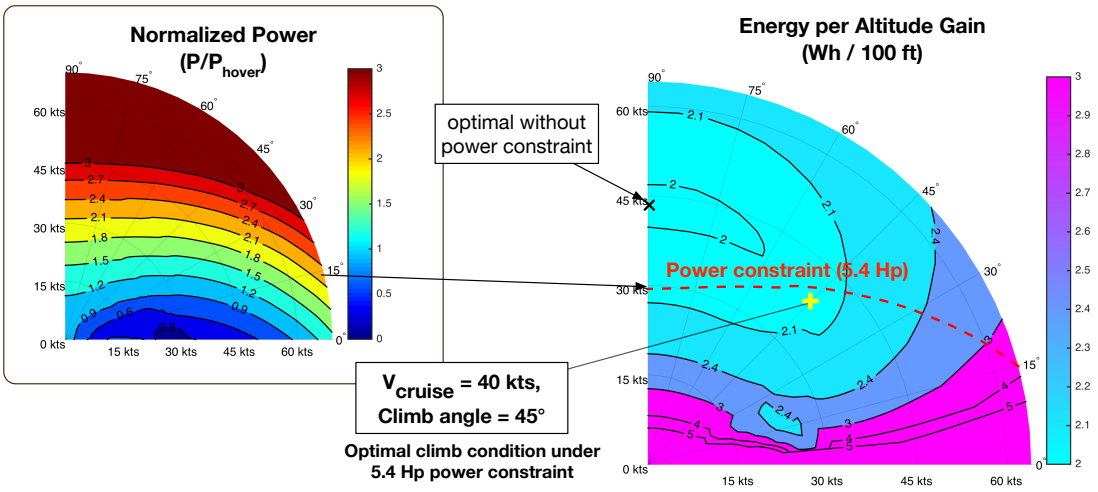

FIGURE 15.6: Distribution of climb energy (E_{climb}).

Fig. 15.4, this is unachievable due to the power constraint. Hence, a flight condition of $V = 40$ kts with $\gamma = 45°$ climb angle is determined to be the constrained optimum climb condition.

To clear the minimum specified altitude, there are three general options that are programmed into the system. Depending on the nature of the urban environment, one of the following will be chosen:

(i) Hover → Optimal climb → Hover → Tumble → Cruise

(ii) Hover → Tumble → Cruise → Optimal Climb → Accelerate → Cruise

(iii) Hover → Optimal climb → Accelerate → Cruise

The third option is the simplest and the most efficient choice. Therefore, the outbound transition is designed so that it incorporates the identified optimal climb condition (Trajectory 2 in Figure 15.5). Starting from hover, the vehicle transitions to a steady optimal climb condition, [40 kts, 45°], maintains the phase until desired altitude (cruise altitude minus the vertical displacement of the remaining maneuver) is achieved, and then transitions to cruise at 55 knots as shown in Figure 15.5 (accelerating climb).

A set of outbound transition choices are illustrated in Figure 15.7. A set of outbound transition choices are illustrated in Figure 15.7. The optimal maneuver requires 5.4 Hp to transition from hover to 55 kts cruise in 17 seconds with 200 ft altitude gain and 350 ft forward travel. However, depending on the environmental conditions, a suboptimal maneuver may be chosen from a set of possible maneuvers to avoide flying close to tall buildings.

The algorithm for choosing the maneuver is shown in Figure 15.7. After slowly and safely climbing up to a safe altitude, where there is no obstacles like tall buildings or cranes, the vehicle measures the remaining altitude (Δh) to the cruise altitude.

- If Δh is greater than the vertical displacement required for the optimal outbound transition (Δh_{opt}), the optimal transition is split into two phases and a steady-climb phase is inserted between the two. The climb angle and velocity of this phase ensures minimum energy consumption per gained altitude among all the flight conditions. Also, this maneuver

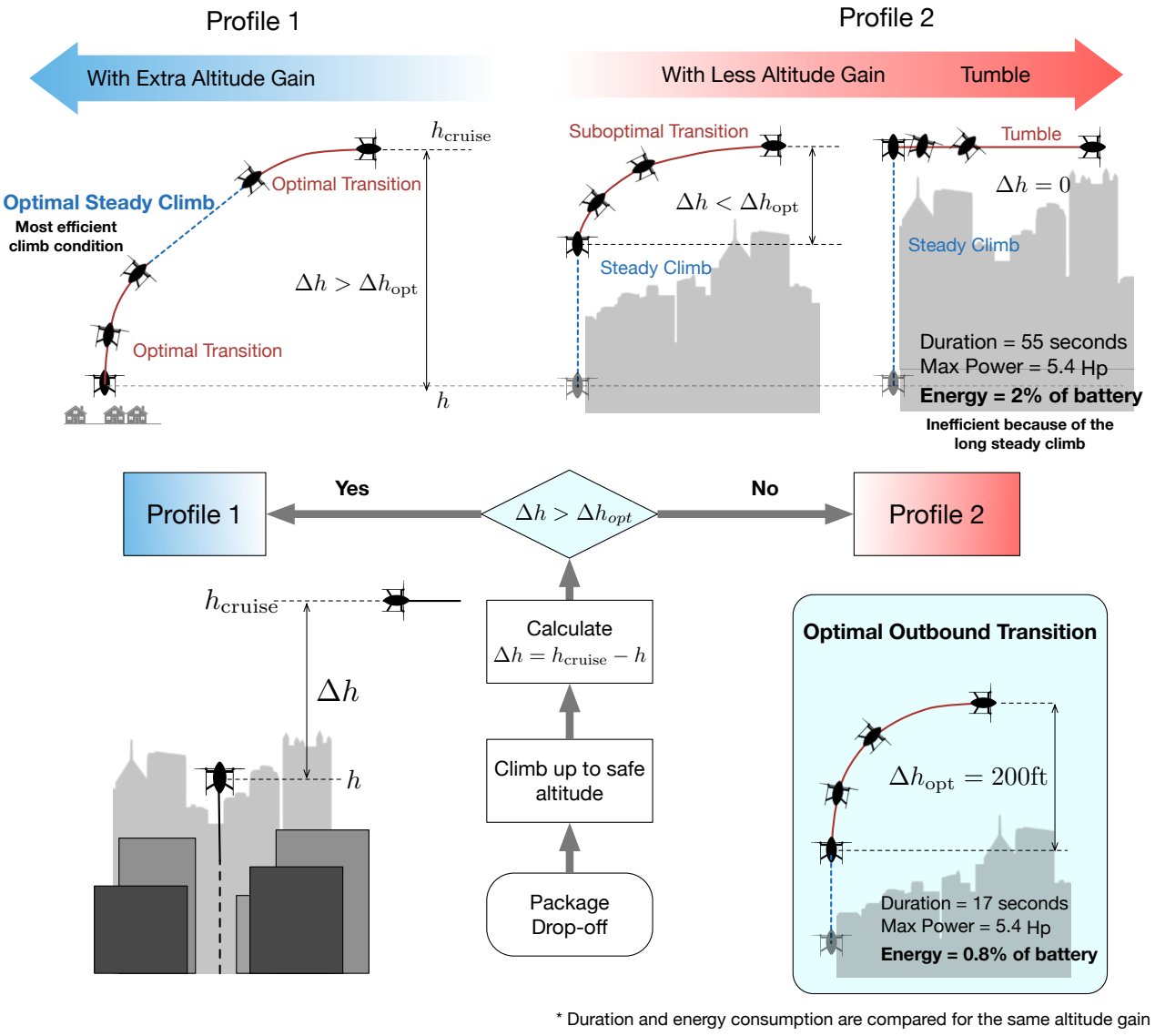

FIGURE 15.7: Selection of outbound transitional maneuver.

guarantees high wing-stall margin throughout the transition since the vehicle flies with near-zero angle of attack with respect to wind.

- If Δh is less than Δh_{opt}, a suboptimal maneuver with 'vertical displacement = Δh' is selected. The extreme case will be the tumbling maneuver with Δh=0, but this is not ideal because of the small wing stall margin The total energy consumption including the steady vertical climb will be higher than the optimal maneuver since the total duration is longer.

The key to minimizing battery energy consumption is to use the optimal transition with optimal climb whenever possible, which guarantees energy efficiency and high wing-stall margin. The desired altitude gain is adjusted by the duration of steady climb portion. The suboptimal maneuver with less altitude gain is performed only when necessitated by the altitude constraint.

The motor power limit is an important consideration during outbound transition when the vehicle tries to accelerate while also gaining altitude (or potential energy). Figure 15.3 shows

the power curve of the *AirEZ* vehicle. The available power ($2.8P_{\text{hover}} = 6.62$ Hp) is designed for safety in the one engine inoperative (OEI) case. To account for gusts, a 15% power margin limit is imposed by the control system.

Therefore, in the design of the optimal and suboptimal outbound transitions, the duration of maneuver is minimized by utilizing 85% of available power preserving 15% margin for gust rejection. The fast transition with maximum of 5.44 Hp can be completed within 15 seconds, and the energy used during the transition is less than 1 % of the total battery energy.

In summary, for the outbound transition, using high power to finish the transition as quickly as possible has the following benefits:

(a) Minimized battery drain

(b) Strong downwash from the rotors delays wing stall

(c) Minimize the time when the vehicle is most vulnerable to gusts

15.2.3 Cruise to Hover (Inbound Transition)

During inbound transition, two methods for deceleration are considered:

(1) Stall brake: Use as much drag as possible from wings, fuselage, and rotor to reduce speed and dissipate kinetic energy

(2) Pull-up: Convert kinetic energy to potential energy by increasing altitude

The two approaches are illustrated in Figure 15.8.

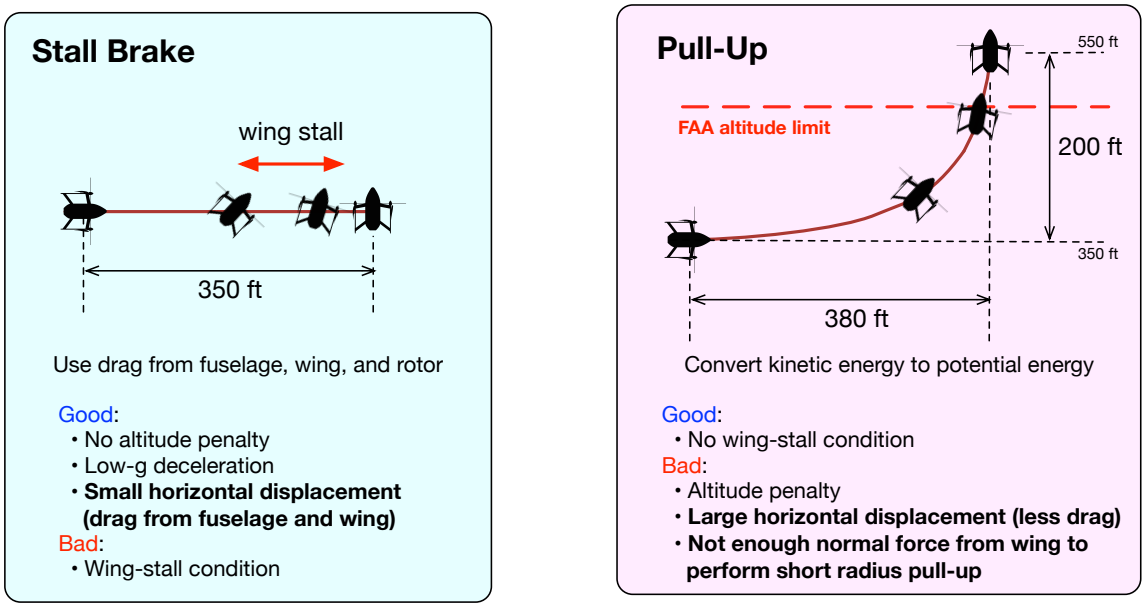

FIGURE 15.8: Options for inbound transition.

The pull-up approach avoids wing-stall and is potentially quicker for tail-sitters with larger wing areas [39]. However, the major disadvantage of the pull-up maneuver is the additional height gained. This altitude gain translates into height that the vehicle has to descend. With the

cruise altitude set to 400 ft and the FAA rule of maximum allowed flight altitude at 500 ft, the maneuver is not feasible, since the flight path radius of 100 ft cannot be achieved with the available wing area. A version of the pull-up maneuver, which includes a dive before the climb was also considered. However, increased maneuver time and a large forward travel covered (more than 400 ft) rendered the choice infeasible due to safety considerations:

(a) An accurate front view during the maneuver is not guaranteed

(b) The vehicle has to know the front clearance beforehand and assume no obstacles exist

However,existing sensors do not have the extended range required for the weight class assumed.

The stall-brake approach is free from these issues, since the vehicle does not change its altitude. The maneuver starts with a pitch-up moment induced by differential rotor thrust. As the vehicle increases its pitch attitude, the effective flat-plate area of the fuselage increases, which aids deceleration. The drag on the fixed wings also increase due to stall and flow separation. The simulation program with the nonlinear vehicle dynamics showed that this maneuver results in smaller forward travel while adhering to rotor power limits. The disadvantage of using this approach lies in maintaining the vehicle stability under the buffeting loads encountered in wing-stall condition. The bio-inspired stability augmentation with distributed sensors (see Section 15.3.3) is designed to overcome this limitation. Since there is no excess power required for the maneuver, the available power $\Delta P_{\max}$ (Figure 15.3) can be used for the vehicle attitude stabilization and tracking.

For these reasons, the *AirEZ* vehicle uses the stall brake approach as the inbound transitioning maneuver.

15.3 Control System

The *AirEZ* vehicle is designed to achieve all the delivery tasks autonomously without any intervention from a human operator. Design requirements for the control system are:

- Maintain stability under various operating conditions
- Perform safe transitions between hover and cruise
- Navigate the vehicle through specified paths using way points

Hierarchical structure of the control system is shown in Figure 15.9.

- **Central command**: The central system monitors all the vehicles and specifies routes to each vehicle.
- **Loop1**: Once the route for a single trip is specified, Loop 1 recognizes and triggers flight modes for the inner loops. Loop 1 is also the level that deals with the health monitoring of the vehicle. If there is any problem with the power system, for example, then it communicates that information to the central system and decides whether the vehicle should continue the mission or come back to the station.
- **Loop 2**: Given the destination, Loop 2 plans the detailed path. Sensing and avoidance of obstacles using sensor information are done in this level. This block computes the desired states of the vehicle (pose, velocity, etc.) required to track the specified path and sends it as a command to the lowest level of the control system.

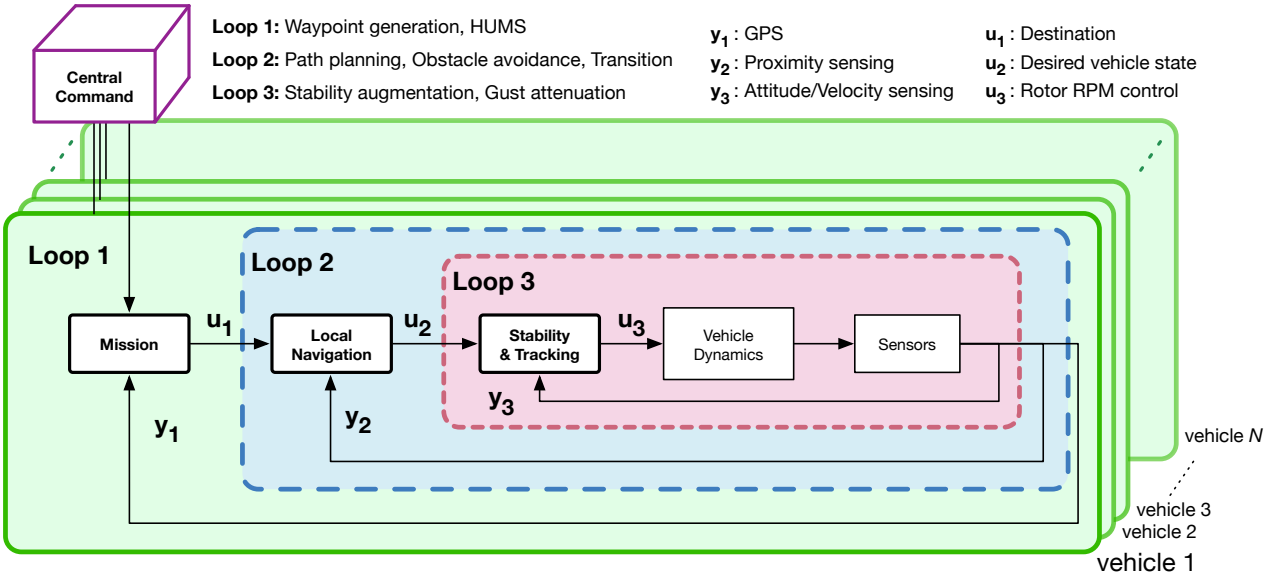

FIGURE 15.9: Control Architecture.

- **Loop 3:** tracks the desired vehicle states specified by the higher level controller, and also maintains the stability of the vehicle. Gust attenuation is done in this level.

The loop in the higher level is dependent on those in the lower level. If Loop 3 fails, then the whole system will fail. Therefore, it is important to have a lower level controller that works robustly in various conditions. The *AirEZ* vehicle uses a Linear Quadratic Regulator in conjunction with bio-inspired disturbance rejection techniques using distributed acceleration sensing.

The full nonlinear vehicle dynamics model described in Section 15.1 is used to design and validate the controller. The model was also utilized in optimizing and simulating the transitional maneuvers.

15.3.1 Path Planning: Loop 2

Loop 2 is based on path planning for high-speed rotary-wing vehicles capable of aggressive maneuvers. The *AirEZ* vehicle utilizes a combination of vision, infrared, laser, sonar based sensing for obstacle avoidance and a hybrid path planner using an optimized Rapidly-exploring Random Tree (RRT) algorithm and minimum snap trajectory generation. The RRT* algorithm uses a sampling-based approach to incrementally construct a graph of state space that expands over time and selects the optimal polynomial trajectory based on performance metrics, including turn radius [40, 41]. Offline path planning with RRT* is performed in advance using pre-computed waypoints on a known map, and online path planning is used to account for dynamically changing obstacles. Forward flight cruise is primarily offline planning using the stored map of buildings and precise positioning data from the DGPS receiver and LATAS module (see Chapter 14). Vertical flight is primarily online planning since the local map around the *AirEZ* vehicle is constantly updated with new obstacles detected by the sensors. Since online planning is performed in real-time, the *AirEZ* vehicle uses the computationally efficient minimum snap trajectory generation method coupled with known vehicle kinematics and dynamics [42]. The optimal collision-free path is chosen using information combined from online and offline trajectory planners.

15.3.2 Stability & State Tracking: Loop 3

The most essential role of the control system is to maintain stable flight. The autopilot in Loop 3 in Figrue 15.9 uses the vehicle states $\mathbf{X}$ (measured by sensors) in a feedback control loop to augment vehicle stability.

Among many different types of feedback controllers, the H_∞ controller is appealing in terms of robust performance in the presence of gusts. However, such a controller requires a large number of controller states that the onboard computer has to integrate online. This is not desirable because most of the computational resource is used for image processing (see Chapter 14).

Therefore, a simple but reliable Linear Quadratic technique is used. The reliability of the controller can be analyzed by robust control techniques. The RPM control $\mathbf{\Omega}$ is described as $\mathbf{\Omega} = \mathbf{\Omega}_{\text{ref}} + \Delta\mathbf{\Omega}$, where U_{ref} is the feedforward term obtained from the trim analysis, and $\Delta\mathbf{\Omega}$ denotes the feedback control. The reference input $\mathbf{\Omega}_{\text{ref}}$ is a prescribed trim input corresponding to the desired state X_{ref}. Since there are uncertainties in the system (external wind, unmodeled vehicle dynamics), feedback control $\Delta\mathbf{\Omega}$ is superposed, where $\Delta\mathbf{\Omega} = -\mathbf{K}(\mathbf{X} - \mathbf{X}_{\text{ref}})$. The static feedback gain $\mathbf{K}$ is provided by gain scheduling with airspeed, i.e., linear-quadratic regulator (LQR) is used with the linearized vehicle dynamics at each airspeed.

To ensure that the measurement error in airspeed does not destabilize the vehicle, eigen values are computed with different airspeeds while a single feedback gain $\mathbf{K}$ for 55 kts cruise condition is used. It was observed that the poles have negative real parts, indicating that the closed-loop system is stable. The gain is also robust to the change in the c.g. location caused by package dropoff. This control strategy enables the vehicle to track the desired airspeed and climb angle during hover, cruise and transition. The full nonlinear vehicle dynamics model was used to simulate the transition shown in the foldout.

15.3.3 Bio-inspired Gust Attenuation

Gust attenuation is one of the biggest challenges for small scale autonomous vehicles. Following the in-house work by Gremillion and Humbert [43], a bio-inspired disturbance rejection technique with distributed acceleration sensing is used in the *AirEZ* vehicle. The advantages of this method are:

(i) Low computational loads, which enables the vehicle to spend the limited computational resource on image processing.

(ii) Short reaction time: disturbance mitigated/attenuated before it grows.

(iii) Rejection of both external disturbances (gusts) and internal disturbances (actuator dynamics and uncertainties).

Inspired by flying insects, this method utilizes redundant sensor arrays to construct a static estimator that requires minimal computational resources compared to standard observer (Kalman filter). The use of distributed accelerometers in the estimation of forces ($\mathbf{F}$) and torques ($\boldsymbol{\tau}$) acting on the vehicle is summarized in Figure 15.10.

The key is to have more sensors (15) than the number of states $\mathbf{z}$ (12). Then matrix C^TC is nonsingular, the pseudo inverse can be constructed and the vehicle states can be evaluated to a high degree of accuracy. Redundant sensors improve the noise to signal ratio.

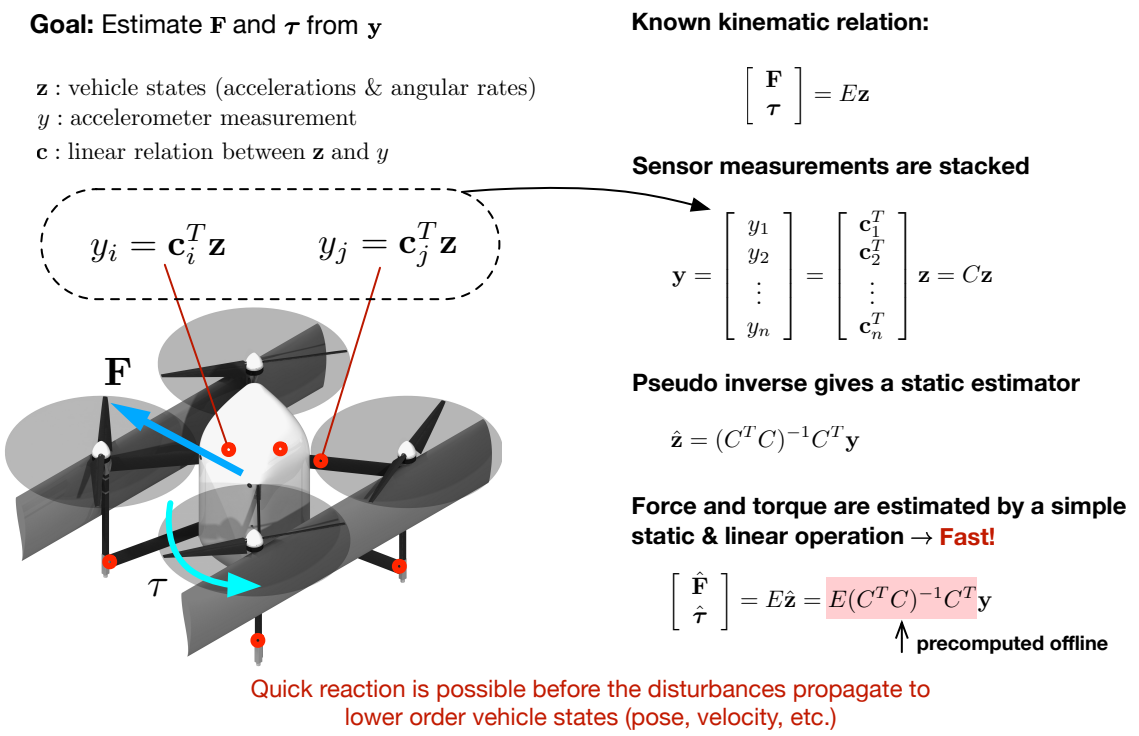

FIGURE 15.10: Distributed accelerometers for force torque estimation.

Figure 15.11 shows how the force-torque estimation is used in the stability augmentation. The estimated forces and torques are fed back to the control commands with proportional control to reject the disturbance. This feedback improves tracking of requested controls in the presence of disturbances by regulating errors between desired and actual loads from individual rotors. Therefore, the rejection works to mitigate both external disturbances (wind gusts) and internal disturbances (motor dynamics).

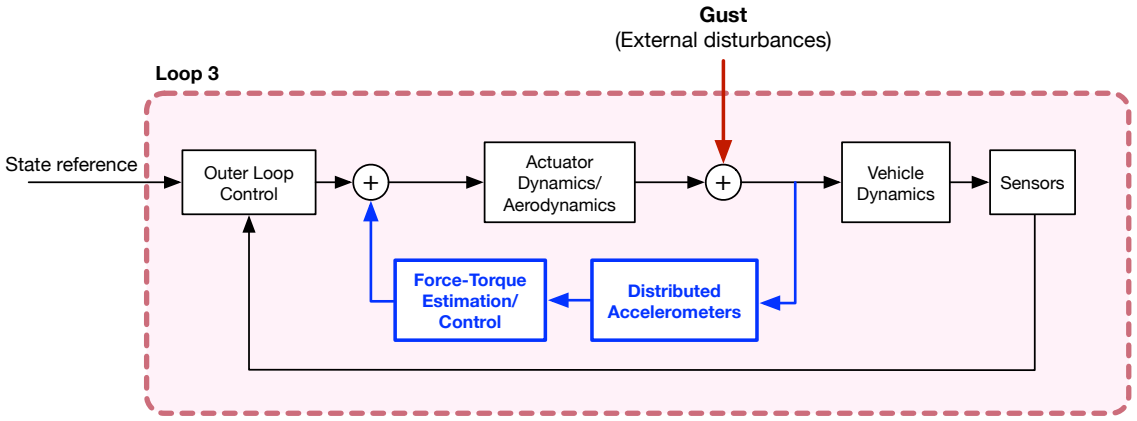

FIGURE 15.11: Block diagram of stability augmentation system.

This bio-inspired gust attenuation technique enables *AirEZ* to operate with a high degree of safety in the presence of gusts using a robust stabilizing system. The technique has been successfully demonstrated in a micro-quadrotor as well as in a mini fixed wing vehicle for a range of

sharp-edge gust loading. [43]. The algorithm was modified to for the *AirEZ* quadrotor biplane tailsitter.

16 Acoustics

To aerially deliver packages in an urban area, noise levels are of major concern and the vehicle should be as quiet as possible. The vehicle must permit safe human operation below and in its immediate vicinity considering that the noise pollution can be intimidating to customers and potentially harmful to the operators.

16.1 FAA Noise Requirements

For an unmanned vehicle of the size of *AirEZ* , there are no official regulations for noise level defined by the Federal Aviation Administration (FAA) for UAV sized quadrotor. However, there are guidelines in reference to tiltrotors provided by the Federal Aviation Regulations (FARs). The quad bi plane tailsitter is similar to the tiltrotor in that the proprotor plane will be parallel to the ground in hover and perpendicular to the ground at high speed. The sound pressure levels (SPL) are obtained on a hemisphere of 16.4 ft radius centered at the vehicle and a plane that is 16.4 ft below the vehicle. Both hovering and cruising conditions are considered in the noise study. The noise level limit for a 40 lb aircraft is a band between 88 and 90 EPNdB (Effective Perceived Noise Level in decibels), as shown in Fig. 16.1.

16.2 Noise Assessment

The four rotors are the main noise source of the vehicle, which is comprised of the thickness noise, loading noise, High Speed Impulsive (HSI) noise and Blade Vortex Interaction (BVI) noise. Noise estimates were obtained using an in-house developed code based on Formulation-1A of the Ffowcs–Williams–Hawkings (FWHA) equation. The FWHA model only calculates

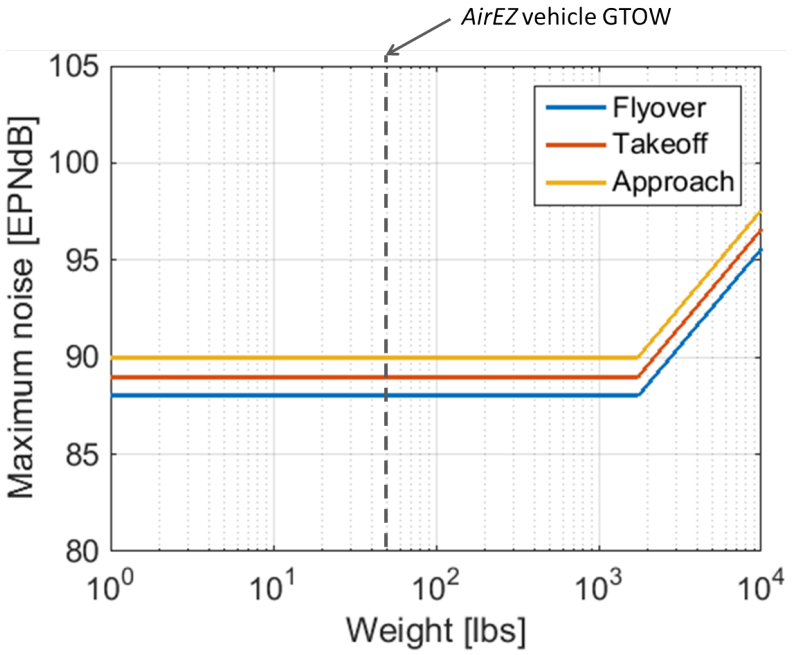

FIGURE 16.1: FAA noise limit requirements (Extrapolated from FAR 36.1103).

thickness noise, which is caused by the air displacement by a blade, and loading noise, which is caused by the accelerating force on the air induced by the blade surface. The HSI noise is not considered because to the low tip speed (maximum Mach number of 0.3 in the flight envelope), and the BVI noise is not studied because it only occurs in specific flight regimes, such as returning vortices in a conventional helicopter.

	Thickness Noise (dB)	Loading Noise (dB)	Total Noise (dB)
Hover	57.4	88.5	88.5
Cruise	32.2	68.8	69.0

TABLE 16.1: The summary of maximum noise level of the acoustics study

The predicted results are shown in Fig. 16.2. As expected, the thickness noise is highest in the plane of rotors, while the loading noise reaches its maximum along the thrust direction. The loading noise is the major source of rotor noise in both hovering and cruising conditions, because the disk loading is relatively high and the RPM is low. In forward flight cruise, the total noise is lower because of the relatively lower disk loading in cruise, and thus the dominating loading noise is lower. The noise patterns are symmetric because of the symmetrical characteristics of the *AirEZ* quad-rotor configuration. The SPL in decibel is summarized in Table 16.1. The noise level is comparable with a well-studied 12 lb quad-rotor with a rotor diameter of 18 in and RPM of 7500 [1].

Besides the rotor, the second largest contributor to noise pollution is internal noise during the flight, which is primarily caused by the engine (typically piston or tubine). However, the powerplant on board *AirEZ* is a battery pack powered by electrical motors. Therefore, the noise level from the power system should be far lower from the rotor noise. In conclusion, the noise levels from the *AirEZ* system during its operation in hover and cruise mode is far lower than those specified by the FAA.

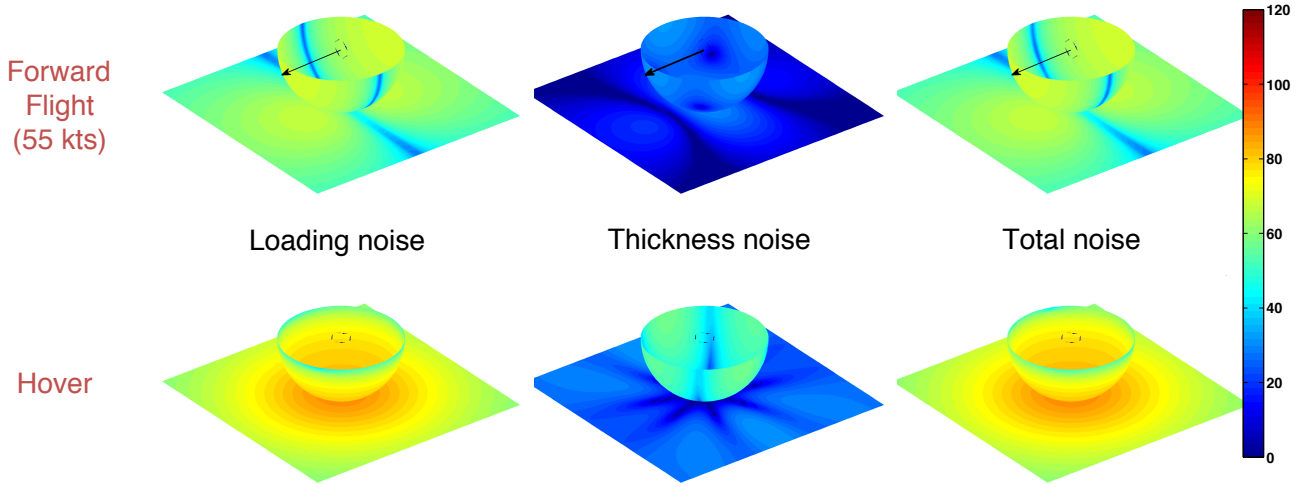

FIGURE 16.2: The thickness/loading/total noise of the vehicle in hovering and cruising conditions

17 Failure Modes Analysis

17.1 Failure Mode, Effects and Criticality Analysis

AirEZ is a system of systems design involving multiple logistics nodes that includes the warehouse, fleet vehicles, communication links and the customers. Each of these building blocks are prone to failure and mishaps, effectively increasing the overall complexity and sensitivity of the system to failures. To ensure a robust and safe design, failure modes must be reviewed at each level of the system, i.e., components, assemblies, and subsystem, and their causes and effects must be identified.

TABLE 17.1: Severity levels of a potential failure mode

Severity Level	**Description**
I	Catastrophic - Injury or loss of life possible
II	Major Concern - Vehicle not recoverable/repairable
III	Moderate Concern - Delivery failure
IV	Low Concern - Delivery delay
V	No concern

TABLE 17.2: Probability of occurrence of any particular failure mode.

Probability Level	
A	Very High Probability (>75%)
B	High Probability (50-75%)
C	Moderate Probability (25-50%)
D	Low Probability (5-25%)
E	Negligible Probability (<5%)

To this end, Failure Mode, Effects and Criticality Analysis (FMECA) was performed to identify the likelihood of a potential failure mode occurring and the impact of the failure on the system. Table 17.1 ranks the severity levels of a failure model from I–V, with I being catastrophic failure and V being an event of no concern. Probability of the occurrence of the failure modes are ranked form A–E, with A indicating very high probability (>75%) and E indication negligible probability (<10%). Therefore, a criticality level of I-A would necessitate immediate attention and resolution of the problem while V-E would be low on a priority list.

Table 17.1 shows a list of potential failure models identified and analyzed for the *AirEZ* system. This list contains primarily the vehicle level failure modes, such as one engine out, failure of delivery mechanism, faulty communication system, etc. The failure modes were identified based on severity and likelihood. Potential consequences and the effects on mission performance were analyzed. Finally, a mitigation strategy, i.e., system or component solutions developed, were implemented as part of the *AirEZ* system to reduce the criticality levels and make *AirEZ* a safe and viable option for quick package delivery in a congested urban airspace.

17.2 Rotor Considerations

During the design of the *AirEZ* vehicle, safety was a chief concern. Therefore, it was imperative that both rotor downwash and kinetic energy remained low throughout the design process. High

Risk	Severity	Likelihood	Consequences	Mitigation
One engine out	II	D	Crash landing of vehicle	Excess power installed to allow transition to hover and safe landing to ground
Total power loss	I	E	Crash landing of vehicle	Parachute installed in vehicle fuselage
Delivery mechanism failure	III	C	Package not delivered, delivered late, packages delivered incorrectly/out of order	Color sensor installed to detect successful/unseuccessful package deliveries, allows for multiple attempts before departing drop location, programmed return to base to restart delivery mission possible if multiple attempts are unsuccessful
Unexpected weather/wind	III	B	Predetermined flight path altered, late deliveries, unexpected wing/rotor stall	Gust and weather detection systems installed
Transceiver failure	III	C	Loss of communication to central warehouse, loss of health monitoring, etc	Mesh networking
Front camera failure	III	E	Collision with bird, crane, other transient objects	Travel in edgewise flight
Door failure	III	C	Failed delivery	Automatic return to base to restart delivery mission
Communication failure 1 (WH -> UAV)	III	D	Loss of relative location information, delivery inaccuracy	Mesh networking
Communication failure 2 (UAV -> WH)	IV	D	Loss of vehicle health monitoring	Mesh networking, automatic return to base
Microprocessor failure	II	D	Loss of onboard computing of sensor data, vehicle crash	2 Odroid-UX3 Lite's have been installed
Loss of Autopilot GPS signal	III	D	Loss of relative location information, delivery inaccuracy	LATAS module includes second GPS system
Loss of monocular camera	III	D	Vehicle cannot find safe landing zone	Multiple visual cameras installed
Loss of IR depth sensor	IV	D	Vehicle cannot detect height from ground, hard landing possible	LIDAR Lites installed
Loss of LED light	V	D	Cameras suffer from low light	Multiple LED lights installed, IR depth sensor, LIDAR Lites, FLIR sensor installed
Loss of a visual camera	III	D	Vehicle cannot see landing zone, cannot know if package was dropped properly	Multiple cameras installed provide awareness, redundant sensor suite allows for total environmental awareness without visual camera, sensor system installed to detect package drop
Loss of IMU data	II	D	Vehicle cannot compute kinematic data, vehicle crash	Health monitoring allows pilot takeover via central warehouse and use visual cameras to navigate
Global map not updated	III	E	Vehicle unaware of new buildings/obstacles, travels to wrong address	Multiple sensor redundancies to avoid objects while delivering, QR codes placed at homes receiving deliveries
Vehicle frame structural failure	II	E	Crash landing of vehicle	Strutural components sized to endure maximum flight loading of 3 g's, routine vehicle maintenance
Control algorithm failure				
Loss of wing	II	E	Loss of lift, crash landing of vehicle	Transition to hover, fly edgewise or land to be picked up by maintenance crew
Battery dislodged	I	D	Loss of power, crash landing of vehicle	Parachute automatic deployment on reserve power

FIGURE 17.1: Identified failure modes for the *AirEZ* system.

rotor downwash can generate high speed debris when landing on an unprepared surface. This debris can cause harm to the vehicle and any surrounding personnel, and therefore, should be avoided. Table 17.3 shows a comparison of the downwash generated by the *AirEZ* vehicle to other popular rotorcraft. It can be seen that the *AirEZ* vehicle generates a 84% slower downwash than an R-22 and a 57% slower downwash than a UH-60 helicopter. Therefore, the *AirEZ* vehicle is proven to generate a low downwash environment.

TABLE 17.3: Rotorcraft downwash velocities

Rotorcraft model	**Downwash velocity [ft/s]**
AirEZ vehicle	20.00
R-22	68.83
UH-60	127.95

Kinetic energy is another rotor characteristic which should be lowered in order to ensure a safe vehicle design. Reference [44] states that an "object which impacts a human is considered likely to be lethal if its kinetic energy is greater than 80 Joules." This means that the rotor should always operate at a tip speed which ensures a kinetic energy less than 80 Joules. This holds true especially during hover, when vehicles are most likely to be operating in close proximity to people. Fortunately, the *AirEZ* vehicle has a kinetic energy far below the 80 Joules threshold in both hover and cruise. During hover, the kinetic energy of a rotor is 43.78 Joules and during cruise, this number drops to 8.32 Joules. These studies help to validate that the *AirEZ* vehicle design is safe to operate in a crowded urban environment.

17.3 Motor Loss

One Motor Inoperative

1. In hover: Immediately spin down the diagonally opposite rotor and perform controlled descent by sacrificing the yaw control. Installed power is enough to generate the thrust required to achieve hover and steady descent with two rotors. Increase collective of the third rotor to stall the blades so that it does not generate thrust but can be used for vehicle yaw control.

2. In cruise: Use the functioning diagonal rotor pair to regulate the thrust and used the third rotor with high collective to control the roll. Immediately apply pitch up moment by increasing the thrusts on the lower rotor to return to hover mode and perform the controlled descent described in case 1.

Two Motors Inoperative

Care was also taken to ensure vehicle survivability in the event of two motor failure. There are two main cases that can occur: diagonal motor losses and adjacent motor losses. If a diagonal pair of motors fail, the other two rotors are utilized to return to hover mode via differential thrust. Afterward, the vehicle performs a controlled descent to the ground. If adjacent rotors fail, the controller must orient the vehicle body in such a manner that the parachute can be deployed in the direction of the wind. The parchute is then deployed and the vehicle descends safely to the ground.

18 Weight Analysis

18.1 Weight Estimates

TABLE 18.1: *AirEZ* weight estimates

	Component description	Weight (lb)	% Empty Weight	z_{cg} (in)
1	Wings	1.91	9.3%	24
2	Rotor Group	1.91	9.3%	28.1
	Blades	0.84	4.1%	28.1
	Hubs	1.07	5.2%	28.1
5	Electric Motor Group	4.4	20.8%	27.0
	BLDC Motors	3.9	18.9%	27.2
	Electronic Speed Controllers	0.5	1.9%	25.5
3	Fuselage Group	4.5	21.8%	21.1
	Forward structure	1.2	5.8%	30.2
	Center structure	2.4	11.6%	20.3
	Aft structure	0.9	4.4%	11.1
4	Landing gear group	2.1	10.2%	13.9
	Upper Struts	0.55	2.7%	26.0
	Lower Struts	0.65	3.2%	7.0
	Landing Stilts	0.8	3.9%	13.0
	Elastomeric Spring	0.1	0.5%	0.5
7	Package Dropoff System	0.55	2.7%	23.2
	Servos	0.25	1.2%	13.3
	Augers	0.11	0.5%	11.8
	Drive Shafts and Gears	0.19	0.9%	11.8
	Door structure	0.5	2.4%	11.8
6	Electronic System	5.36	27.9%	28.1
	Sense and Avoid	2.53	12.3%	20.5
	Parachute	2.75	13.3%	35.1
	HUMS	0.03	0.1%	26.9
	Gust Rejection	0.05	0.2%	13.9
	Empty weight	**20.63**	**100%**	**24.4**
	Battery	12.85		28.12
	Package	5		11.8
	Gross weight	**38.48**		**24.0**

19 Summary

The *AirEZ* fleet has redefined the way the next generation aerial delivery will be conducted — A fast, efficient and agile configuration integrated into a system of systems approach capable

of delivering around 5,000 packages in a dense urban environment in 10 hours. A fleet of 400 vehicles working together in a mesh networking system ensures delivery to the customer's door within 90 minutes of order placement at a low delivery price of $9.03 dollars per package. As part of the logistics network, the vehicles function as a completely self aware node capable of grid communications, mesh networking, HUMS, and precise navigation in an urban canyon.

AirEZ combines the most desirable characteristics of fixed and rotary wing concepts to operate efficiently in both hover and forward flight regimes. Boasting a figure of merit of 0.74 and a propulsive efficiency of 0.85, *AirEZ* is able to operate in cruise at 55 kts, attain maximum dash speeds of 87 kts, hover at altitudes of over 8,000 ft, and fly for up to 7 hours. The hot and high capabilities of the craft allow the delivery system to be located in virtually any urban city in the United States. Considering that *AirEZ* operates as part of a large fleet, the components and subsystems are designed in a modular fashion utilizing validated manufacturing techniques that allow for ease in maintenance and repair.

The *AirEZ* system is a multi-redundant system with safety measures built into every logistics node. The avionics suite onboard the *AirEZ* vehicle features multiple power loss and sensors capability loss failure mode mitigation strategies built in to safely guide the vehicle away from high-risk scenarios. Furthermore, the vehicle design is such that in the case of battery/motor failure, the rotors can either autorotate to the ground or safely operate in an one-motor inoperative condition. If however, a system level failure occurs, an inbuilt parachute system can guide the vehicle safely to the ground.

The 2015 Student Design Competition Request for Proposals, issues by the American Helicopter Society desired the development of a system of systems solution for package delivery. This proposal has defined the design of the *AirEZ* system, a novel autonomous quadrotor biplane tailsitter design capable of successfully meeting the RFP requirements while outperforming in certain areas.

With regard to the stated Measures of Effectiveness, the *AirEZ* system offers the following performance:

- **System acquisition and yearly operating costs: $6.77 million, $7.39 million.**
- **Number of packages delivered per vehicle per day: 11 packages.**
- **Number of events where the time between customer's request for a package and actual delivery exceeds 90 minutes: 0 packages weighing less than 5 lb and smaller than 12 x 12 x 16 in.**
- **Pounds of CO_2 emitted per delivery mile flown: 0.067 lb/mile**
- **Percentage of delivery missions successfully completed: 86%, which is similar to any major carrier's success rate for express deliveries.**

Bibliography

[1] "FedEx same day quotes," https://www.fedexsameday.com/fdx_quick_quote.aspx, Accessed: 05-29-2015.

[2] Tishchenko, M. and Nagaraj, V. T., "ENAE634 Helicopter Design Lecture Notes," University of Maryland, College Park, 2008.

[3] Stoll, A. and Bevirt, J., "Drag Reduction Through Distributed Electric Propulsion," *Aviation Technology, Integration, and Operations Conference, Atlanta, Georgia*, June 2014.

[4] Pinsker, W. J. G., "Theoretical Assessment of the General Stability and Gust Response Characteristics of STOL Aircraft," Tech. rep., Procurement Executive, Ministry of Defence, Aeronautical Research Council, UNKNOWN 1971.

[5] Sion Power, *Lithium Sulfur Rechargeable Battery Data Sheet*, 10 2008.

[6] Song, M.-K., Zhang, Y., and Cairns, E. J., "A Long-Life, High-Rate Lithium/Sulfur Cell: A Multifaceted Approach to Enhancing Cell Performance," *NANO Letters*, Vol. 13, No. 12, 11 2013, pp. 58915899.

[7] Nagaraj, V. T. and Chopra, I., "Explorations of Novel Powerplant Architectures for Hybrid Electric Helicopters," *AHS Forum 70, AHS Forum and Technology Display, Montreal, Canada*, May 2014.

[8] "BU-1101: Cost of Power," 2014, [Online; accessed May-2015].

[9] Gaines, L. and Cuenca, R., "Costs of Lithium-Ion Batteries for Vehicles," Tech. rep., Center for Transportation Research, Energy Systems Division, Argonne National Laboratory, 9700 South Cass Avenue, Argonne, Illinois 60439, May 2000.

[10] "Fuel Properties Comparison," Tech. rep., Alternative Fuels Data Center, October 2014.

[11] Bailey, R., "Electric Vehicles," 2014, [Online; accessed May-2015].

[12] Stahlhut, C., *Aerodynamic Design Optimization of Proprotors for Convertible-Rotor Concepts*, Ph.D. thesis, University of Maryland.

[13] Robert E. Sheldahl, P. C. K., "Aerodynamic Characteristics of Seven Symmetrical Airfoil Sections Through 180-degree Angle of Attack for Use in Aerodynamic Analysis of Vertical Axis Wind Turbines," Tech. rep., Sandia National Laboratories.

[14] Selig, M., "UIUC Wind Tunnel Data on the Web," March 1998, [Online].

[15] Nagaraj, V., "Relationship Between Fundamental Natural Frequency and Maximum Static Deflection for Rotating Timoshenko Beams, Journal of Sound and Vibration," *Journal of Sound and Vibration*, Vol. 201.

[16] Selig, M., Guglilmo, J., Broeren, A., and Giguere, P., *Summary of Low-Speed Airfoil Data*, SoarTech Publications, 1st ed., 1995.

[17] Selig, M. and McGranahan, B., "Wind Tunnel Aerodynamic Tests of Six Airfoils for Use on Small Wind Turbines," Tech. rep., American Institute of Aeronautics and Astronautics, Inc., UNKNOWN 2004.

[18] Nixon, M., P. D. C. L. and Popelka, D., "Aerodynamic Tailoring for Stability Augmentation and Performance Enhancements of Tiltrotor Aircraft," *55th Annual Forum of the American Helicopter Society*.

[19] Singh, S. P., Burgess, G. J., Singh, J., and Kremer, M., "Measurement and Analysis of the Next-day Air Shipping Environment for Mid-sized and Lightweight Packages for DHL, FedEX and United Parcel Service," *Packaging Technology and Science*, Vol. 19, No. 3, April 2006, pp. 227–235.

[20] Brackins, K., "2014-2015 32nd SDC Questions," American Helicopter Society, March 2015.

[21] Raymer, D. P., *Aircraft Design: A Conceptual Approach*, American Institute of Aeronautics and Astronautics, Inc., 2nd ed., 1992.

[22] Prouty, R., *Helicopter Performance, Stability, and Control*, PWS Engineering, Boston, 1986.

[23] Gur, O., Mason, W., and Schetz, J., "Full-Configuration Drag Estimation," *Journal of Aircraft*, Vol. 47, July 2010.

[24] Fradenburgh, E. A., "A Simple Autorotative Flare Index," *Journal of the American Helicopter Society*, Vol. 29, July 1984, pp. 73–74.

[25] Forster, C., Faessler, M., Fontana, F., Werlberger, M., and Scaramuzza, D., "Continuous On-Board Monocular-Visionbased Elevation Mapping Applied to Autonomous Landing of Micro Aerial Vehicles," Tech. Rep. 200021-143607, Robotics and Perception Group, University of Zurich, 2014.

[26] "Scanning range finder (SOKUIKI sensor) UTM-30LX," 2014, [Online].

[27] "Velodyne LiDAR PUCK," [Online].

[28] "STOPPING SIGHT DISTANCE AND DECISION SIGHT DISTANCE," Discussion Paper 8.A, Transportation Research Institute Oregon State University, Corvallis, Oregon 97331-4304, February 1997.

[29] Fitch, T., "How good can those antique car headlights be?" 2014, [Online; accessed April-2015].

[30] Ratti, C., Burian, S. J., Brown, M. J., Velugubantla, S. P., and Linger, S., "Building Height Characteristics in Three U.S. Cities," Tech. rep., SENSEable City Lab, Massachusetts Institute of Technology, 2002.

[31] "NDGPS GENERAL INFORMATION," April 2015, [Online].

[32] Reich, L., "PrecisionHawk Joins NASA Collaboration to Develop Tools for UAS Traffic Managemnt System for Low-Altitude Drone Operations," 2015, [Online; accessed April-2015].

[33] Collins, T., "Phone Interview on LATAS," April 2015, [Personal Phone Interview].

[34] Elliott, A. W., *VISION BASED LANDMARK DETECTION FOR UAV NAVIGATION*, Mres thesis, CRANFIELD UNIVERSITY, 2012.

[35] Kimchi, G. and et al., "UNMANNED AERIAL VEHICLE DELIVERY SYSTEM," 04 2015.